THE INFLUENCE OF H_2S ON PALLADIUM AND PALLADIUM-COPPER ALLOY MEMBRANES

by

Bryan David Morreale

B.S. in Chemical Engineering, University of Pittsburgh, 1999

M.S. in Chemical Engineering, University of Pittsburgh, 2001

Submitted to the Graduate Faculty of

the School of Engineering in partial fulfillment

of the requirements for the degree of

Doctor of Philosophy

University of Pittsburgh

2006

UNIVERSITY OF PITTSBURGH

SCHOOL OF ENGINEERING

This dissertation was presented

by

Bryan David Morreale

It was defended on

August 22, 2006

and approved by

Anthony Cugini, Professor, US DOE National Energy Technology Laboratory

Joseph McCarthy, Professor, Chemical and Petroleum Engineering Department

D. Sholl, Professor, Carnegie Mellon University, Chemical Engineering Department

Goetz Veser, Professor, Chemical and Petroleum Engineering Department

Dissertation Director: Robert Enick, Chairman, Chemical and Petroleum Engineering Department

THE INFLUENCE OF H_2S ON PALLADIUM AND PALLADIUM-COPPER ALLOY MEMBRANES

Bryan David Morreale, Ph.D.

University of Pittsburgh, 2006

Dense metal membranes have been identified as a promising technology for post-gasifier forward water-gas shift membrane reactors. Unfortunately, the impurities present in the gasifier effluent streams, such as H_2S, can have adverse effects on the mechanical and chemical stability of potential metal membranes in the form of corrosion or catalyst deactivation, respectively. Thus, this study has focused on the identification and characterization of dense metal membranes that can tolerate the harsh environments encountered in the gasification process without significant detrimental effects on permeability.

Pd-Cu alloys have been of interest in recent years due to its catalytic activity for hydrogen dissociation, high permeability relative to Pd, suppression of the hydride-phase transition and limited reports of stability in the presence of H_2S. Initially, the permeability of pure palladium, pure copper and palladium-copper alloys containing 80wt%, 60wt% and 53wt% Pd was evaluated with hydrogen retentate streams at temperatures and pressures ranging from 350 to 900^{o}C and 0.1 to 2.86 MPa, respectively. Results indicate that crystalline phase plays a

significant role in membrane performance, with the B2, 60wt%Pd-Cu alloy exhibiting the highest permeability of the alloys tested at temperatures below approximately 500^{o}C. However, at temperatures corresponding to an fcc crystalline temperature for all of the alloys, membrane performance increased with increasing palladium content of the alloy.

Additionally, the permeability the above mentioned alloys, along with pure palladium, have been evaluated in a H_2S containing retentate gas mixture at temperatures of 350, 450 and 635^{o}C. Permeability measurements coupled with SEM and XRD analysis of post tested membranes indicate that the mechanisms influencing performance is strongly dependent on operating temperature, alloy composition, crystalline structure, and exposure time.

Gravimetric analysis of the growth rate of the metals sulfides observed on the palladium-copper alloys and pure palladium during the transient period of flux measurements was conducted. A model of hydrogen transport through a composite membrane with a Pd base and a growing palladium sulfide film was then developed and fit to the transient flux results and sulfide growth rate. The optimization of the model resulted in the first reported values of the permeability of palladium sulfide.

TABLE OF CONTENTS

LIST OF TABLES

LIST OF FIGURES

ACKNOWLEDGMENTS

I would like to take this opportunity to thank everyone that has helped made this process a reality. First, I would like to thank my advisor, Robert M. Enick for his long hours of discussion and guidance through this work. Additionally I would like to acknowledge the financial and resource support of the University of Pittsburgh, the US DOE National Energy Technology Laboratory and Parsons Project Services in the evolution of this project.

Next I would like to thank the engineering technicians and computer personnel of Parsons Project Services for construction of the test apparatuses their long and attentive hours of collecting permeability data on the HMT units. Within Parsons Project services, I would like to extend a special thanks to Jeremy Brannen, Bill Brown, Paul Dieter, Ron Hirsh, and Ray Rokicki for making my experience fruitful for my professional career by instituting the importance of relationships with fellow workers.

Furthermore, I would like to thank Mike Ciocco, Anthony Cugini, Rich Killmeyer, and Kurt Rothenberger for their professional guidance over the duration of this study. I would like to extend a special thanks to Bret Howard for his long hours of discussion and patience within the subject matter as well as the extensive analytical analysis performed within this work.

Lastly, and most importantly, I would like to dedicate this work to the most important person in my life, my loving wife Kelly. Without her this accomplishment would not have been feasible. “Kel, we did it!”

1.0 INTRODUCTION AND BACKGROUND

As the world embarks on the 21st century, the US Government has dedicated a great deal of resources towards the identification of new energy sources and the enhancement of energy production processes. The interest in energy advancement stems from the concern over the depletion of fossil fuel resources, the increasing importance of a "clean" environment, and the desire of fuel independence. As a result, the scientific community has aggressively pursued the identification of the "future energy" from sources including biomass, coal, geothermal, nuclear, hydropower, natural gas, petroleum, solar energy and wind.

Renewable energy sources, such as power derived from biomass, wind and solar energy, have the potential as future energy sources because of their abundance and "green" characteristics. Hydrogen, however, has been of increasing interest because of its vast production possibilities and its flexibility of use in either combustion processes or fuel cells. Further, there is (currently) tremendous political support from the Bush administration for movement toward a "Hydrogen Economy" based on the aforementioned concerns of the current petroleum economy. Nonetheless, major obstacles impeding the rapid movement into a society based on hydrogen fuels include the identification of economically viable hydrogen production (and associated CO_2 sequestration) techniques, the transportation of hydrogen from production to local distributors, hydrogen storage, and finally safe delivery to the consumer.

Although, the road to a Hydrogen Economy may be a long, tortuous path, implementing hydrogen production during a period of petroleum instability may facilitate the evolution of the petroleum economy to a hydrogen economy. It is widely acknowledged, even by those opposed to reliance on coal-based technologies, that the gasification of coal and/or biomass is one of the few processes that have the potential of generating the large amounts of hydrogen (mixed with other gases) required to supply a hydrogen economy, especially during the next few decades. Gasification is a process that produces a fuel gas mixture of CO, CO_2, H_2 and trace contaminants including hydrogen sulfide, ammonia, mercury, halides (MX, where X is chlorine, fluorine, iodine, bromine, and M is another element) and fly ash[1, 2]. The fuel stream, rich in carbon monoxide, can be further reacted with steam to promote conversion of carbon monoxide to hydrogen and carbon dioxide via the water-gas shift (WGS) reaction, Equation 1-1.

$$CO + H_2O \leftrightarrow H_2 + CO_2 \qquad (1\text{-}1)$$

The WGS reaction is an exothermic reaction (ΔH = -171 kJ/mol) whose equilibrium conversion is favored at low temperatures. Therefore, the WGS reaction is commonly conducted at relatively low temperatures in order to attain high conversions, while introducing a heterogeneous catalyst to enhance the reaction rate [3]. This approach, however, increases the costs associated with the additional utilities (such as cooling) and catalysts. Systems analysis studies by Parsons indicate that the overall efficiency of the plant may be significantly improved if the WGS reaction and hydrogen separation can be conducted at elevated temperature and pressure conditions, immediately after gasification[4]. Hydrogen separation membranes have been

identified as a promising technology for the separation and purification of hydrogen from the mixed gas effluent stream at temperatures and pressures up to 1000^{o}C and 6.8 MPa. A synergistic approach to reaction and separation in a membrane reactor would also shift the CO conversion beyond that which would be attained in a conventional reactor. Although the value of the equilibrium constant for the WGS reaction decreases with increasing temperature causing low CO conversions to be attained in a conventional reactor, the ability to remove hydrogen from the reactor would lower H_2 concentration, allowing higher conversions of CO to be realized (especially with low H_2 pressures on the membrane permeate). Therefore, a membrane reactor would be required to shift the CO conversion well beyond that which could be attained in a conventional reactor while high temperature operation would also mitigate the need for the introduction of a heterogeneous catalyst. Hence, a selective, stable, highly permeable hydrogen membrane that can withstand the severe conditions associated with gasification product streams (up to 1273 K, up to 6.8 MPa, dilute concentrations of H_2S, NH_3, HCl, Hg, etc.) must be identified.

The application of a mechanically stable membrane reactor that was perfectly hydrogen-selective would produce two effluent streams, a low-pressure hydrogen stream and a high-pressure water/carbon dioxide stream. If the permeate stream was fed to a compressor, the suction of the compression could maintain the high purity hydrogen at a low pressure (required for high conversions of CO). Alternately, a sweep gas composed of an inexpensive component that is easily separable from hydrogen (e.g. steam) could be used to lower the hydrogen partial pressure; but would require the resources for the generation of steam and separation of the water. The high-purity hydrogen stream could serve as a chemical feedstock, a fuel or a feed stream for a hydrogen fuel cell, while the water/carbon dioxide stream could be cooled to condense the water, yielding a high-pressure carbon dioxide stream that is amenable for sequestration.

There are several technologies available for the production of hydrogen and its separation from gas mixtures. Some of the most common commercial hydrogen separation technologies are cryogenic separation, pressure swing adsorption, polymer membrane diffusion and catalytic purification[5]. Separation via membrane technologies have been of increasing interest due to their simplicity of operation (no moving parts) and potential ability to produce highly pure hydrogen and will be the focus of this work.

1.1 MEMBRANE TYPES

There are numerous membrane candidates being considered for the separation of hydrogen from a post-gasifier stream composed primarily of H_2, H_2O, CO and CO_2. The membrane candidates can be categorized based on the mechanism of hydrogen transport across the membranes: molecular, atomic, and ionic[6].

1.1.1 Porous Membranes

Porous membranes, generally composed of ceramics, carbon, metals, or a combination thereof are known to have very high permeability values for hydrogen, but often lack the selectivity required for implication. The characteristics governing performance of these membrane technologies include the pore diameter, mean free path, membrane thickness, tortuosity and kinetic diameter of the molecules of the gases of interest. Materials commonly employed in molecular transport membranes are zeolites, silicon carbide, silica, alumina and metal composites[6]. Currently institutions including, but not limited to Oak Ridge National Laboratory, Sandia National Laboratory and Los Alamos National Laboratory are investigating the performance characteristics of porous based membrane technologies for the separation of hydrogen from mixed gas streams.

1.1.2 Ion Transport Membranes

Ion proton transport membranes have been of increasing interest over the past 20 years due to their potentially high selectivity and chemically stability. Ion transport membranes are generally fabricated from pure mixed ionic conductors such as a dense perovskite or a combination of a dense ceramic and metallic phase, known as cermets[6]. The performance of ion transport membranes is governed by the ability to of the ceramic and metal phases to transport hydrogen protons and electrons, respectively. Ion transport membranes often exhibit infinite selectivity to hydrogen (and oxygen at elevated temperatures, >900^{o}C) but are rather low performing, limited to a very high operating temperature (>700^{o}C), and are mechanically brittle. Extensive work on ion transport membranes is being conducted by institutions including Argonne National Laboratory, Eltron Research Inc. and Oak Ridge National Laboratory.

1.1.3 Atomic Transport Membranes

Currently, organizations including ExxonMobil, IdaTech, Worcester Polytechnic Institute, Eltron Research Inc., the National Energy Technology Laboratory and many others are exploring the viability of atomic transport membranes. Atomic transport membranes are generally composed of a dense metal and/or metal alloy. The widely accepted mechanism for an atomic transport membrane, from high hydrogen pressure to low pressure surface, is: 1) the adsorption of hydrogen molecules, 2) the dissociation of the adsorbed hydrogen molecules into hydrogen atoms, 3) the transport of atomic hydrogen through the bulk of the metal via hopping of atomic hydrogen from defects within the metal lattice, 4) recombination of atomic hydrogen to molecular hydrogen, 5) followed lastly by the desorption of molecular hydrogen from the

membrane surface[7-9]. Metal membranes are generally infinitely selective to hydrogen, due to the abovementioned transport mechanism, with the hydrogen flux being inversely related to membrane thickness. Unfortunately, many metals of interest for membrane application are known to be susceptible to both thermal and chemical degradation[7].

Although dense metals have been studied as hydrogen membranes materials for over a century, a surprisingly small amount of flux and selectivity data are available for promising metal alloys in the presence of gasifier effluent products and impurities, especially H_2S. Therefore, the permeability, hydrogen selectivity, and robustness of metal alloy membranes at post-gasifier conditions must be addressed in effort to advance membrane technologies.

1.2 PALLADIUM MEMBRANES

Initial diffusion experiments with metal membranes began as early as the middle of the 19th century with palladium[10-12]. Since the initial diffusion experiments, Pd has been the most widely investigated membrane material, with the most recognized studies being conducted in the mid-20th century[13-18]. Additionally, several comprehensive review studies have been conducted summarizing the developments of palladium membrane technologies over the past 150 years[5, 19].

The interest in palladium as a membrane research stems from its relatively high permeability as compared to other pure metals (Figure 1), infinite selectivity for hydrogen, reasonable mechanical characteristics, and highly catalytic surface[20, 21]. Although palladium has

been the most highly investigated membrane material, properties including cost and chemical stability inhibit its widespread application to large scale processes such as gasification.

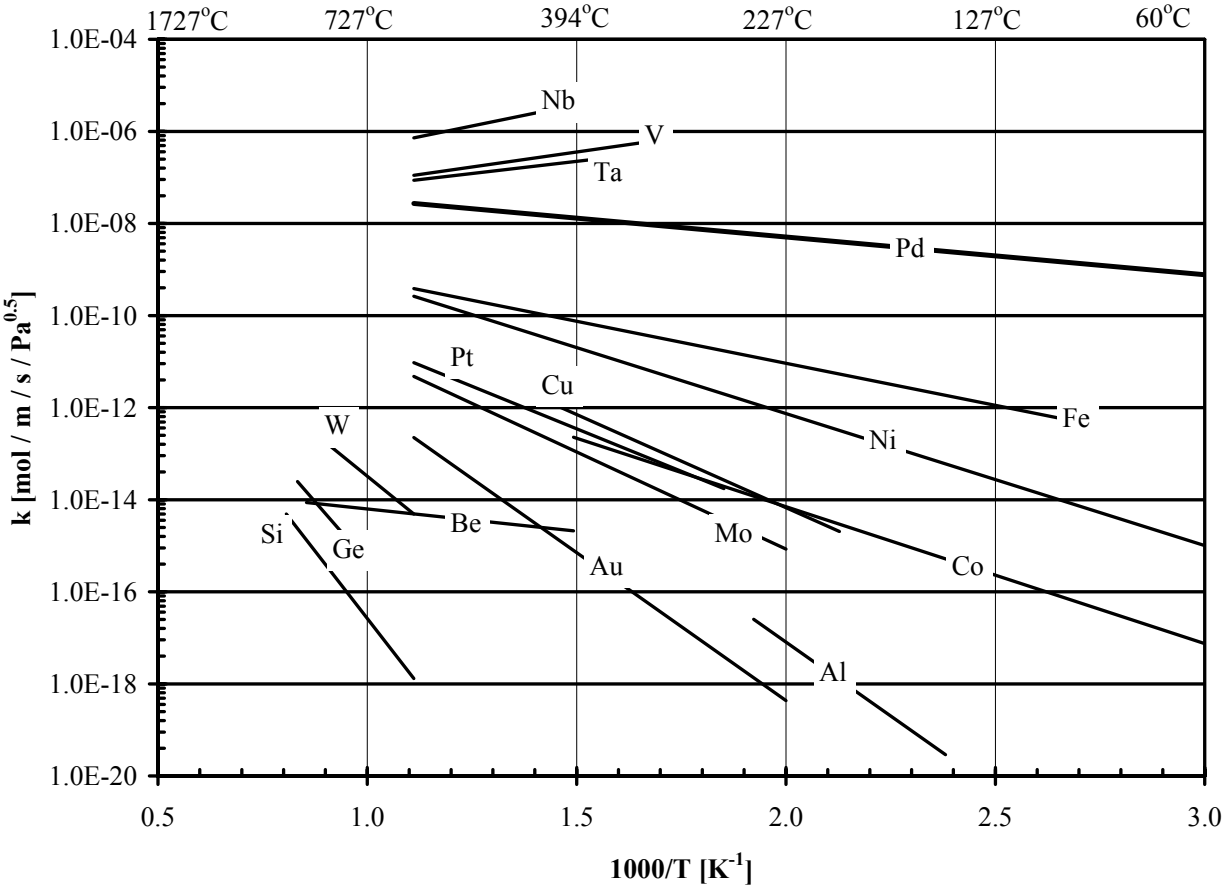

Figure 1. Hydrogen permeability of various pure materials[20].

The cost of palladium, historically varying between $180 and $1000 per troy-ounce, makes it economically impractical as a membrane material for large processes in which a thickness of greater than 25-microns is employed. Current membrane research is focusing on the development of new and more efficient technologies to circumvent the high capital costs of palladium. These technologies include alloying palladium with lower cost materials, applying very thin films of palladium and palladium alloys to highly permeable substrates, and identifying efficient means of recycling "used" membranes[22-70].

Although palladium has many advantages as a "hydrogen" membrane, ironically hydrogen can have adverse affects on the mechanical integrity of pure palladium. In the presence of hydrogen, palladium forms a continuous solid solution, exhibiting an fcc (face-centered-cubic) crystal structure[71]. However, at temperatures below 573K, the phase diagram illustrates the formation of two distinctly different phases, a hydrogen-rich phase and a palladium-rich phase. Although the two low temperature phases are both fcc in crystal structure, they exhibit slightly different lattice parameters. Thermal cycling palladium in the presence of hydrogen throughout the region of hydride formation can lead to distortion and severe embrittlement[5]. However, technologies including alloying palladium with other metals have been identified as a means of mitigating mechanical failure due to hydride formation[5, 9]. Alloying palladium with metals including silver and copper has been identified as a means of lowering the temperature of the miscibility gap[7], thus mitigating mechanical failure due to hydride formation.

Operation of metal membranes at elevated temperatures can have deleterious effects on mechanical durability, which is linked to the thermodynamic process of the minimization in surface free energy. The reduction in free surface energy is accomplished by crystal recovery, recrystallization and/or crystal grain growth in which there is a strong correlation between mechanical strength and the coarseness of the crystal distribution. Thus, prolonged exposure at elevated temperatures (as low as 1/3 of the melting temperature or 517^{o}C for palladium) can significantly increase crystalline size and reduce mechanical strength[72, 73]

1.2.1 Chemical Stability of Palladium Membranes

Of additional importance to the advancement of palladium membrane technologies is the impact of chemical species other than hydrogen on performance. Several researchers have demonstrated the influence of various chemical species, such as O_2, H_2S, CO_2, H_2O, on the performance of palladium-based membranes[7, 74-76].

Many palladium membrane studies often initiate testing with an oxygen exposure prior to characterizing hydrogen performance. The oxygen pretreatment is claimed to "activate" the membrane by the removal of surface contaminants, and has been shown to vastly influence performance values[75, 77-79]. Although the operation of a palladium membrane in an oxidizing atmosphere can remove surface contaminants, it has been revealed that such exposures can highly influence surface morphology even though palladium oxides are not observed. Oxygen exposures can vastly increase surface roughness and membrane surface area, which could cause significant technical issues with respect to thin film integrity[74].

Studies have also focused on the influence of major gasifier effluent species (CO, CO_2, and H_2O) on the performance and viability of palladium-based membrane materials[63, 73, 78, 80-83]. A thorough review conducted by Gao et al. indicated all of the major gasifier effluent species exhibit adverse effects on palladium performance. A reduction in performance in the presence of H_2O and CO_2 was attributed to the blocking of hydrogen adsorption sites. While the influence of CO was slightly more complex, varying from competitive adsorption to decreases in permeability due to the formation of graphitic carbon within the interstitials of the palladium crystal structure[73].

Additionally, the influence of minor gasification effluent species, especially H_2S, is of importance to the advancement of palladium membrane technologies. While studying the performance of a 25-micron palladium foil in 1961, Hurlbert and Konecny showed an ~83% reduction in hydrogen flux in less than ~120 minutes at 350^oC in the presence of $5e^{-5}$mol%H_2S (50ppm H_2S). The reduction in performance observed was attributed to the formation of a "dark gray" surface film and appeared to be irreversible[75].

While patenting several palladium alloys in 1967, McKinley and Nitro demonstrated the effects of H_2S on the hydrogen flux through a palladium membrane at 350^oC. Upon exposure of a 25-micron foil to 20ppm H_2S, a gradual reduction in hydrogen flux was observed in the first four days of exposure followed by a constant performance over the next 2 days. The total reduction observed for the palladium foil over the six day exposure period was ~70%. Upon visual inspection of the post-tested palladium membrane, the surface appeared dull and lost its initial luster. Additionally, a second palladium foil was exposed to 20ppm H_2S at 350^oC for approximately 4 days, in which a gradual reduction of ~70% was also observed. However, upon the removal of H_2S and the introduction of hydrogen, the performance of the membrane was restored to its initial value in only two days. McKinley and Nitro therefore hypothesized the reduction in performance observed in his study was due to the adsorption of H_2S on the palladium surface rather than chemical attack or sulfide formation on the surface[84].

In an effort to enhance the reliability of a palladium based hydrogen sensor, Lalauze and co-workers explored the influence of surface contaminants on the hydrogen diffusion process through palladium. Temperature Programmed Desorption and Auger analysis of the palladium

surface showed significant concentrations of C, O and S, as high as 54, 5, and 18at%, respectively. Therefore, Lalauze and co-workers concluded the variances in performance observed for the palladium samples was attributed to the chemisorbed species on the palladium surface[78].

In 1993 and 1994, Edlund and co-workers explored the viability of hot-pressed composite membranes for high temperature hydrogen separations. The composite membranes consisted of a 25-micron thick palladium or platinum layer on each side of the 30-micron thick vanadium substrate. The performance of the Pd-based composite membrane yielded considerably higher flux values in the presence of hydrogen as compared to the Pt-based membrane[85]. The hydrogen flux Pd- and Pt-composite membranes were then characterized in the presence of pure H_2S at 700^{o}C and 115 psia for an 8 hour exposure. The Pt-coated membrane showed no changes in hydrogen flux in the presence the presence of H_2S and remained lustrous in appearance during post test visual inspections. However, the Pd-coated membrane failed within seconds under similar conditions. Upon removal of the palladium based composite membrane after H_2S exposure, the membrane exhibited numerous holes which was attributed to complete corrosion of the metals[86].

In 1999, Kajiwara and co-workers explored the stability and behavior of palladium and platinum coated porous alumina membranes in the presence of 6200 ppm H_2S in hydrogen. Similar to the results observed by Edlund[85, 86], the palladium based membrane ruptured within an 20 minutes of operation at 400^{o}C. Scanning Electron Microscopy (SEM) analysis of the post test membrane sample revealed cracks in the surface of the membrane (up to several centimeters

long). The failure of the membrane sample was attributed to the formation of a palladium sulfide, which has a lattice constant roughly twice that of palladium, thus creating structural stresses which were relieved by the formation of cracks in the membrane[87].

In a recent study, Kulprathipanja and co-workers (2005) explored the inhibition of H_2S on the hydrogen permeation of a ~4-micron, electroless-plated (on asymmetric α-alumina tubes) palladium membrane. Several Pd membranes were exposed to H_2S concentrations ranging from 100 to 1000ppm at 450^{o}C. SEM analysis of the Pd membranes exhibited pore and particle formation on the surfaces after ~100ppm H_2S exposure. After exposure to a 20ppm $H_2S/H_2/N_2$ gas mixture, the performance of the membrane sample decreased 33%, while a 36% decrease in the H_2/N_2 selectivity was observed. Moreover, two Pd membrane samples were tested in the presence of 100ppm H_2S, the first membrane sample resulted in failure in less than 2 hours while a similar test resulted in a 95% reduction in performance without failure. Kulprathipanja and co-workers hypothesize that the reduction in performance observed was due to "site-blocking" with complete inhibition taking place at H_2S concentrations greater than 100ppm while pores, cracks and defects were a result of surface rearrangement due to metal-sulfur interactions[88].

1.3 SUPER-PERMEABLE METALS

In the past 20 years select, refractory metals (niobium, tantalum, vanadium, and zirconium) have been of increasing interest to the scientific community due to their very high permeability (relative to palladium), Figure 1, and has been the focus of a comprehensive review

by Mundschau and co-workers[89]. Although these "super-permeable" materials show very high performance capabilities, the application of these materials to large scale applications have been prohibitive due to an insufficient catalytic surface (due to oxide formation associated with even brief exposure to dilute concentrations of oxygen during handling, transport, installation or testing) and embrittlement issues attributed to the formation of metal-hydrides[5, 90-93]. Efforts by numerous researchers have focused on incorporating these super-permeable metals and super-permeable metal alloys (ex. $V_{85}Ni$, $V_{85}Cu$) into an applicable composite membrane [21, 24, 27, 48, 53-55, 60, 85, 86, 90, 93-104]. These composite membranes generally revolve around the application of a highly catalytic surface material (such as palladium) on an oxide free super-permeable metal or metal alloy substrate. The resultant composite membranes will thus demonstrate a very high performance (governed by the super-permeability metal), reduced costs (reduced amounts of palladium), and increased mechanical strength (high strength of the refractory metals). Additionally, since the "super-permeable" substrate is applied as a dense foil, a highly pure hydrogen product will be produced, even upon defects in the coating materials, unlike the use of porous substrates. Further, defects in the coating materials over a dense substrate will result in only a minor loss in permeance and virtually no change in selectivity, while defects in palladium films on porous substrates leads to substantial losses in selectivity.

1.4 PALLADIUM ALLOY MEMBRANES

Palladium alloy research has been conducted in an effort to minimize the amount of palladium needed in membrane fabrication, increase the performance, promote chemical

robustness and increase mechanical integrity by reducing the effect of the hydride phase change [5, 105, 106]. Palladium has been the parent material for binary membranes, alloyed with an array of elements including boron[84, 107], cerium[84, 107-109], copper[32, 39, 63, 84, 88, 107, 110-114], gold[84, 107], iron[115], nickel[33, 49, 50, 84, 107, 116],silver[9, 22, 26, 36, 47, 57, 63, 77, 84, 107, 110, 116-118], yttrium[109, 119, 120], and others. Although all the metals alloyed with palladium have some effect on performance and deformation resistance, cerium, copper, gold, silver and yttrium are unique in that these alloys can exhibit higher permeability values than each of the metals exhibit individually[5, 84, 106], Figure 2. The observed change in permeability of a metal alloy is attributed to increasing either the solubility and/or the diffusivity of hydrogen within the metal, and thus increasing permeability[5, 121-125].

The palladium-silver alloy membrane system was successfully commercialized in the early 1960's[5] but the reduction of palladium and addition of silver would still not be a significant cost-effective alternative for large-scale processes[48] unless micron-scale thin films could be prepared; a goal currently being addressed by many researchers including Way from the Colorado School of Mines, Ma from Worcester Polytechnical Institute, and Buxbaum of REB Research.

Additional research has focused on the Pd-Cu system due to the relative high performance of the 60wt%Pd-Cu alloy, which has exhibited flux values comparable to pure palladium in the presence of hydrogen at 350^{o}C[84]. Hydrogen solubility studies of the Pd-Cu system indicate that the solubility of the fcc crystalline phase increases with increasing palladium content[125, 126]. The B2 composition yields significantly higher solubility values as compared to

the fcc Pd-Cu alloys, with a maximum solubility at a composition of ~60wt%Pd-Cu[124]. Additionally, studies conducted by Piper and Zetkin revealed that the B2 phase of the Pd-Cu alloys exhibit higher diffusion coefficients as compared to fcc alloy compositions[122, 123], while dissolved hydrogen shifted the B2-fcc phase boundaries to higher palladium concentrations (but the B2 phase remained unstable at temperatures greater than 600°C)[123]. Lastly, Kuranov and coworkers demonstrated the enhanced mechanical properties of bcc Pd-Cu alloys as compared to fcc compositions[127]

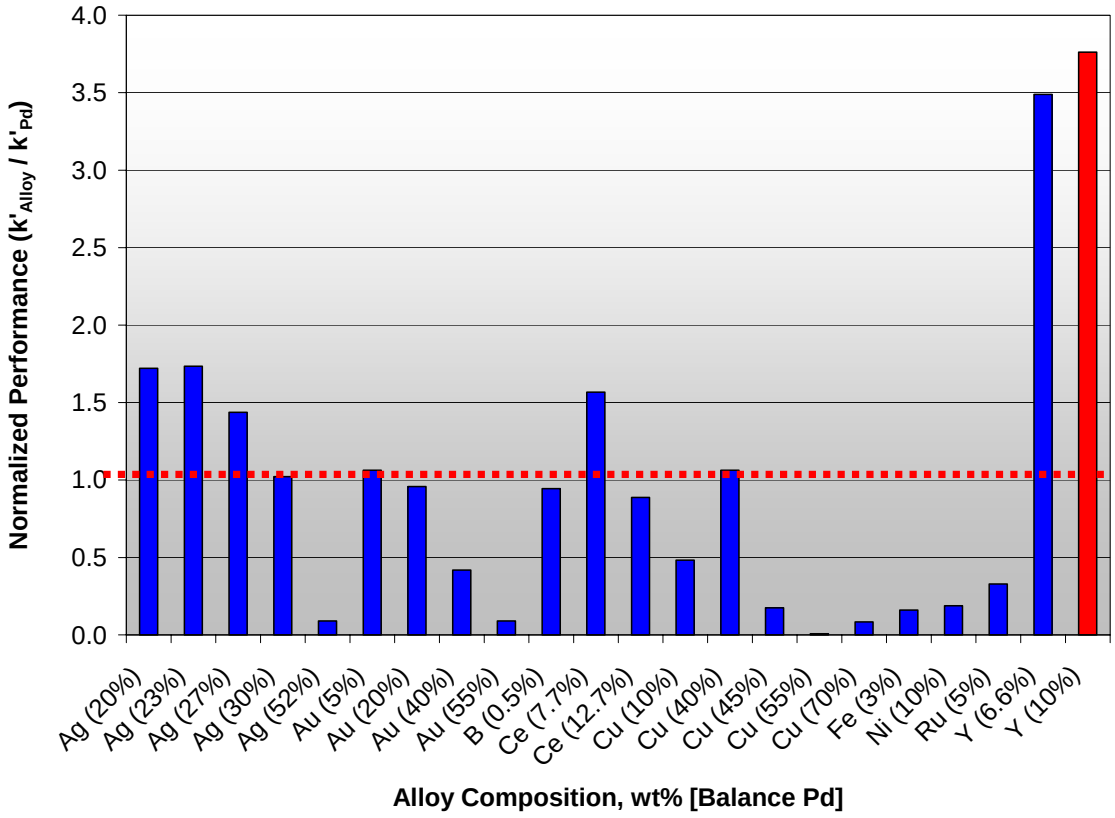

Figure 2. Permeance of select palladium alloys relative to pure palladium at a temperature and feed pressure of 623K and ~2.16MPa, respectively[84, 106, 115].

1.4.1 Chemical Stability of Palladium Alloy Membranes

As was demonstrated in the previous section, the success of these membrane alloys towards the implementation to the gasification process relies on the chemical stability in the presence of both major and minor gasifier effluent components. Several studies have been conducted on the influence of major gasifier components (CO, CO_2 and H_2O) on palladium alloys[22, 73, 115, 128, 129]. Although the results observed with palladium alloys are similar to the aforementioned results for pure palladium in the presence of major gasifier species (but will not be reviewed in this work), results in the presence of H_2S are more interesting and will be the focus of the subsequent paragraphs.

In 1967, while patenting metal alloys for hydrogen purification and separation, McKinley and Nitro conducted the first thorough study on the influence of H_2S on the performance of various ~25-micron palladium-alloy foils at 350^{o}C and a feed pressure of 75psig. H_2S concentration in the experiments conducted by McKinley and Nitro ranged from 3.5 to 4.7ppm, unless otherwise noted[84].

The 73 wt% palladium-silver alloy (the most commonly used alloy in commercial applications) exhibited a 99% reduction in performance over a six day period, although the majority of the flux reduction was observed over the first 6 hours of exposure. The palladium-silver alloy exhibited "regenerable" characteristics when H_2S was removed from the system after 2-days of exposure. Following 1-day of exposure to hydrogen (after 2 days of H_2S exposure), the palladium-silver alloy regained some of its original performance, exhibiting an 80% reduction in flux from the pre-H_2S exposure. Over the next three day of exposure to hydrogen, the flux of the membrane gradually increased to a value of 67% of the pre-exposed results[84].

An alloy containing 60wt%Pd-Cu was also studied by McKinley and Nitro. Likewise, the palladium-copper alloy exhibited significant hydrogen flux decreases in the presence of H_2S, an 82% reduction immediately decreasing to a 90% reduction after 6-hours of exposure, to a limiting value yielding a 95% reduction at day 3, and holding relatively constant for the next 5-days of exposure. The palladium-copper foil was also tested to determine the "regenerability" of the alloy upon removal of the H_2S gas mixture. After a 95% reduction in hydrogen flux was observed over the first 2-days of H_2S exposure, the palladium-copper alloy retained its performance only after 2 days of H_2 exposure[84].

The most promising alloy studied by McKinley and Nitro with regards to the smallest influence of H_2S was the 60wt% palladium-gold alloy at 350^{o}C. Although the initial performance of this alloy was relatively low (Figure 2), only a 20% reduction was observed over a 6-day exposure. A second palladium gold alloy was tested in an effort to characterize the regenerability of the alloy. After 2-days of exposure in the presence of H_2S a 10% reduction was observed.

However, upon the removal of the sulfur gas mixture and the introduction of H_2, the membrane actually performed better, yielding a flux ~120% of the original. McKinley and Nitro also studied the influence of other H_2S concentrations (20ppm and 6.6%) on the performance of the palladium-gold alloy. The higher the concentration of H_2S exposed to the membrane, the larger in the decrease in performance was observed. However, with both concentrations, a flux of ~120% of the original was experienced after H_2S was removed and pure hydrogen was re-introduced[84]. The aforementioned performance data in the presence of H_2S reported by McKinley and Nitro is summarized in Table 1.

While studying the influence of pressure, temperature, and membrane thickness on the diffusion rate of the hydrogen-palladium-silver system in 1963, Darling exposed a ~75 micron drawn 73wt% palladium-silver tube to several H_2S concentrations. At 500^{o}C and 200 psi the palladium-silver alloy exhibited negligible changes in flux in the presence of 490 and 1280ppm H_2S, although 1600ppm H_2S dramatically reduced performance. Furthermore, exposure of such an alloy to 1500 ppm H_2S for 16 hours resulted in the formation of a palladium-sulfide layer on the membrane surface. Darling continues to state that mild poisoning (defined by <25% reduction in performance), is usually temporary and the membrane performance can be regenerated by operation of the poisoned membrane in the presence of neat hydrogen for 24 hours at 500^{o}C. While instances where reductions in membrane performance of greater than 50% observed are probably permanent[9]. Similar results were observed for the palladium-silver system by Philpott and Coupland, where 1600ppm H_2S reduced performance by 50% in only 16hrs at 500^{o}C[7].

Table 1. Effect of hydrogen sulfide on the performance of select Pd and Pd alloy membranes as presented by McKinley and Nitro[84].

Alloy Composition	Normalized Performance (k'_{Alloy}/k'_{Pd})	Normalized Performance ($k'_{4ppm\ H2S}/k'_{H2}$)	"Regenerability" ($k'_{H2,\ After\ H2S}/\ k'_{H2,Initially}$)
Pure Pd	1.00	0.29	1.00
27.18wt%Ag-Pd	1.73	0.01	0.67
39.7wt%Au-Pd	0.46	0.85 0.43* No flux observed**	1.18 1.22 1.18
38.7wt%Cu-Pd	1.35	0.05	1.00

Performance data was collected at a temperature of 350°C, a feed pressure of 790kPa and an atmospheric permeate pressure.*Denotes results in the presence of 20 ppm H_2S. ** Denotes results in the presence of 6.6% H_2S. The values in column 5 demonstrate the results after the feed gas is switched from a H_2S containing mixture to neat hydrogen [84].

In 1994, Ali and co-workers studied the influence of methylcyclohexane, toluene, sulfur and chlorine on the performance of palladium-silver membranes. As previously mentioned for pure palladium membranes, Ali and co-workers employed an oxygen activation procedure to their palladium-silver alloy membrane to remove surface impurities. Upon flux testing at 633°C in the presence of 0.12% dimethyl-disulfide (1630ppm S), a ~83% reduction in performance was observed. Ali and co-worker then attempted to regenerate the membrane by air cycling and increasing temperature. Air exposures at 633, 673, and 713°C resulted in flux comparisons of 50%, 75% and 108%, respectively, as compared to the original flux results in the presence of hydrogen at 633°C. Ali and co-workers contributed the decrease in performance in the presence of S to the blocking of hydrogen adsorption and dissociation sites on the membrane surface.

While attempting to develop a membrane process for the thermal decomposition of H_2S, Edlund and coworkers (1996) studied the potential of several palladium alloys for chemical stability. The alloy foils tested were approximately 25-microns thick and were operated at 500°C in the presence of 1000ppm H_2S in hydrogen at ~115 psia. A 75wt% palladium silver alloy,

which exhibited a flux of ~97 $cm^3/cm^2/min$ in the presence of neat H_2 showed a flux of less than 1 $cm^3/cm^2/min$ in the presence of 50ppm H_2S and no detectable flux in the presence of 1000ppm H_2S. Additionally, a gold coated palladium membrane, which had a flux of ~18 $cm^3/cm^2/min$ in neat hydrogen, exhibited a 29% decrease in performance in the presence of 50ppm H_2S. Lastly, a 60wt% palladium-copper alloy was tested which exhibited a hydrogen flux of ~33 $cm^3/cm^2/min$ in the presence of neat hydrogen. Flux testing of the 60wt%Pd-Cu alloy in the presence of 50 and 1000ppm H_2S resulted in a 23% and 85% reduction in performance, respectively. Based on the results of the this study, Edlund and co-workers hypothesize that the observed resistance of the 60wt%Pd-Cu alloy should increase with increasing temperatures[110].

In 2002, while studying the influence of grain size on the performance of a palladium-iron membrane, which was fabricated by a pulsed electrodeposition technique, Bryden and Ying conducted diffusion experiments in the presence of 51.9ppm H_2S at 200^oC. The H_2S exposure of the 10-micron thick, 94at% palladium-iron alloy, resulted in immediate decreases of 75 and 95% in performance for the membranes with a grain size of 28 and 100 nm, respectively, Furthermore, after 2-hrs of exposure, the H_2S gas mixture was removed in an effort to determine the "recovery" of the 28 and 100 nm samples. The hydrogen flux of the 28 nm sample recovered 100% of its performance in approximately 30 minutes, while over 400 minutes was needed for the 100 nm sample to achieve a similar recovery[115].

Additionally, in 2005 Kulprathipanja and co-workers studied the influence of varying H_2S concentrations on the permeability of palladium and various palladium-copper membranes, with Pd compositions ranging from 27wt%Pd to 80wt%Pd. The majority of the membrane

samples were prepared using an electroless plating technique while one of the samples tested was in the form of a dense foil. The membranes were exposed to various concentrations of H_2S with resulting flux and surface information detailed in the manuscript. The Pd-Cu alloys studied exhibited significant surface modification after exposure to H_2S, which included pore and particle formation detected by SEM as well as significant surface roughness measured by AFM measurements. Surface modification observed for the electroless plated membrane samples was more evident as compared to the membrane foil. Differences observed by EDS measurements of pre- and post-tested membranes indicated alloy segregation, which was evident by increases in the fcc crystalline content in the top 1 μm of the surface as well as the detection of S in post-tested samples. However, XRD studies could not verify the formation of the metal sulfides. Moreover, decreases in hydrogen flux were observed for all of the Pd-Cu alloys reported, and were attributed to competitive adsorption. The authors hypothesized that total membrane inhibition would take place at a H_2S concentration of only 300 ppm. At H_2S concentrations greater than 300 ppm, Kulprathipanja and co-workers propose mechanical failure, which is attributed to the formation of palladium and copper sulfides rearranging the surface and forming large pores and causing membrane rupture[88].

1.5 MEMBRANE POISONING MECHANISMS

As has been detailed in the previous sections, the reduction in performance of palladium based membranes can be attributed to, in a broad sense, the formation of a "sulfur" layer. The sulfur layer inhibiting performance can further be differentiated into: a) adsorption of S on the membrane surface inhibiting hydrogen adsorption and dissociation, and/or b) the formation of a "low-permeability" sulfide scale.

1.5.1 Competitive Adsorption

As noted above, several researchers attribute the observed reduction in the performance of palladium based membrane materials to the "deactivation" of the catalytic surface by adsorbed S[9, 77, 78, 84, 88]. The influence of S on the capability of palladium to adsorb and dissociate hydrogen has been the focus of numerous experimental and theoretical studies, which will be the focus of the following section. Although the following material is by no means a comprehensive review of Pd-S interactions, it gives a foundation of understanding of the pertinent phenomenon as it relates to hydrogen membranes.

In 1987 Campbell and Koel studied the influence of H_2S on a Cu based WGS catalyst. In their study Campbell and Koel reported that H_2S dissociates into H_2 and adsorbed S bonded on the top of a Cu(111) single crystal. The researches continue to demonstrate a considerable decrease in the catalytic activity of the Cu(111) surface with increasing S coverages at temperatures of 339^{o}C with respect to the WGS reaction, where approximately an order of

magnitude decrease in reaction rate was observed for a S/Cu AES surface ratio of 0.42 (θ_s=0.34). Campbell and Koel attributed the observed decrease in catalytic activity to sterically blocking H_2O adsorption sites. Furthermore, they conclude that the desorption of S from the Cu(111) surface is very slow[130].

In 1990, Burke and Madix studied the influence of S on the hydrogen adsorption on a Pd(100) surface by temperature programmed desorption (TPD). The study indicates that the saturation coverage of adsorbed hydrogen decreases linearly with adsorbed sulfur, with hydrogen adsorption being completely blocked at a sulfur coverage of 0.28 monolayer (ML). The researches hypothesize that this phenomenon is attributed to the direct blocking of adsorption sites on the Pd(100) surface as well as the adsorbed S extending a steric influence to the four nearest adsorption sites[131].

In 1992 Forbes and coworkers used analytical techniques including STM, LEED and AES to characterize sulfur overlayers on a Pd(111) surface. STM images reveal $(\sqrt{3} \times \sqrt{3})R30^o$ over-layers on the surface while the formation of the $(\sqrt{7} \times \sqrt{7})R19^o$ is more complex in that the sulfur may exist in the subsurface Pd lattice[132]. The presence of sulfur in the sub-layers of the Pd-S system may indicate a high atomic mobility of the system as well as that the influence of S on a membrane may be more significant than just competitive adsorption.

In 1992, Vazquez and co-workers explored the morphological and activity influences of sulfidation on hydrodesulfurization catalysts at temperatures ranging from 400 to 450^{o}C. TEM analysis indicated particle growth of the palladium particles on a Si substrate, which was

attributed to the sulfidation of the Pd and was more significant with increasing temperature. Additionally, thiophene conversion decreased over 60% at 400^{o}C for a sulfided catalyst as compared to a sulfide free Pd catalyst[133].

In 1994, Feuerriegel and coworkers explored the effect of H_2S on the deactivation of a Pd-based catalyst during the oxidation of methane. At 240^{o}C, H_2S concentrations of 5.4, 13.3 and 21.6 ppm all resulted in complete deactivation of the commercial palladium-supported on γ-Al_2O_3 catalyst, however, higher concentrations of H_2S resulted in more rapid catalyst deactivation (total deactivation was observed in as little as 14 hrs and as long as 80 hrs). Additionally, an H_2S surface coverage of 0.08 ML completely poisoned the catalyst. XPS analysis of the post tested catalyst exhibited metallic palladium and sulfur in a highly oxidized state (>SO_2). Thus, Feuerriegel and co-workers attributed the decrease in activity to the adsorbed sulfur species on the catalyst surface[134].

In 1995, Wilke and Scheffler studied the co-adsorption of hydrogen and sulfur on a Pd(100) surface using theoretical methods. Wilke and Scheffler studied the adsorption of hydrogen on clean and sulfur covered Pd(100) using density functional theory. The theoretical calculations illustrate that low sulfur surface coverages ($\theta_S \leq 0.25$) reduces the hydrogen adsorption energy at sites close to adsorbed sulfur, while at higher surface coverages ($\theta_S = 0.5$), strong repulsive H-S interactions strictly block the adsorption of hydrogen in the vicinity of sulfur adatoms. Additionally, the influence of sulfur adatoms also influences the dissociation of hydrogen by the formation of additional energy barriers[135].

In 1999, Gravil and Toulhout used first principle calculations to theoretically model the interaction of S and Cl on a Pd(111) surface. These researchers demonstrated that a 0.33 ML of adsorbed S is sufficient to completely inhibit H_2 adsorption. Additionally, Gravil and Toulhout elude that lower S coverages inhibit H_2 dissociation on the Pd(111) surface which is strongly dependent on the lateral separation of the adsorbed S and H[136].

In recent computational studies by Alfonso and co-workers, the interaction of several membrane materials with S and H_2S has been examined. Alfonso and co-workers demonstrated that the binding energy of S on potential membrane metals shows the following trend: $E_{Pd(111)}>E_{Cu(111)}>E_{Ag(111)}$, while Pd-alloys with Cu and Ag show weaker binding energies than pure Pd[137]. Additional studies conclude that although H_2S will adsorb and dissociate relatively easily on a Pd(111) surface, S is the most stable adsorbed species at low surface coverage ($\theta_S \leq 0.5$). While at a surface coverage of sulfur greater than 0.5 ML, adsorbed sulfur has a tendency to form S-S bonds on the Pd surface[138, 139].

In summary, adsorbed sulfur on a metal surface can significantly impact the hydrogen adsorption and dissociation properties of the catalyst with the impact increasing with increasing surface coverage. Researchers note that a sulfur surface coverage of as little as 0.28 ML can completely inhibit the catalytic process of the Pd-H_2 system. Additionally, adsorbed sulfur was shown to decrease the reaction rate as well as conversion of several reactions involving hydrogen. The aforementioned decreases in catalytic activity due to the presence of sulfur may have significant impacts on the performance of hydrogen membranes due to the inability for hydrogen to adsorb and dissociate on the membrane surface.

1.5.2 Corrosion

High temperature corrosion is a widespread problem in industries including power generation, aerospace and gas turbines, heat treating, mineral and metallurgical processing, chemical processing, petrochemical and refining, automotive, pulp and paper as well as waste incineration. Corrosion mechanisms that are important to these industries include oxidation, sulfidation and carburization and are named based on the corrosion product. Of importance in this study is the interaction of potential membrane materials with an H_2S containing gas stream, therefore, sulfidation is the primary corrosion mechanism of concern.

Sulfidation is a typical high temperature corrosion failure mechanism of metals and is analogous to metal oxidation. In sulfidation, sulfur containing gaseous species reacts with the metal to form a new compound on the surface, assuming thermodynamic favorability. Ellingham

diagrams (standard free energy of formation versus temperature) are qualitative tools used to visualize the relative stability of oxides, sulfides or carbides An Ellingham-type diagram for various metal sulfides as they pertain to membrane materials are given in Figure 3, where a lower y-axis value represents a more stable corrosion product[140, 141]. Once an observation is made in the determination of the stability of a corrosion product, the rate of scale growth can be fit to three main kinetic models: parabolic, logarithmic, and linear. The parabolic and linear rate laws illustrate the underlying mechanism of corrosion. For the linear rate law formation of corrosion product is only limited by the rate of scale growth. While at very short times for the parabolic relationship, the formation of the scale is also limited by the rate of reaction. However, as the sulfide scale thickens the rate becomes limited by the diffusion of electrons, metal cations and/or gas anions through the scale. Lastly, when neither the parabolic or linear rate laws describe the scale growth, a logarithmic law is employed. The logarithmic rate law is strictly used as an empirical relation describing sulfur uptake and yields no fundamental insight into the corrosion mechanism.

Figure 3 illustrates the stability of several metals of interest in this study, including palladium-based sulfides. Unfortunately, only two references were obtained detailing the thermodynamics of the palladium-sulfur system, which differed significantly from one another. The Gibbs free energy values obtained from the reference book compiled by Barin, which summarizes the work of Niwa, is roughly two times greater than those reported by Taylor[140-142]. The discrepancy in these thermodynamic values, and the disagreement of the predicted stability based on the values of Niwa with other membrane researches yields doubt of the integrity of the data presented by Niwa.

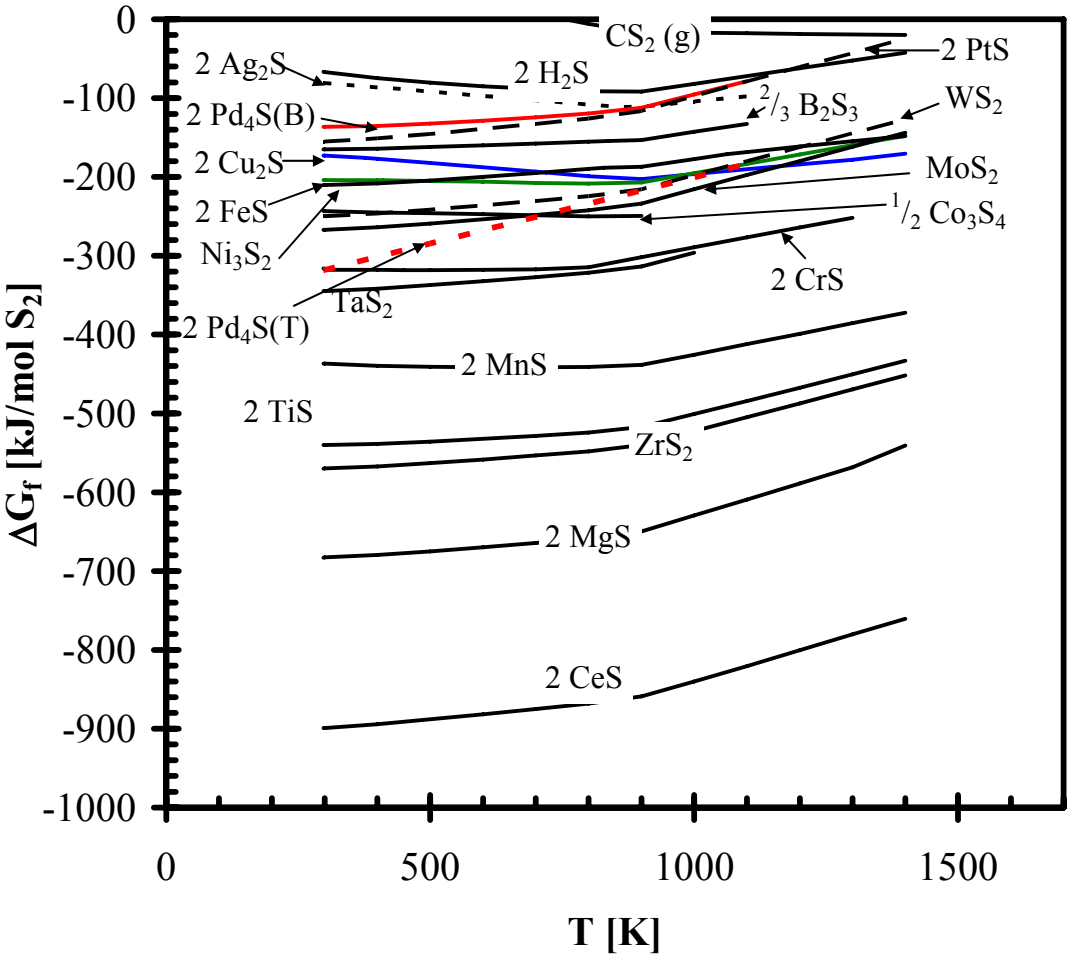

Figure 3. Gibbs free energy of formation for various potential metal sulfides as a function of temperature. Parenthetical reference besides the Pd_4S compositions refers to (B)arin and (T)aylor[140, 141].

The formation of a metal sulfide layer on a membrane surface can have significant impacts on the overall membrane performance (and mechanical life), but the influence relays heavily on the structure/formation of the scale. One method of impact can involve the formation of a scale which only partially covers the membrane surface, such as a porous scale, a scale that spalls, and/or a scale exhibiting cracks resulting from relieving surface stresses (Figure 4). The partially covered membrane surface may still exhibit enough catalytic surfaces to promote the

adsorption and dissociation of hydrogen but would yield a smaller amount of atomic hydrogen due to the reduced surface area.

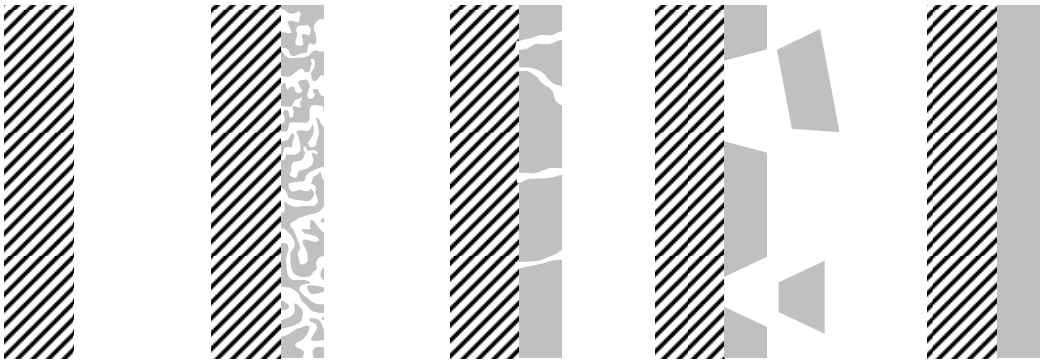

Figure 4. Possible scale phenomenon as it pertains to membrane transport: (a) Cross section of un-sulfided membrane, (b) membrane with porous sulfide scale, (c) membrane with cracked sulfide scale, (d) membrane with spalling sulfide scale, (e) membrane with continuous, dense scale.

A second method may involve the formation of a continuous, dense scale on the membrane surface. The continuous scale, which would entirely cover the catalytic surface of the original membrane, would inhibit the interaction of the gas phase molecular hydrogen with the original catalytic surface of the membrane. However, if the sulfide scale exhibits transport properties for molecular hydrogen (i.e. though grain boundaries) that would permit hydrogen to contact the membrane at the metal/scale interface, hydrogen may have the potential to dissociate and diffuse through the membrane. Additionally, if the sulfide scale exhibits catalytic properties for dissociating hydrogen (into atomic H or a H-proton and electron) and diffusive properties for

atomic H or H^+/e^- the membrane would transport hydrogen to the scale-metal interface followed by diffusion through the metal. The performance of the sulfide scale with respect to hydrogen transport would depend on the diffusion properties of hydrogen through the scale and the scale thickness.

If the ability of the membrane to transport hydrogen as well as the mechanical integrity of the system is dependent on the sulfide scale, it is important to understand the growth rate of the scale, whether the scale formation is at the gas/scale or scale/metal interface, and the sulfide species being formed.

2.0 RESEARCH OBJECTIVES

From the preceding introduction and background it is clear that the influence of H_2S on palladium and palladium alloy membranes may be a significant barrier to the success of integrating a membrane separation device to the gasification process. Therefore, the objective of this work is to evaluate the permeability and possible deactivation mechanism of palladium and palladium copper alloy membranes in the presence of H_2S at temperatures and pressures associated with the proposed positions of the water-gas shift membrane reactor in the gasification process. Although the thicknesses of the membranes used in this study (100 to 1000 microns) are orders of magnitude greater than commercial feasible membranes, the results presented will enable those researchers developing ultra-thin coating strategies to focus on mechanical fabrication while selecting a membrane composition based on the results presented in this study.

Membrane testing will initially be conducted in the presence of neat hydrogen or hydrogen with inert diluents at temperatures associated with various locations within the gasification process, 350 to 900^{o}C. Permeability results will be correlated with factors including temperature, palladium concentration, hydrogen pressure and crystalline structure.

Additionally, permeability testing as well as corrosion studies of various palladium and palladium-copper alloy will be conducted in the presence of hydrogen-sulfide in hydrogen.

Membrane permeability and/or hydrogen flux results will attempt to be correlated with temperature, crystalline structure, palladium concentration and sulfide scale thickness. The results of membrane testing and corrosion analysis will support the identification of the poisoning mechanism often observed for Pd-based membrane studies found in literature.

For the first time, the permeability of the palladium-sulfide layer will be quantified over a wide range of temperatures based on experimental flux measurements and gravimetric measurements of sulfide scale growth rate. The only adjustable parameters used in the model to predict the permeability of Pd_4S was the partial pressure exponent.

2.1 HYPOTHESIS FOR DECREASES IN H_2 FLUX IN THE PRESENCE OF H_2S

2.1.1 Sulfide Scale

The decrease in hydrogen flux associated with the palladium and palladium-copper alloys in the presence of H_2S is hypothesized to be attributed to the formation of a sulfide surface scale which has low transport properties for hydrogen. Thus, the flux through the sulfided membrane will be governed by the flux through the sulfide scale. In this case, the mechanism of hydrogen transport through the sulfide scale will attempt to be evaluated.

2.1.2 Competitive Adsorption

The decrease in hydrogen flux associated with the palladium and palladium-copper alloys in the presence of H_2S is hypothesized to be attributed to competitive adsorption between adsorbed S and H. In cases where no sulfide scale growth is evident on the membrane surface, the decrease in flux is credited to sulfur ad-atoms blocking the necessary surface reaction required to initiate the atomic hydrogen transport mechanism established for dense metal membranes.

3.0 EXPERIMENTAL

In an effort to determine the influence of hydrogen and hydrogen-sulfide on select membrane materials at conditions associated with the gasification process, several test apparatus and analytical instruments were utilized at the U.S. D.O.E. National Energy Technology Laboratory. The materials and equipment used throughout this study will be described as follows:

3.1 MEMBRANE FABRICATION & PREPARATION

The hydrogen permeability and corrosion characteristics of several Pd-Cu alloy membranes of varying thickness and composition were evaluated over a wide range of temperatures and pressures, which are typical of the coal gasification process. Several mounting methods were utilized for permeability testing of the Pd-Cu alloys due to the wide range of conditions studied (350 to 900^{o}C), difficulties with the gaseous environments on fabrication, and varying membrane thicknesses and compositions. The thickness, crystalline phase structure, and alloy composition of the as received foil samples were verified by micrometer, X-Ray Diffraction (XRD), and Inductively Coupled Plasma (ICP) measurements, respectively, prior to use.

3.1.1 Pure Metals

The pure metals of used in this study were of pure palladium and copper. The pure metal foils were purchased from Alfa Aesar®, generally as 100 mm-by-100 mm sheets with thicknesses of either approximately 100 or 1000 microns. The as received pure palladium and copper foils appeared lustrous and had a purity of 99.9% and 99.999% on a metal basis, respectively.

3.1.2 Metal Alloys

The Pd-Cu alloys used in this study were obtained from two sources. The 80wt%Pd-20wt%Cu, 60wt%Pd-40wt%Cu, 53wt%Pd-47wt%Cu and 40wt%Pd-60wt%Cu foils were purchased from ACI Alloys of San Jose, California. The foils were generally 120 mm-by-120 mm sheets with thicknesses of approximately 125 and 1000 microns. The as received foils were generally dull in appearance, probably due to surface oxidation and/or residue from fabrication. Therefore, the foils were polished with 400 to 1200 grit silicon carbide paper, followed by an acetone rinse prior to use in an effort to remove any "gross" contaminants on the surface prior to testing. XRD analysis of the 80wt%Pd-20wt%Cu as-received foil revealed a fcc crystal structure, while the as received 60wt%Pd-40wt%Cu and 53wt%Pd-47wt%Cu alloys exhibited both fcc and bcc crystalline structure. The 60wt%Pd-40wt% and 53wt%Pd-47wt%Cu alloys were annealed in pure hydrogen at ~350^{o}C in an attempt to obtain the desired B2 phase or at 700^{o}C when the fcc phase was preferred. The annealed alloys were once again polished with varying grades of silicon-carbide paper and rinsed with acetone to ensure that any surface contaminants formed during annealing was removed prior to testing. For simplicity, the alloys will use the following nomenclature for the duration of this work and is assumed to represent wt % unless otherwise noted, a alloy composition of 60wt%Pd-40wt%Cu will be represented as 60Pd-Cu.

3.1.3 Mounting Procedure

Three methods were generally used for "mounting" membrane foils for permeation testing. Membranes with thicknesses greater than 500-microns where reduced to the proper

diameter (~19mm) using a shim punch made by ShopAid Inc. The membrane disk, a porous Hastelloy® C-276 alloy (69wt%Ni, 28wt%Mo, 1wt%Cr, <1wt% Co, Mn, Si, C) support and in most cases a diffusion barrier were then TIG welded between two pieces of high-temperature alloy tubing of predetermined length, as illustrated in Figure 5. The diffusion barrier was used to prevent intermetallic diffusion between the membrane foil and the porous Hastelloy C-276 support and consisted of a Whatman® Anodisc 13 (60 microns thick with a pore diameter of 0.1 microns). The high-temperature tubing, 19.1mm O.D. Inconel® Alloy 600 (72wt%Ni, 15wt%Cr, 8wt%Fe, <1wt% Si, Mn, C, Cu, S), acted as "extension tubes" and served to contain pressure and carried feed and permeate gases to and from the membrane. An example of the mounting configuration is illustrated in Figure 5.

Unfortunately, due to the fragility of the thin metal foils and the extreme temperatures encountered during the welding process, the thin membrane samples could not be mounted in the abovementioned manner. Therefore, the "thin" membrane samples, which were generally less than ~150μm, were mounted using two alternative methods. In both methods, the foils were cut to the proper diameter using stainless steel scissors.

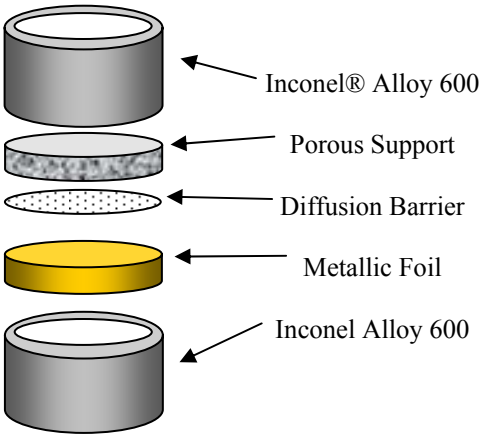

Figure 5. Illustration of the "sandwich weld" mounting method used for membrane foils of ~100 microns.

The first method for mounting the thin foils consisted of a brazing technique developed at NETL. A gold paste consisting of 99.96+wt% gold powder (Alfa Aesar), water and ethanol was placed on the surface of a 316 stainless steel (65wt%Fe, 17wt%Cr, 12wt%Ni, 2.5wt%Mo, 1wt%Si, <1wt%C, P, S) washer, towards the center. The water and ethanol was used to help in the application of the gold to the washer. The metal foil was then pressed onto the gold seat and placed in a ceramic crucible. The membrane and washer was covered with boric acid in an effort to promote braze flow and reduce oxidation during heating. The crucible, membrane and boric acid were then placed in a high temperature box furnace for 5 minutes at 1400 K. The crucible was removed and allowed to cool to ambient temperature. The cooled, brazed membrane was extracted from the crucible and boiled in de-ionized water for a minimum of 8 hours to remove residual boric acid flux. The brazed membrane was then bubble tested for gross leaks by applying ~100 kPa of N_2 across the membrane. The successfully leak tested, brazed membrane was then welded to extension tubes of predetermined lengths, as illustrated in Figure 6.

However, a second method for the permeation testing of thin membrane foils was needed due to the incompatibility observed between the brazed mounting assembly and a flowing sulfur stream at temperatures above 500^{o}C, as will be described in detail in the following sections.

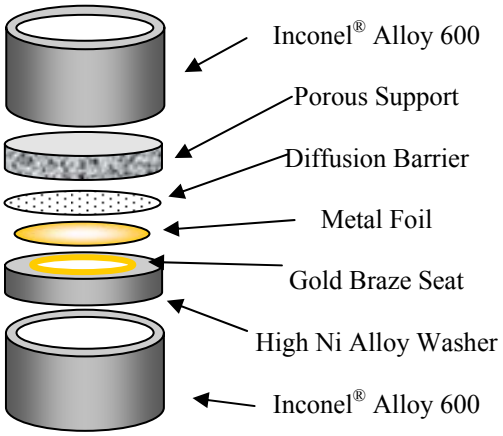

Figure 6. Mounting assembly for membrane foils with thicknesses of ~100-microns using a gold brazing method.

The second method used for mounting thin membrane samples consisted of a "off-the-shelf" 316 stainless steel VCR® fitting purchased from Swagelok®. Similar with the previously described mounting methods, a porous support, a diffusion barrier and the metallic foil were placed in the VCR® fitting, as shown if Figure 7. However, rather welding the assembly, as done the previously described methods, the VCR® fitting allowed the membrane to be sealed by the compression of a "knife-edge" seal onto the membrane. In an effort to reduce the amount of intermetallic diffusion between the VCR® fitting and the membrane as well as the premature failure observed in the brazed assemblies, a platinum washer was often employed to the assembly between the VCR® gland and the membrane foil, as illustrated in Figure 7.

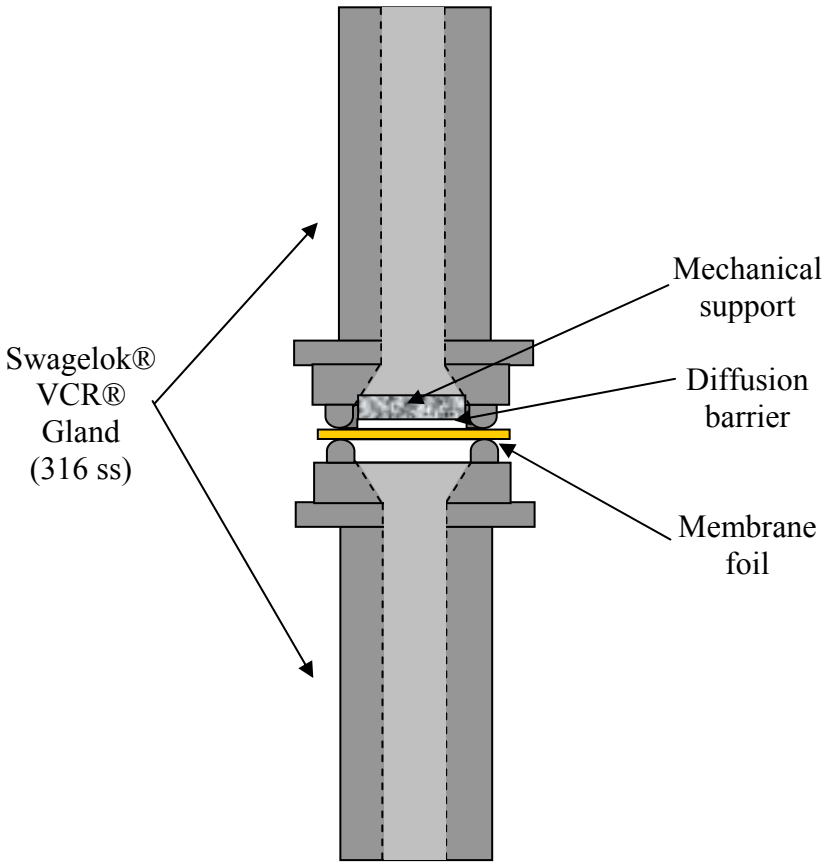

Figure 7. Illustration of the Swagelok® VCR® assembly used for mounting membrane foils with thicknesses of ~100 microns.

3.2 BATCH HYDROGEN MEMBRANE TEST UNIT

A schematic of the Batch Hydrogen Membrane Test (b-HMT) unit used in this study is illustrated in Figure 8. The b-HMT unit allowed for the determination of membrane permeability of potential materials. Permeability tests conducted in the b-HMT generally consisted of short durations (typically <4hrs), which was determined by the volume of hydrogen and the diffusion rate of the membrane material.

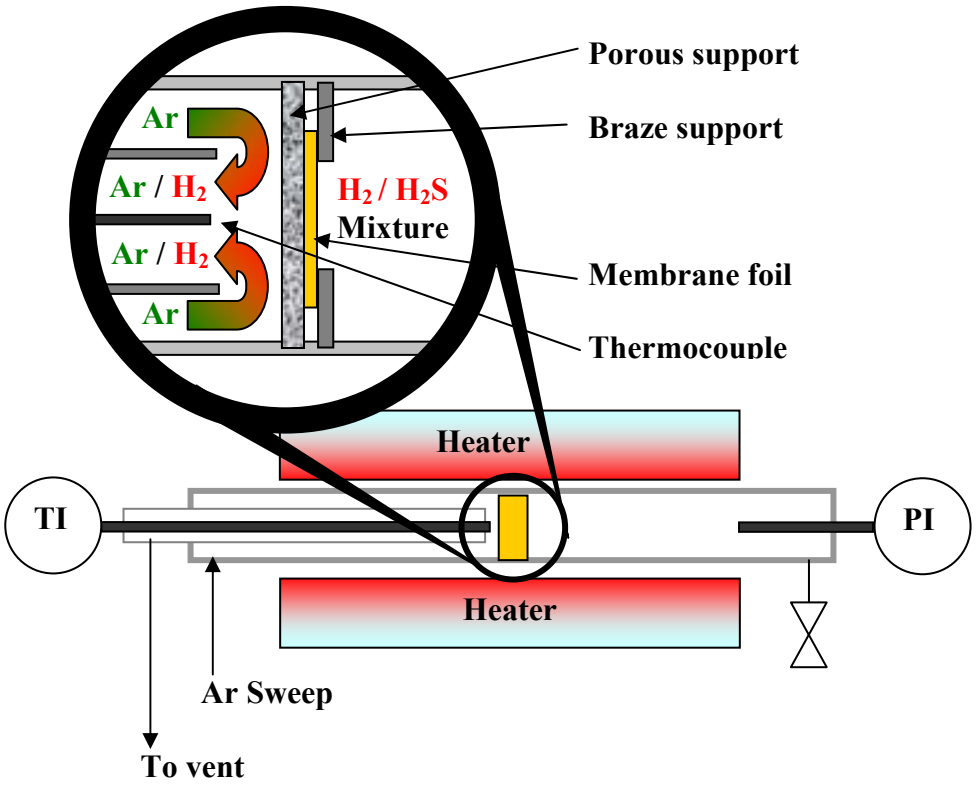

Figure 8. Schematic of the Batch-Hydrogen Membrane Test unit.

The retentate side of the membrane was charged with the test gas of interest (up to 75 psi), either pure hydrogen or a 1000 ppm H_2S/balance H_2 mixture. The operating temperature of

the b-HMT was up to 900°C, in which the heat was supplied by a Lindberg/Blue Mini-Mite™ tube furnace (model TF55035A) while the temperature of the system was monitored with a dual element, Inconel® sheath type-K thermocouple and a Omega HH12 temperature readout. Concentric tubes placed on the permeate side of the brazed mounting assembly allowed a constant argon sweep to evacuate the surface of the membrane of diffusing hydrogen. The system was then heated to the desired temperature and the retentate transient pressure data was used to calculate the rate of hydrogen transport through the membrane.

3.3 STEADY-STATE HYDROGEN MEMBRANE TEST UNIT

In an effort to characterize the performance of select membrane materials in a flowing gas stream and for varying durations, two steady state hydrogen membrane test (ss-HMT) units were utilized. The ss-HMT units were designed, fabricated and operated at NETL. A simplified schematic of the ss-HMT unit is illustrated in Figure 9, in which all three of the mounting methods previously described were tested. The two ss-HMT units utilized in this study were very similar, with the major difference being that one allowed for the investigation of membrane permeability in the presence of hydrogen while the second was used for testing in the presence of hydrogen and hydrogen-sulfide gas mixtures. The membrane assembly incorporated a coaxial tube configuration which allowed the feed and sweep gases to enter through the annulus tubes, contact the membrane, and exit through the inside tube. The membrane unit was heated by a Watlow 120 V (152 mm long, 51 mm inner diameter, 102 mm outer diameter) concentric resistance heater placed around the membrane assembly. The heater was controlled by an Iconic

Genesis® or Wonderware® process control program in conjunction with two coaxially mounted type-K thermocouples with Inconel® sheaths, which were placed approximately 6 mm from each of the membrane surfaces. The membrane unit and resistance heater were insulated with ceramic fiber insulation and housed inside a 7.5 liter stainless steel containment vessel that was continuously purged with nitrogen. The containment vessel was used to ensure that any hydrogen escaping from the membrane apparatus would be diluted, cooled, and vented.

The membrane unit feed gases, pre-mixed and cylinder fed, consisted of UHP He, UHP Ar, 10%He-H_2 and/or a 1000 ppm H_2S-10%He-H_2, and were purchased from Butler Gas. Helium was a common component in the gas mixtures because it was used as an internal check for membrane leaks. Since helium does not have the ability diffuse through dense palladium and its alloys, its detection in the permeate stream was indicative of a leak in the membrane or membrane-to-holder seal. The feed and sweep gas flow rates were controlled by Brooks Series 5890i mass flow controllers, while the process feed and sweep pressures were regulated by pneumatic, stainless steel Badger Research control-valves. In some cases, the sweep gas was maintained at atmospheric pressure, while in other cases, the sweep gas was pressurized to minimize the pressure drop across the membrane ($\Delta P_{minimum}$>20psi) in an effort to mitigate mechanical failures. The non-permeated hydrogen feed stream and the hydrogen-containing permeate stream was carried to a Hewlett Packard 5890 Series II gas chromatograph equipped with dual 3.2 mm O.D., 3 m long, zeolite packed columns and dual thermal conductivity detectors for quantification.

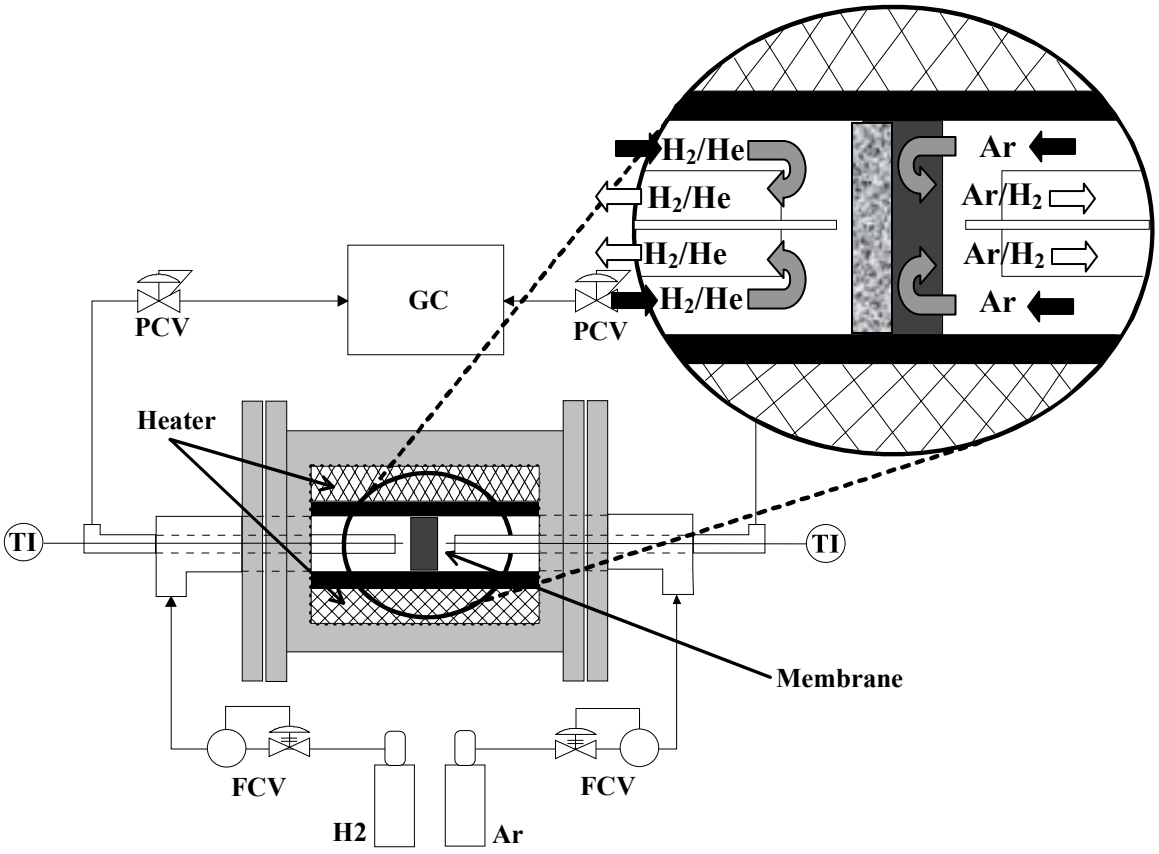

Figure 9. Schematic of the steady-state hydrogen membrane test unit.

3.4 SAMPLE CONDITIONING UNIT

Sulfide scale layers on the membrane surface can possibly influence performance, as was demonstrated in previous sections of this work. Therefore, a sample conditioning unit was designed and utilized in this study to investigate the scale growth rate of sulfide scales on palladium and palladium-copper alloys. The conditioning unit, illustrated in Figure 10, utilized cylinder fed gases of either UHP He or a mixture of 89.9%H_2-10%He-1000ppmH_2S. The gas flows to the unit were controlled with a Variable Control Rotameter equipped with a glass float

and a high-precision control valve. The flows were directed into a specially designed quartz reaction chamber (fabricated at the University of Pittsburgh's Glass Shop), where all of the surface of the metal foils and platinum catalyst were exposed to the test gases, as illustrated in Figure 11. The platinum catalyst was used to ensure an equilibrium mixture of the feed gas was obtained prior to contact with Pd-Cu alloy coupons. The heat of the reaction chamber was maintained with a Lindberg/Blue Mini-Mite™ tube furnace (model TF55035A). The temperature of the system was monitored with an Omega HH12 temperature readout in conjunction with an Inconel® sheathed type-K thermocouple. In an effort to minimize the interaction with the test gases and the thermocouple material, a quartz liner was employed over the thermocouple.

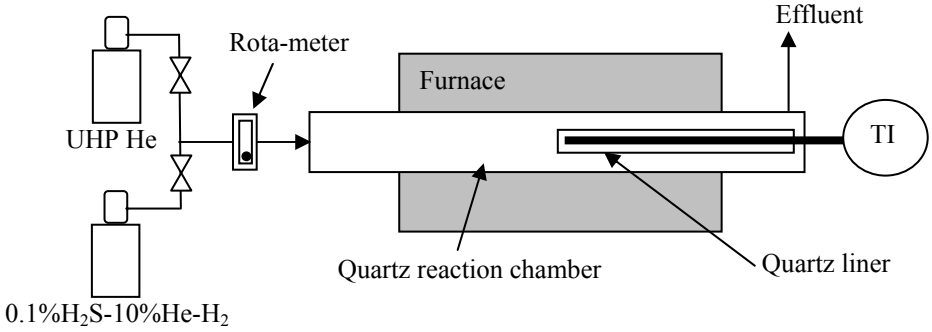

Figure 10. Illustration of the Sample Conditioning Unit utilized in this study.

The metal samples used for condition testing were obtained from the same ~100 micron thick foils used for membrane testing. The metal alloys were scissor cut to the proper dimensions (approximately 10 mm- by-10 mm square coupons), polished with silicon carbide paper (600 to 1200 grit) followed by an acetone rinse. The coupons were placed in the center of the quartz reaction chamber with the thermocouple positioned roughly 5 mm downstream of the last sample. Prior to inserting the quartz reaction chamber into the preheated furnace, the reaction

chamber was purged with UHP He at ~100 ml/min for 15 minutes in an effort to remove any residual oxygen present, followed by the introduction of the 1000 ppm H_2S-10% He- H_2 gas mixture at a flow of ~10 ml/min. Once the furnace was pre-heated to the desired temperature and the H_2S gas mixture was introduced, the quartz reaction chamber and the metal coupons were positioned in the center of the heated zone. Immediately following the placement of the reaction chamber into the furnace, the flow of the H_2S gas mixture raised to ~100 ml/min. Upon completion of the desired exposure time (typically ranging from 30 to 120 minutes), the H_2S flow was reduced to ~10 ml/min and the reaction chamber was immediately removed from the furnace. After the samples were cooled to room temperature, the coupons were removed from the quartz reaction chamber and weighed. This procedure was repeated several times until a total exposure time of 120 hours was achieved. The insertion of the quartz reaction chamber into the pre-heated furnace as well as its removal of the chamber upon test completion facilitated a maximum heating and cooling rate in attempt to preserve coupons structure. The typical time required for heating and cooling was ~10 minutes each.

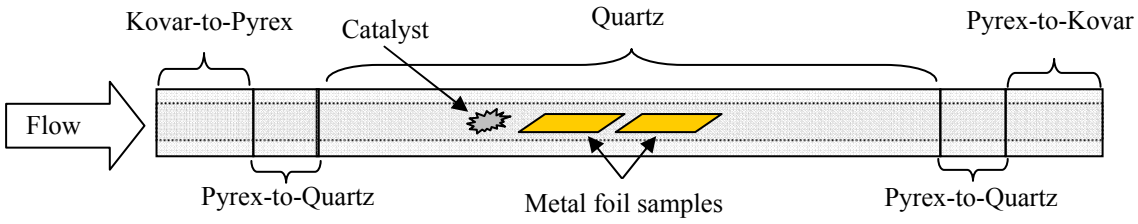

Figure 11. Schematic of the reaction chamber used in the conditioning unit.

3.5 ANALYTICAL INSTRUMENTATION

To determine the influence of H_2S on the performance of palladium-based membranes, several pieces of analytical equipment were utilized.

3.5.1 Scanning Electron Microscopy (SEM)

In an effort to determine the influence of test conditions on surface topology and elemental identification, an Aspex Personal SEM 2000 was utilized. The SEM was equipped with a Secondary Electron Detector (SED) for topological characterization, a Quadrant Backscatter Electron Detector (QuadBSED) for compositional and topological insight and an Energy Dispersive Spectrometer (EDS) for quantitative elemental analysis. The manufacturer's specification for magnification for this SEM was approximately 100,000x although only 10,000x was realistic due to infrastructure vibrations.

3.5.2 X-Ray Diffraction (XRD)

A PANanalytical XRD was utilized in this study to determine crystalline information as well as surface compounds present of pre- and post-tested membrane materials. The PANalytical X'Pert Pro MPD powder diffractometer having a theta-theta configuration, a Cu X-ray source operated at 45 kV and 40 mA and an X'Celerator detector equipped with a monochromator.

3.5.3 Inductively Coupled Plasma-Optical Emission Spectroscopy (ICP-OES)

The metal concentrations in the alloys of interest were verified prior to testing using a Perkin Elmer Optima 3000 ICP-OES. The alloys were digested in hot aqua regia, diluted and analyzed for Cu, Pd, and selected trace elements. The Optima 3000 uses a Glass Expansion Sea Spray nebulizer and glass cyclonic spray chamber in the sample introduction system. An yttrium solution was used as an on-line internal standard to adjust for any variations in sample introduction due to sample fluctuations in solids loading or viscosity.

4.0 RESULTS & DISCUSSION

The palladium-copper system has been of great interest in membrane research in recent years due to its reported high flux and the stability the alloy has shown in the presence of low levels of hydrogen-sulfide[84, 110], as demonstrated in Section 1.0 of this work. This study will evaluate the hydrogen permeability of several palladium and palladium-copper alloy membranes over a wide range of temperatures and pressures (up to 900^{o}C and 400psig) using flowing and static gas systems in the presence of either a hydrogen/helium or hydrogen/helium/hydrogen-sulfide gas mixture. The metals selected for permeability evaluation include pure palladium and copper as well as the 80Pd-Cu, 60Pd-Cu and the 53Pd-Cu alloy. Figure 12represents the relationship between alloy composition, crystalline phase and temperature of the selected alloys. However, it should be noted that Figure 12 gives representation of the Pd-Cu system in the absence of hydrogen, which has been documented to change transition lines between phases[123].

The 60Pd-Cu alloy was selected due to it being the most widely investigated Pd-Cu alloy as well as reports of it yielding the highest performance values of the Pd-Cu system[84, 107, 110, 112, 113, 123, 143-147]. According to the phase diagram, the 60Pd-Cu alloy exhibits a mixed B2-fcc phase at temperatures below ~540^{o}C, while the high-temperature (T>~540^{o}C) phase is fcc (the B2 crystalline phase is often referred to in literature by its ordered bcc phase). The 53Pd-Cu alloy was chosen due to its intersection of the apex of the phase transition which undergoes a transformation from the B2 to fcc phase at ~600^{o}C, without the presence of a mixed crystalline

phase. Lastly, the 80Pd-Cu alloy was chosen due to its fcc crystalline structure throughout the entire temperature range of interest and its intermediate composition between pure palladium and the 60Pd-Cu alloy Details of the as received alloys evaluated in this study are listed in Table 2.

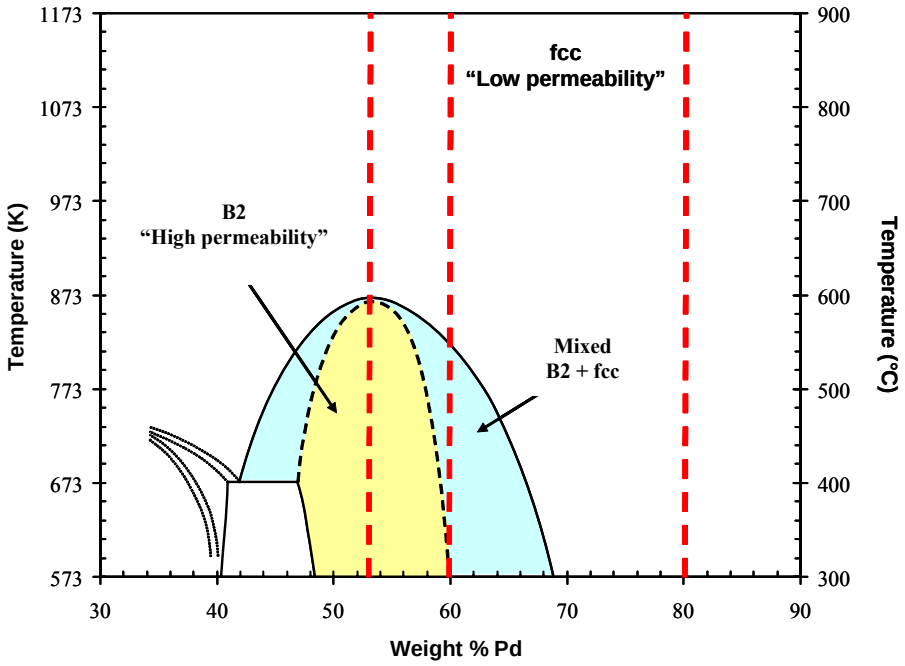

Figure 12. Phase diagram of the palladium-copper system where the vertical dashed lines represent the Pd-Cu alloys of interest in this study[71].

Table 2. As-received membrane foil thickness, composition and crystalline structure as determined by micrometer, ICP, and XRD measurements, respectively.

Alloy	Supplier	Foil Thickness (μm)	Wt% Pd (metal basis)	Wt% Cu (metal basis)	Crystalline Structure
Pd	Alfa Aesar	102 ± 0	99.5 ±2.06	0	fcc
		993 ± 4	99 ± 1.50	0	fcc
80Pd-Cu	ACI Alloys	124 ± 4	80.65 ± 1.31	19.60 ± 0.33	fcc
		977 ± 28	80.15 ± 0.77	19.9 ± 0.24	fcc
60Pd-Cu	ACI Alloys	143 ± 5	59.97 ± 3.28	40.03 ± 0.43	fcc
		932 ± 15	60.8 ± 1.88	40.85 ± 1.33	fcc
53Pd-Cu	ACI Alloys	171 ± 8	53.8 ± 6.66	46.7 ± 0.58	fcc
		1002 ± 23	52.4 ± 2.84	46.8 ± 2.60	fcc
Cu	Alfa Aesar	100 ± 2	0.02 ± 0.001	100.5 ± 2.66	fcc
		1031 ± 1	0.02 ± 0.0003	96.6 ± 0.422	fcc

4.1 STEADY STATE PERFORMANCE IN THE PRESENCE OF H_2

4.1.1 Pure Pd and Cu

Permeability testing conducted in this study initially focused on pure palladium and copper foils. Flux analysis of these pure metals allowed for the development of a testing procedure, which included the influence of various process variables on performance, unit operation and data collection. Initial flux testing of the pure palladium and copper foils also validated the mechanical assembly used for the membranes. Moreover, the data generated with the pure palladium foils gave a basis for comparison with literature results along with a comparative measure for future membrane materials conducted in this study. The flux results of three ~1000 μm palladium tested at temperatures and pressures ranging from 350 to 900^{o}C and atmospheric to 2.86 MPa, respectively, are illustrated in Figure 13 as a function of the expected

transport driving force, $P_{H2,Retentate}^{0.5}$ - $P_{H2,Permeate}^{0.5}$. The three pure palladium membranes had designation numbers of 6-59, 6-109 and 6-120, which refers to the notebook and page number detailing specifics about fabrication, mounting and testing.

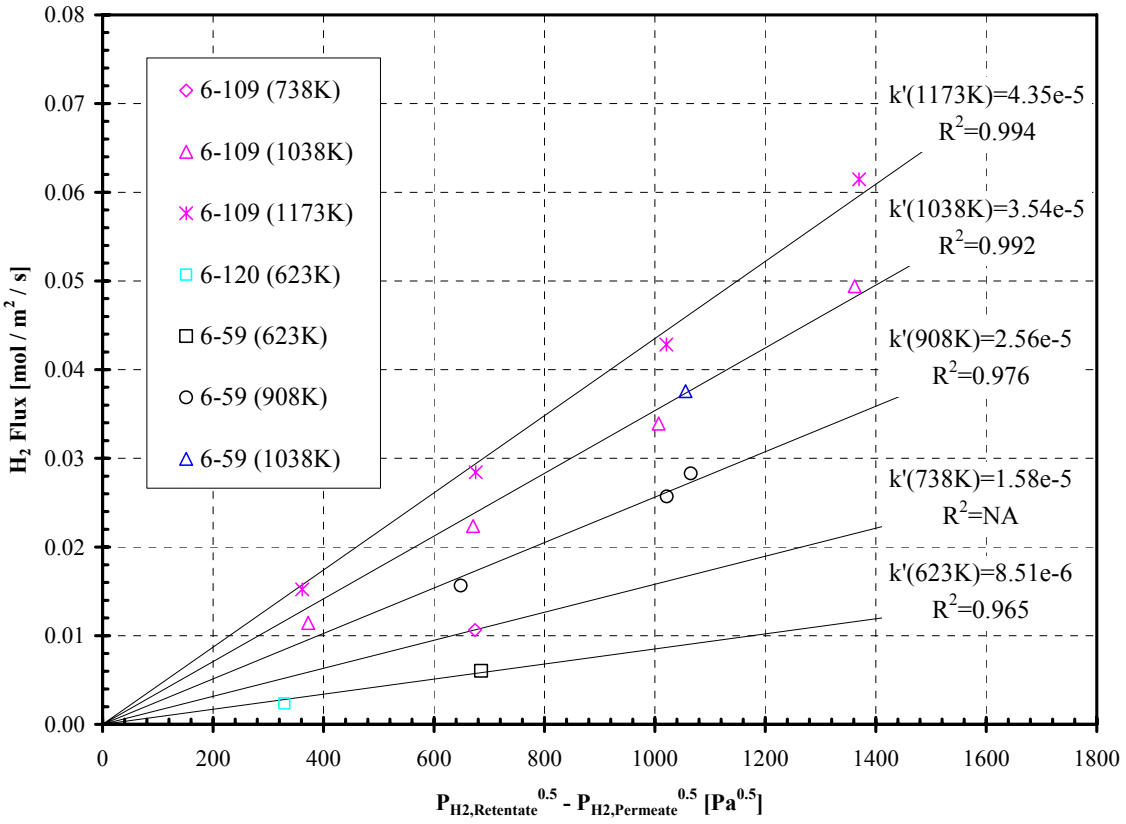

Figure 13. Steady state flux results of the ~1000 μm pure palladium membranes tested in the presence of a H_2/He mixture. The permeance values presented in the plot were calculated from the slope of the data forced through the origin and have units of [mol / m^2 / s / $Pa^{0.5}$].

The partial pressure exponent of 0.5 is indicative of a rapid surface reaction (adsorption and dissociation), thus implying that the rate limiting step in the transport mechanism being the transport of atomic hydrogen through metal. The three 1-mm thick membrane foils were assembled as illustrated in Figure 5, without the use of a mechanical support or diffusion barrier. The isotherms presented in Figure 13 yielded R^2 values ranging from 0.965 to 0.994, with an

average value of 0.982, which supports the assumed transport mechanism. These isotherms can be further evaluated to calculate the permeability values by application of the Richardson's Equation, Equation 4-1. Appendix 6.2 illustrates a detailed derivation of Equation 4-1.

$$N_{H2} = \frac{k}{X_M}\left(P_{H2,Retentate}^{0.5} - P_{H2,Permeate}^{0.5}\right) = k'\left(P_{H2,Retentate}^{0.5} - P_{H2,Permeate}^{0.5}\right) \qquad (4\text{-}1)$$

Where $\mathbf{N_{H2}}$ ***[mol/m^2/s]*** is the hydrogen flux through the membrane, **k** ***[mol/m/s/Pa$^{0.5}$]*** is the permeability, $\mathbf{X_M}$ ***[m]*** is the membrane thickness, **k´** ***[mol/m^2/s/Pa$^{0.5}$]*** is the permeance (or permeability divided by thickness) and $\mathbf{P_{H2,Retentate}}$ ***[Pa]*** and $\mathbf{P_{H2,Permeate}}$ ***[Pa]*** represents the hydrogen pressure of the retentate and permeate streams, respectively. The partial pressure values used for the retentate and permeate were obtained from the average hydrogen partial pressure of the feed and effluent (if the total pressure of the retentate stream is 100 MPa, but the feed composition consisted of 90%H_2 and the effluent consisted of 80%H_2, the driving force for the retentate was presumed to be 85 MPa).

The isothermal permeability values can also be represented as a function of temperature (Figure 14), with the permeability values fit to an Arrhenius-type expression, Equation 4-2. Where $\mathbf{k_o}$ ***[mol/m/s/Pa$^{0.5}$]*** represents the pre-exponential factor, $\mathbf{E_P}$ ***[J/mol]*** is the activation energy of permeation and **R** ***[J/mol/K]*** and **T** ***[K]*** are the universal gas constant and absolute temperature, respectively.

$$k = k_o * \exp\left(\frac{-E_P}{RT}\right) \qquad (4\text{-}2)$$

Figure 14 illustrates the results for 1000 μm Pd data displayed in Figure 13 along with the results obtained for four 100 μm thick samples, where the permeability values were calculated in a similar manner to the 1000 μm samples. Two of the four 100 μm membrane samples were fabricated as illustrated in Figure 6 (with the use of an unpassivated porous support on each side of the membrane) while the other two samples were mounted as illustrated in Figure 7 (one in the presence of and one in the absence of a passivated support). The pre-exponential constants of the 100 and 1000 μm palladium samples were 1.41e-7 and 2.76e-7 mol/m/s/$Pa^{0.5}$, respectively, while the associated activation energy values were 14,045 and 17,893 J/mol. The pre-exponential constant and activation energy values attained for the two pure copper membranes tested were 1.42e-7 mol/m/s/$Pa^{0.5}$and 63,690 J/mol, respectively.

The palladium data collected in this study along with selected literature values illustrated in Figure 14 are in relatively good agreement. The agreement in palladium data validates the test apparatus and the testing protocol that will be used for further steady-state flux testing. Additionally, the aforementioned methodology, nomenclature and equations (4-1 and 4-2) will be utilized for determining the performance of the membranes of interest under "steady-state" conditions for the duration of the work unless otherwise noted.

Lastly, the best-fit Arrhenius expression fit through both the 100 and 1000 micron samples will be used for comparative purposes throughout the duration of this study. The "best-fit" pre-exponential constant and activation energy of permeation for the 100 and 1000 μm Pd data is given in Equation 4-3, and is illustrated graphically in Figure 14 by the bold, solid line.

$$k_{Pd}\left(\frac{mol}{m\ s\ Pa^{0.5}}\right) = 2.09e^{-7}\exp\left[\frac{16{,}260\left(\frac{J}{mol}\right)}{R\left(\frac{J}{mol\ K}\right)T(K)}\right] \qquad (4\text{-}3)$$

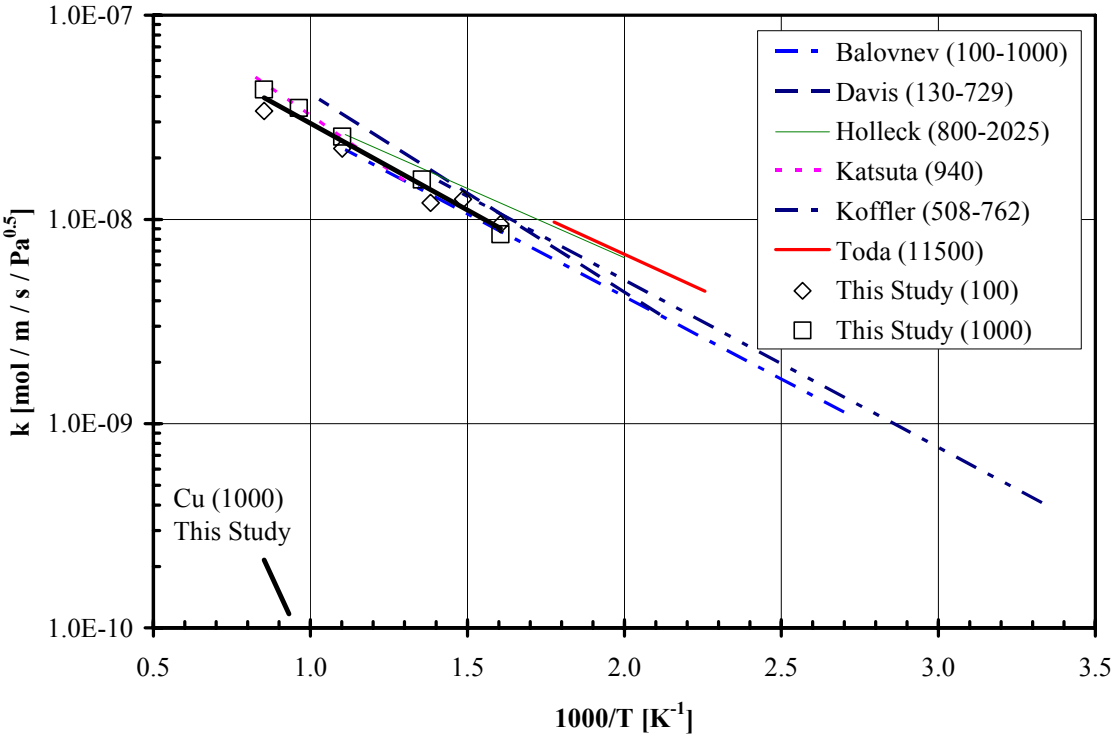

Figure 14. Comparison of the permeability values (k) of palladium and copper obtained in this study in the presence of a H_2/He mixture and compared to selected literature values. Parenthetical values in the legend refer to the thickness of the membrane data presented in microns[13-18].

4.1.2 80Pd-Cu

Five 80Pd-Cu membranes were investigated in the presence of a hydrogen-helium gas mixture. The first sample (6-187) had a thickness of ~1000 μm and utilized the mounting

technique illustrated in Figure 5. The next four samples evaluated (6-104, 6-107, 6-187 and 8-39) had a thicknesses of ~100 μm. Samples 6-104, 6-107, and 6-187 were mounted for testing using the method illustrated in Figure 6, although a diffusion barrier was only utilized for sample 6-187. The last sample evaluated utilized the mounting method illustrated in Figure 7, with the use of a diffusion barrier between the metallic support and test foil.

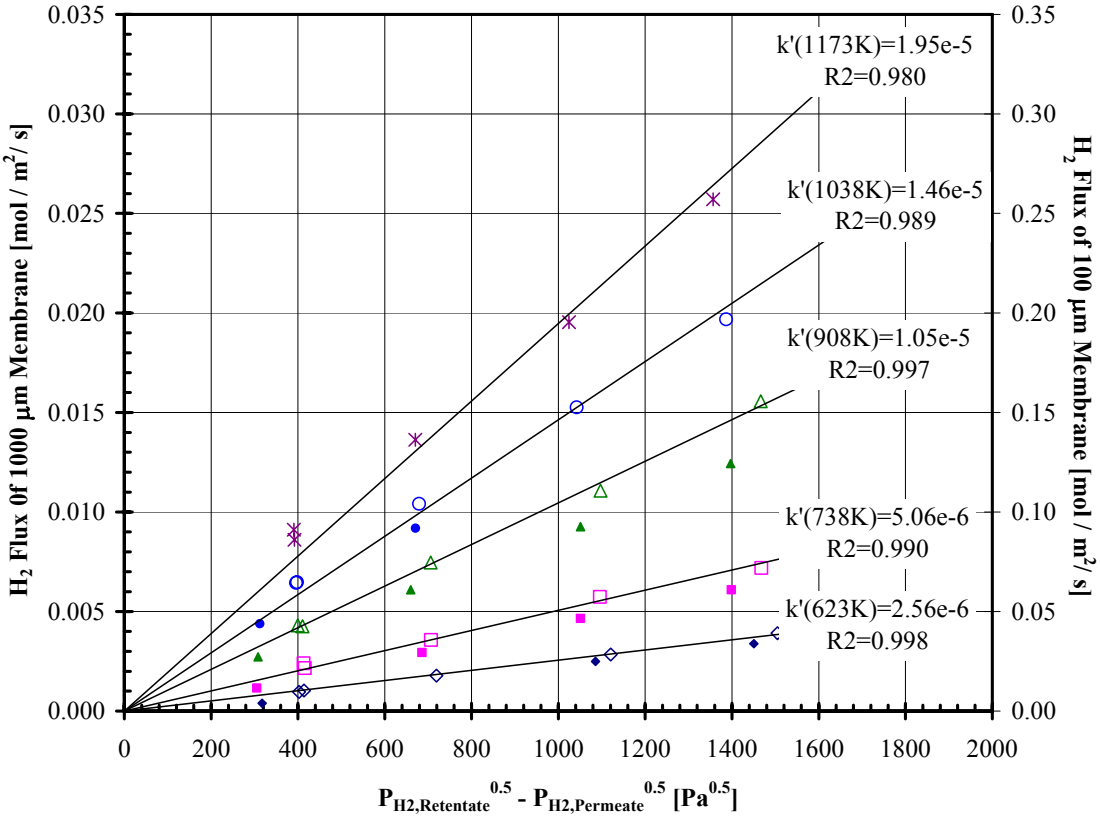

Figure 15. Flux dependence of 100 (solid shapes) and 1000 μm(hollow shapes), 80Pd-Cu membrane as a function of the assumed driving force. The permeance values presented in the plot were calculated from the slope of the data forced through the origin for the 1000 μm samples and have units of [mol / m^2 / s / $Pa^{0.5}$].

Figure 15 illustrates the relationship obtained for the hydrogen flux through two 80Pd-Cu membranes (6-104 and 6-187) as a function of the assumed driving force, $\Delta P_{H2}^{0.5}$. Relatively high R^2 (>0.980) values observed in the isotherms in Figure 15 validates the assumed rate-limiting-step to be atomic diffusion through the bulk of the foil for both the 100 and 1000 μm samples. As expected from equation 4-1, the relationship between the flux of the 100 and 1000 μm samples roughly differs by a factor of ten, as illustrated in Figure 15. Furthermore, the permeability values obtained for the five 80Pd-Cu membrane samples are presented in Figure 16 as a function of temperature. Additionally, the permeability values obtained for the 80Pd-Cu samples (6-187 and 8-39) tested under isobaric (~0.62 MPa) conditions are illustrated in Figure 16.

The pre-exponential constant and activation energy of permeation for the 100 and 1000 μm foils were approximately $2.53e^{-7}$ and $1.98e^{-7}$ mol / m / s / $Pa^{0.5}$, and 23,630 and 22,527 J / mol, respectively. The performance of the 80Pd-Cu membrane was approximately 75% lower than the permeability of palladium at 623 K as reported by Koffler. However at a temperature of 1173 K, only a ~50% reduction was observed.

Lastly, the "best-fit" pre-exponential constant and activation energy of permeation for both the 100 and 1000 μm 80Pd-Cu are give by Equation 4-4 and illustrated in Figure 16, by the bold dashed line.

$$k_{Pd_{80}Cu}\left(\frac{mol}{m\ s\ Pa^{0.5}}\right) = 2.34e^{-7}\exp\left[\frac{23{,}166\left(\frac{J}{mol}\right)}{R\left(\frac{J}{mol\ K}\right)T(K)}\right] \qquad (4\text{-}4)$$

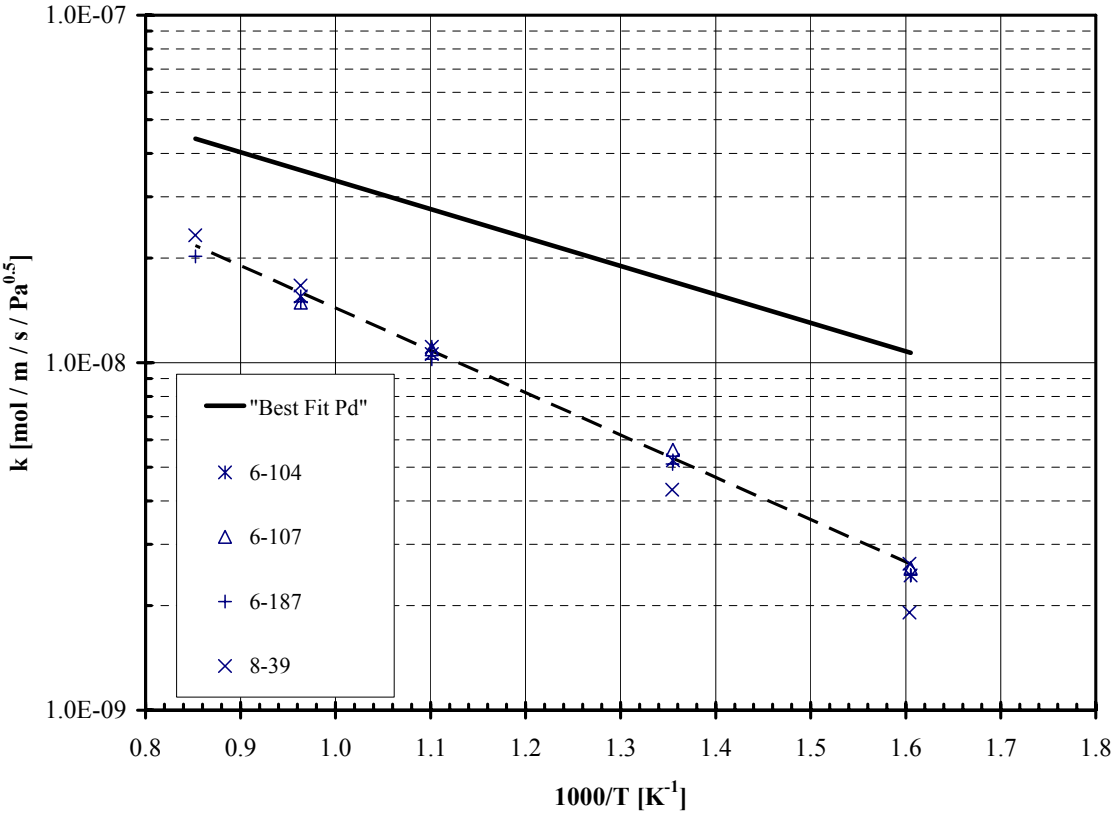

Figure 16. Permeability values obtained for various 80Pd-Cu membranes tested in the presence of flowing H_2.

4.1.3 60Pd-Cu

The performance of the 60Pd-Cu alloy was more complex as compared to the two previous membrane compositions (Pd and 80Pd-Cu) which exhibited crystalline homogeneity through the conditions studied. The complexity with the 60Pd-Cu alloy arises due to the possibility of two phases being present (B2 and fcc) as evident in Figure 12. Increasing the complexity of the alloy further is that the transitions between B2 and fcc phase has been documented to be dependent on temperature and hydrogen concentration[123].

Four 60Pd-Cu membranes were tested in the presence of a flowing H_2-He gas mixture. Samples 6-92 and 6-93 were approximately 100 μm thick and were mounted for testing as illustrated in Figure 6, without the use of a diffusion barrier between the metallic support and the test foil. The second two samples tested (8-54, 8-64) were approximately 1000 μm thick and were mounted for testing as illustrated in Figure 5, with a diffusion barrier. Due to the high temperatures associated with welding in both of the mounting procedures, the membrane foils were installed in the test units with an fcc crystalline structure and was independent of the crystalline structure of the foil prior to welding. Therefore, in attempt to convert the mounted membrane to the desired B2 crystalline structure, initial testing was conducted at 350 or 450oC in the presence of hydrogen. Once no changes in hydrogen flux were observed, the membrane was assumed to exhibit a steady-state crystalline phase, which required exposures as long as 200 hours.

Figure 17 illustrates the relationship observed for the hydrogen flux versus the difference of the square root of the partial pressure for the 100 μm 6-93 membrane sample. The high R^2

value (>0.978) observed for the 6-93 validates the assumption the transport of hydrogen through the 100 μm, 60Pd-Cu membrane is limited by the diffusion of hydrogen though the crystalline lattice.

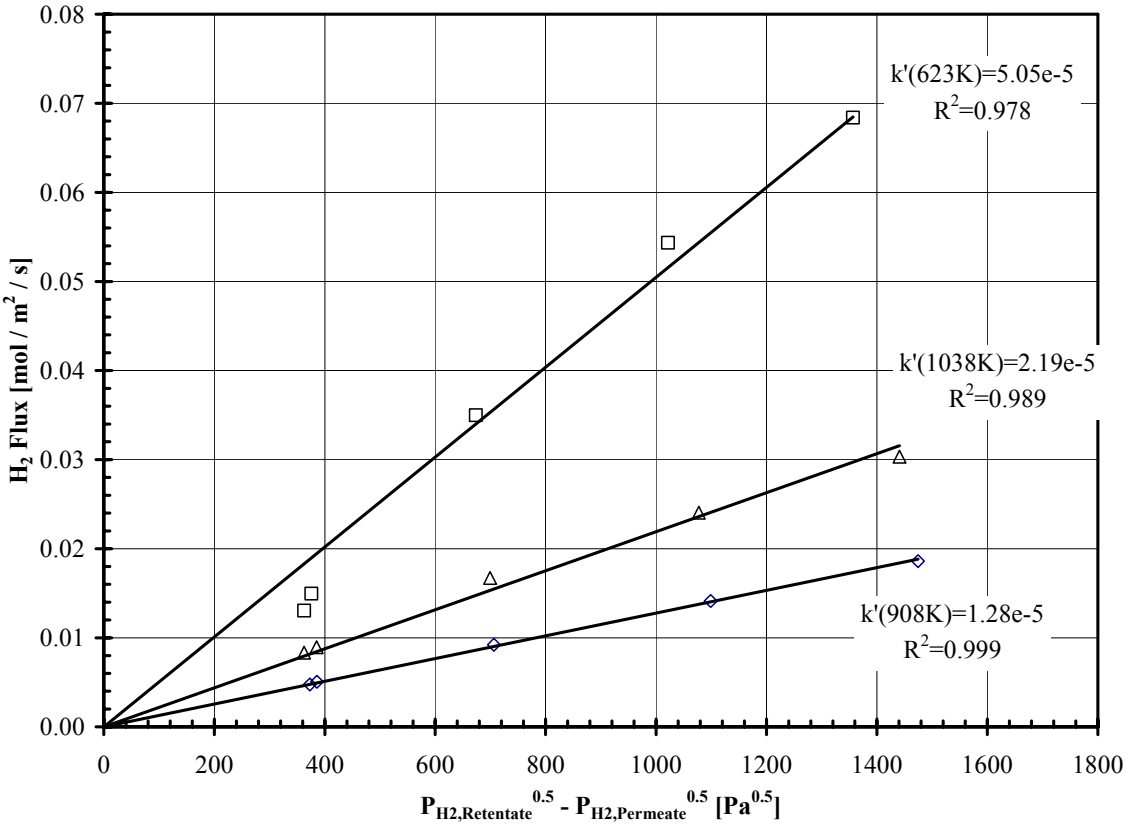

Figure 17. Flux dependence of 100 μm, 60Pd-Cu membrane (sample 6-93) as a function of the assumed driving force. The permeance values presented in the plot were calculated from the slope of the data forced through the origin and have units of [mol / m^2 / s / $Pa^{0.5}$].

The hydrogen flux of the four samples is illustrated in Figure 18 as a function of temperature. At temperatures below approximately 475°C, the permeability values increase with increasing temperature and corresponded to a B2 structure which was observed in a parallel XRD study. The parallel XRD study consisted of "conditioning" the desired 60Pd-Cu alloy

samples in the presence of hydrogen, quenching the samples (cooling on the order of <10 min) and analyzing the metal sample for crystalline phase as a function of temperature.

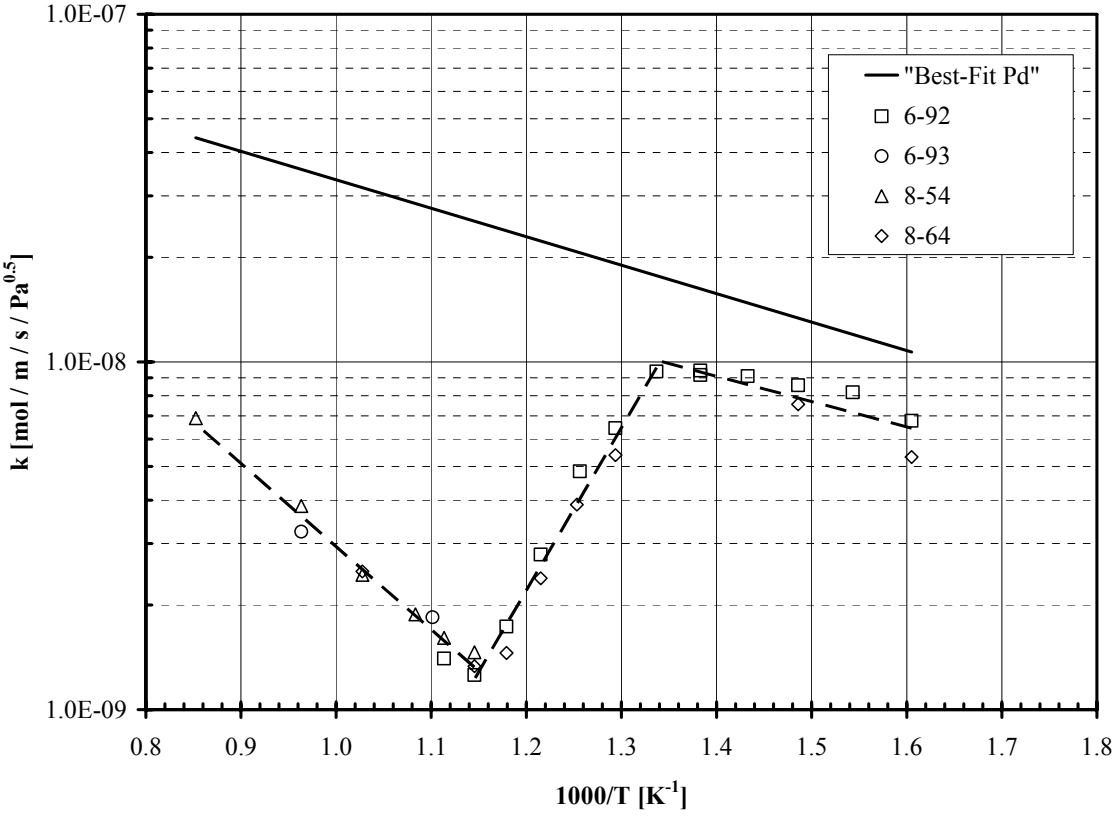

Figure 18. Permeability values of the 100 and 1000 μm 60Pd-Cu membrane samples as a function of temperature. The dashed line represents the "best-fit" relation for the 60Pd-Cu membranes tested in this study.

At temperatures ranging from ~475 to 600°C, the observed permeability values decreased with increasing temperature. The 475 to 600°C temperature range corresponding to a mixed crystalline phase where both the B2 and fcc phases are present. At temperatures above 600°C the permeability once again increases with increasing temperatures, corresponding to the expected fcc crystalline phase. The observed decreases in permeability associated with the mixed

crystalline phase is most likely corresponds to the ratio of the "high permeability" B2 phase and the "low permeability" fcc phase.

Lastly, the "best-fit" pre-exponential constants and activation energy of permeation for the 100 and 1000 μm 60Pd-Cu are given in Table 3 as a function of the apparent crystalline phase and are illustrated in Figure 18 as a function of temperature.

Table 3. Arrhenius values for the 60Pd-Cu membrane as a function of temperature.

Temperature Range [K]	Pre-exponential Constant k_o [mol / m / s / $Pa^{0.5}$]	Activation Energy E_P [J / mol]
623 to ~748	$9.53e^{-8}$	13,947
~748 to ~873	$5.13e^{-15}$	-89,573
~873 to 1173	$7.19e^{-7}$	45,704

The values presented in this table are the "best-fit" values for the 100 and 1000 μm thick samples presented in Figure 18.

4.1.4 53Pd-Cu

The 53Pd-Cu alloy was the last composition of the Pd-Cu system of interest in this study, in which testing was conducted on a total of seven samples in the presence of a hydrogen-helium gas mixture. Of the seven 53Pd-Cu membrane samples tested, four had a thickness of approximately 1000 μm while three had thicknesses of ~100 μm. The 1000 μm samples (8-11, 8-22, 8-28, and 8-129) were all mounted as illustrated in Figure 5 with the use of a diffusion barrier between the porous support and the membrane foil. The three 100 μm samples (6-100, 6-101, and 6-102) were mounted for testing as illustrated in Figure 6, however none of the samples employed a diffusion barrier.

Figure 19 depicts the relationship between the hydrogen flux through the 100 μm, 6-100 membrane sample as a function of the assumed driving force. The relatively high R^2 values (>0.96) validates the transport assumption that the surface reaction (adsorption/dissociation) is much faster than the diffusion of hydrogen through the bulk of the metal for the 100 μm 53Pd-Cu membrane.

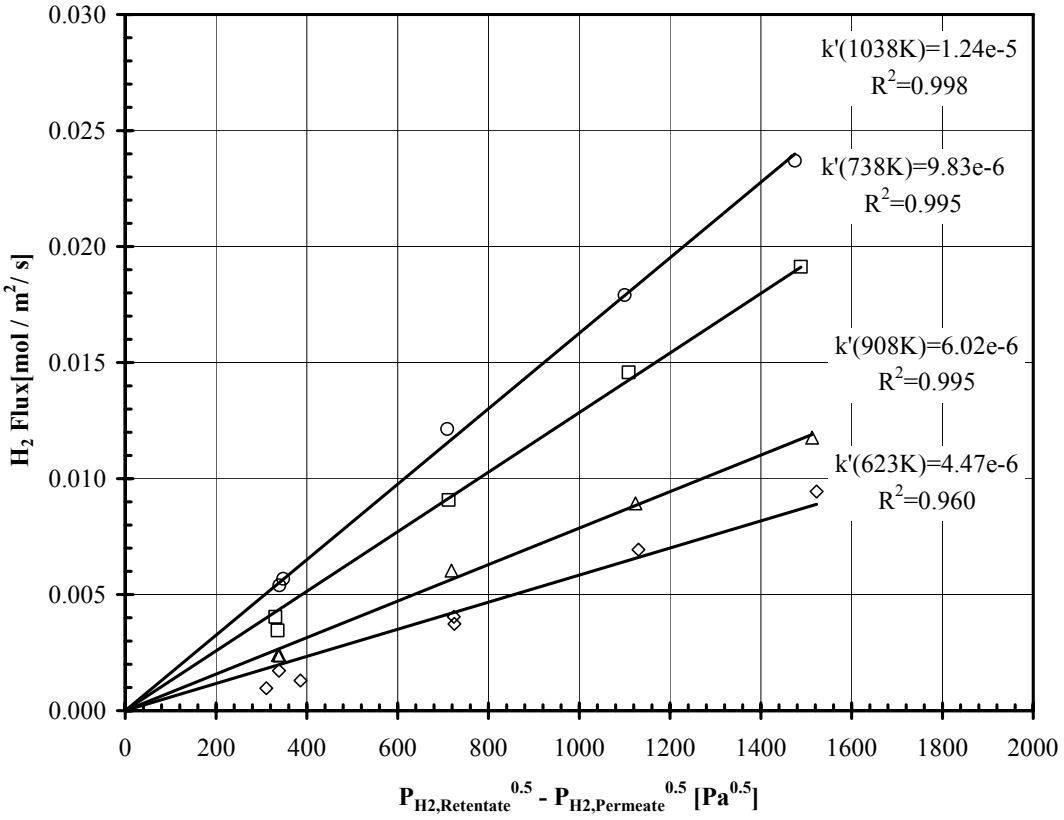

Figure 19. Flux dependence of 100 μm, 53Pd-Cu membrane (sample 6-100) as a function of the assumed driving force. The permeance values presented in the plot were calculated from the slope of the data forced through the origin and have units of [mol / m^2 / s / $Pa^{0.5}$].

Furthermore, the hydrogen flux of the seven 53Pd-Cu membrane samples is illustrated in Figure 20 as a function of temperature. As expected based on the phase diagram (and previous

testing with the 60Pd-Cu alloy), at temperatures associated with a B2 crystalline phase, the hydrogen permeability increases with increasing temperature. At the phase transformation temperature for the 53Pd-Cu alloy (~600^{o}C, Figure 12), the permeability decreases approximately by a factor of 3, followed by an increasing permeability trend with increasing temperature for the fcc phase of the 53Pd-Cu alloy. The permeability values obtained for the 53Pd-Cu alloy was approximately 8 to 11 times less than the pure palladium sample over the entire temperature range of study.

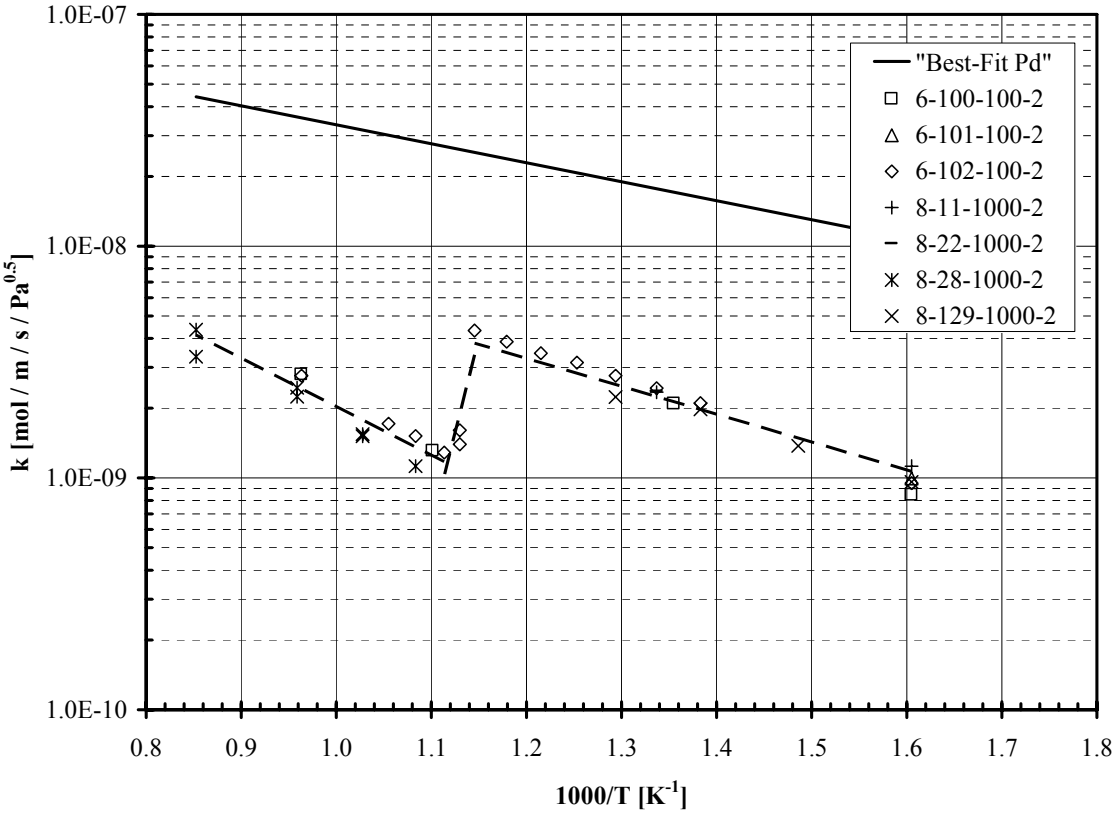

Figure 20. Permeability values of the 100 and 1000 μm 53Pd-Cu membrane samples as a function of temperature. The dashed line represents the "best-fit" relation for the 60Pd-Cu membranes tested in this study.

Lastly, the "best-fit" pre-exponential constants and activation energy of permeation for the 100 and 1000 μm 53Pd-Cu are given in Table 4 as a function of apparent crystalline phase and are illustrated in Figure 20 as a function of temperature by the bold dashed line.

Table 4. Arrhenius values for the 53Pd-Cu membrane as a function of temperature.

Temperature Range [K]	Pre-exponential Constant k_o [mol / m / s / $Pa^{0.5}$]	Activation Energy E_P [J / mol]
623 to ~873	$9.11e^{-8}$	23,027
~873 to ~898	$6.18e^{-28}$	-313,193
~898 to 1173	$2.53e^{-7}$	40,096

The values presented in this table are the "best-fit" values for the 100 and 1000 μm thick samples presented in Figure 20.

4.1.5 Steady State H_2 Permeation Summary

As evident in the previous sections, the permeability of the selected alloys (Pd, 80Pd-Cu, 60Pd-Cu and 53Pd-Cu) are strongly dependent on the crystalline structure of the metal. Alloys exhibiting a crystalline phase change show significantly higher permeability values for the B2 crystalline phase as compared to the fcc phase. Additionally, it is apparent by the agreement of the data with a partial pressure exponent of 0.5 that the hydrogen transport through the membrane is limited by the diffusion of atomic hydrogen through the bulk of the metal.

Although early reports by McKinley and Nitro indicate that the permeability of the 60Pd-Cu alloy is greater than pure palladium, the trend was not observed in this study[84]. The discrepancies observed in this study as compared to that of McKinly and Nitro may be due to small variations in membrane composition. Moreover, the permeability values of all of the Pd-

Cu alloys studied were less than that of pure Pd (Figure 21). However, at temperatures below approximately 475°C, which corresponds to the B2 structure of the alloy, the 60Pd-Cu alloy exhibited the highest permeability values of the Pd-Cu alloys studied. At temperatures above approximately 500°C, the 80Pd-Cu alloy exhibited the highest permeability of the alloys studied. Furthermore, both the 53Pd-Cu and 60Pd-Cu foils exhibited significant decrease in permeability corresponding to the B2 to fcc phase transformations, with the B2 phase yielding higher permeability values than the fcc phase.

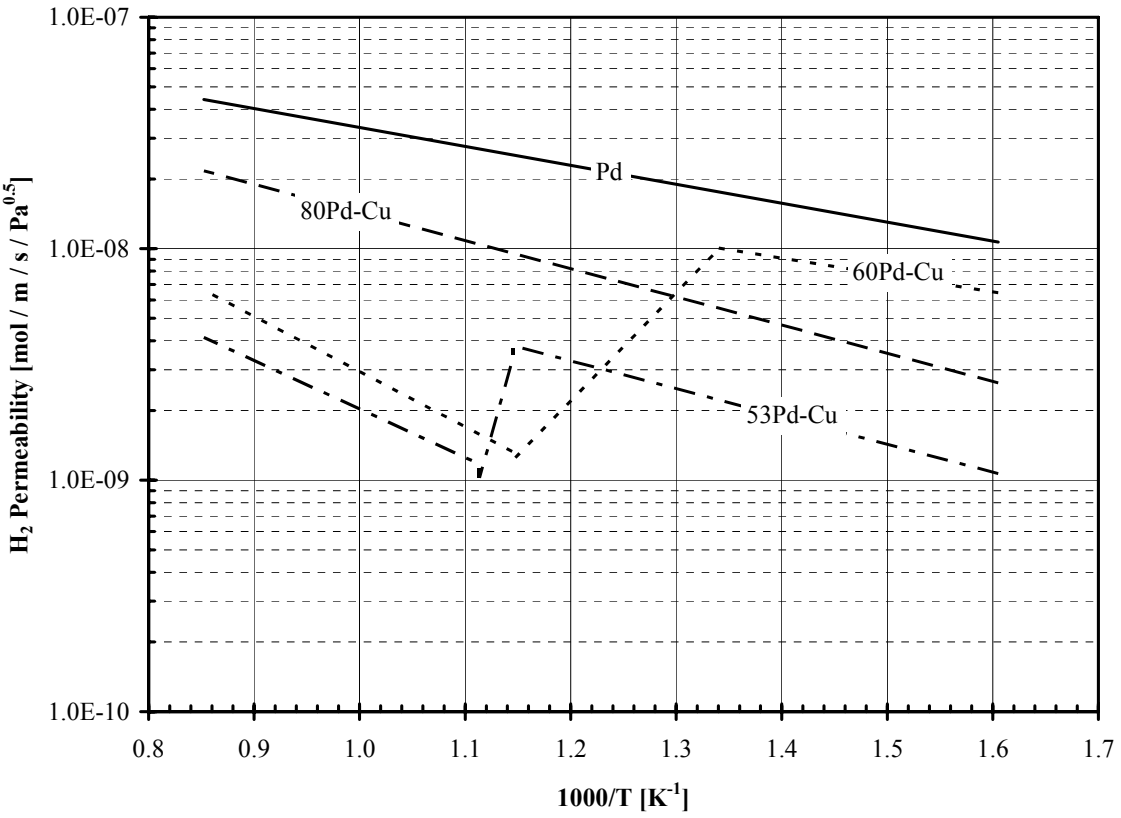

Figure 21. Summary of the "best-fit" permeability values obtained in this study in the presence of a hydrogen-helium gas mixture as a function of temperature.

Lastly, the permeability corresponding to the B2 and the fcc-phase appears to be proportional to the Pd content of the membrane (Figure 22), where higher palladium content yields high permeability values. The observed trend is somewhat expected based on the previous studies of Burch and Flanagan, which demonstrated that the solubility of the fcc-phase Pd-Cu system being proportional to the Pd content[125, 126].

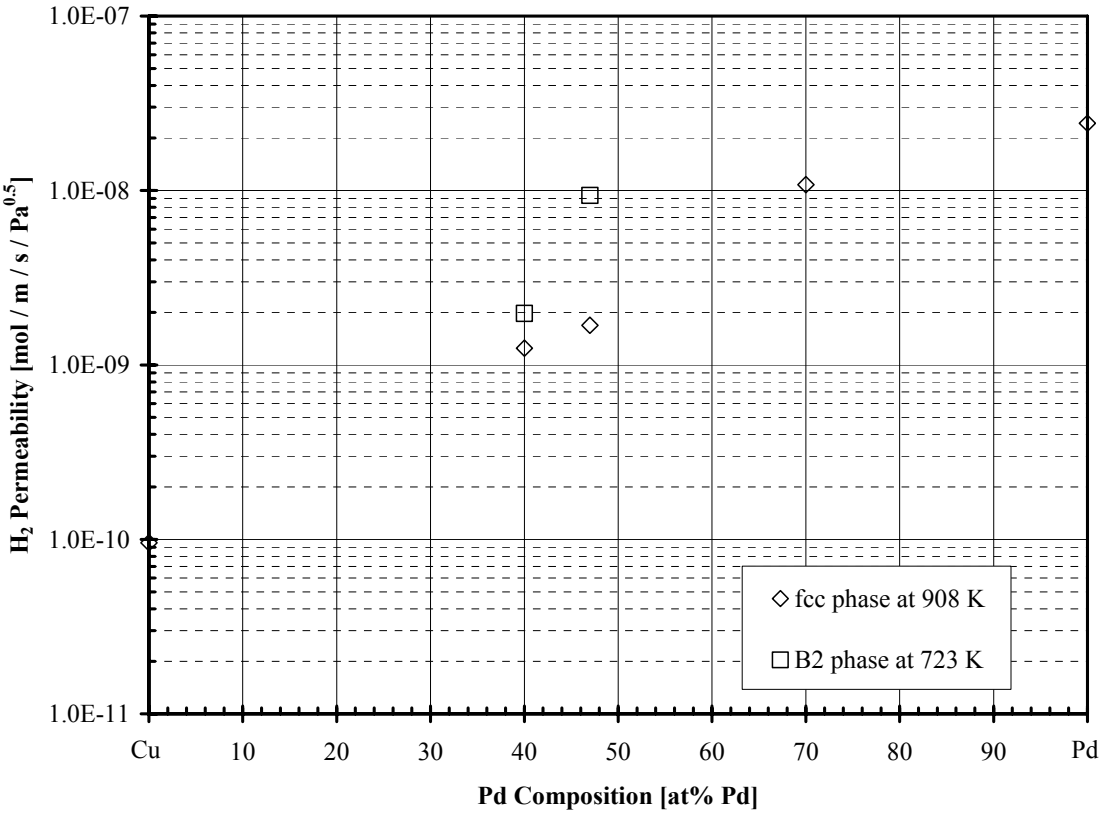

Figure 22. Permeability of the Pd-Cu alloys as a function of crystalline phase and alloy composition.

4.2 BATCH RESULTS OF PD-CU ALLOYS IN THE PRESENCE OF H_2S

Preliminary testing of the Pd-Cu alloys in the presence of H_2S was conducted in the batch Hydrogen Membrane Test unit, as described in Section 3.2. The batch testing method was utilized in an effort to obtain a qualitative understanding of the Pd-Cu-H_2S system. Testing in the presence of H_2S was initiated in the small scale (~0.003 mol H_2) and short duration (generally less than 4 hrs) batch unit due to the concerns with permanent contamination of the ss-HMT unit, which had a capital cost roughly 15-times greater than the b-HMT.

Flux testing was conducted with several Pd-Cu alloys (80Pd-Cu, 60Pd-Cu, and 53Pd-Cu) in the presence of either a hydrogen or hydrogen-hydrogen sulfide mixture. The membranes were mounted for testing as described in Figure 5. Due to the nature of the test procedure, in which the membrane samples were repeatedly heated and cooled in the presence of H_2, pure palladium was not studied using this test method due to the well documented mechanical issues of cycling palladium through the hydride phase transition temperature, ~300^{o}C.

Figure 23 presents an example of the test data and transient model for both a H_2 and H_2-H_2S gas mixture. Under the experimental conditions of this study, hydrogen was considered as an ideal gas and the partial pressure of hydrogen on the permeate side of the membrane was assumed to be negligible due to the use of a sweep gas. Further it was assumed that the time required to poison the membrane was very short relative to the duration of the transient test, hence the permeability of the membrane was invariant with respect to time. Under these conditions the variation of the retentate pressure is related to the permeability of the membrane (k), Equation 4-5.

$$\frac{dP_{H2,retentante}}{dt} = \frac{kA_M}{X_M} P_{H2,retentate}^{0.5} \quad (4\text{-}5)$$

An integrated form of Equation 4-5 was used to correlate the transient hydrogen retentate pressure with the membrane in terms of hydrogen permeability, k, Equation 4-6. Thus, the permeability value was determined by Equation 4-6, relating the permeability to the "best-fit" slope of the data.

$$P_{H2,Ret}(t) = \left[P_{H2,Ret,Initial}^{0.5} - \frac{1}{2} A_M \frac{k}{X_M} \left(\frac{RT}{V} \right) t \right]^2 \quad (4\text{-}6)$$

The permeability results for the 80Pd-Cu, 60Pd-Cu and 53Pd-Cu alloy membranes are presented in Figure 24 as a function of temperature. The permeability values obtained using the b-HMT unit and the corresponding methodologies were slightly lower than the previously reported values obtained in the flowing system as reported in Section 4.1.

Figure 24(a) shows the relationship of the 80Pd-Cu alloy membrane (6-145) with temperature, both in H_2 and H_2/He/H_2S retentate-side atmospheres. The sample was initially operated in the presence of neat hydrogen in the following temperature sequence: ~330, ~430, ~537, ~640, ~740^oC. Next, the membrane was operated in the presence of a 1000 ppm H_2S/10%He/H_2 gas mixture at 330^oC followed by a similar test sequence as done in the presence of H_2 (~430, ~537, ~640, ~740^oC). The 80Pd-Cu alloy membrane exhibited essentially no change in hydrogen permeability in the presence of 1000 ppm H_2S over the entire temperature

range as compared to the results observed in the absence of H_2S. The 80Pd-Cu alloy corresponds to an fcc crystalline phase over the temperature range of the study, as depicted in Figure 12.

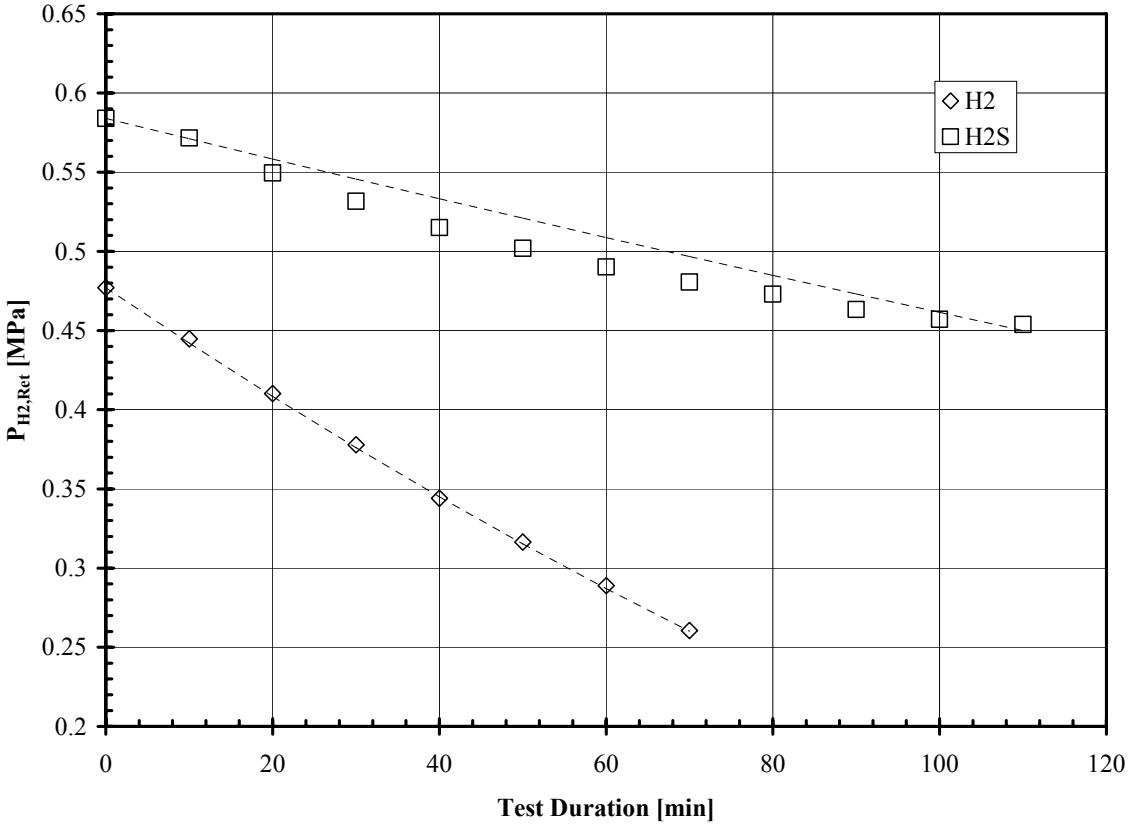

Figure 23. Example of the batch test results for a 60Pd-Cu membrane conducted at ~440°C.

Due to the nature of the mounting method, which included high temperature exposure during the welding process, the phase of the membrane could not be verified upon the initiation of testing. In an effort to ensure the proper crystalline phase, the 60Pd-Cu sample was operated at ~330°C until no observed changes in permeability was observed, which took 4-runs with a total exposure of ~20 hours at temperature. The membrane sample was then operated with the following temperature sequence in the presence of a neat hydrogen gas mixture to develop a comparative baseline: 440, 540, 650, 750, and 850°C. Upon completion of testing in the presence

of hydrogen at the aforementioned temperature sequence, the membrane was conditioned for testing in the presence of a H_2S gas mixture. Condition of the membrane was conducted at a temperature of ~330^oC until no changes in permeability was observed, which verified the crystalline phase conversion to B2. Next, testing of the membrane sample was conducted in the presence of a 1000ppmH_2S/10%He/H_2 gas mixture with a similar temperature sequence as used for the 80Pd-Cu membrane sample.

The permeability of the 60Pd-Cu alloy membrane (6-140) exhibited significant changes in permeability over the temperature ranges and gas compositions of this study as illustrated in Figure 24 (b). The permeability values of the 60Pd-Cu increased with increasing temperatures between 623 K and 723 K, decreased with increasing temperature from 723 K to 913 K, and continued increasing from 913 K to 1173 K. Similar trends were also observed in the results utilizing a flowing gas system (Section 4.1) and are attributable to the crystalline phase of the alloy changing from B2 to fcc with increasing temperature. At the temperatures corresponding to the fcc crystalline phase (above ~823 K) the 60Pd-Cu alloy membrane exhibited only a ~10% decrease in hydrogen permeability when H_2S was present in the retentate. However, at temperatures less than 823 K (the B2 crystalline phase), the 60Pd-Cu alloy exhibited decreases in permeability values of approximately one to two orders of magnitude.

Two 53Pd-Cu samples were tested (6-136 and 6-161) using the b-HMT unit using a similar test methodology as compared to the 60Pd-Cu samples. The 53Pd-Cu alloy exhibited similar trends as the 60Pd-Cu alloy, as shown in Figure 24(c). Permeability values corresponding to neat hydrogen increased with temperature below ~723 K and above ~913 K for the B2 and fcc

phases, respectively, while decreasing at temperatures between 723 K and 913 K in the mixed phase region. The 53Pd-Cu alloy also showed similar trends with respect to the H_2/H_2S mixture as observed for the 60Pd-Cu alloy. The 53Pd-Cu alloy exhibited the greatest resistance to H_2S at temperatures above 913 K, which corresponds to the fcc phase of the alloy. The temperatures associated with the fcc phase exhibited decreases in permeability values of less than 10% in the presence of 1000 ppm H_2S, while permeability values decreased as much as one order of magnitude for the B2 crystalline phase of the alloy.

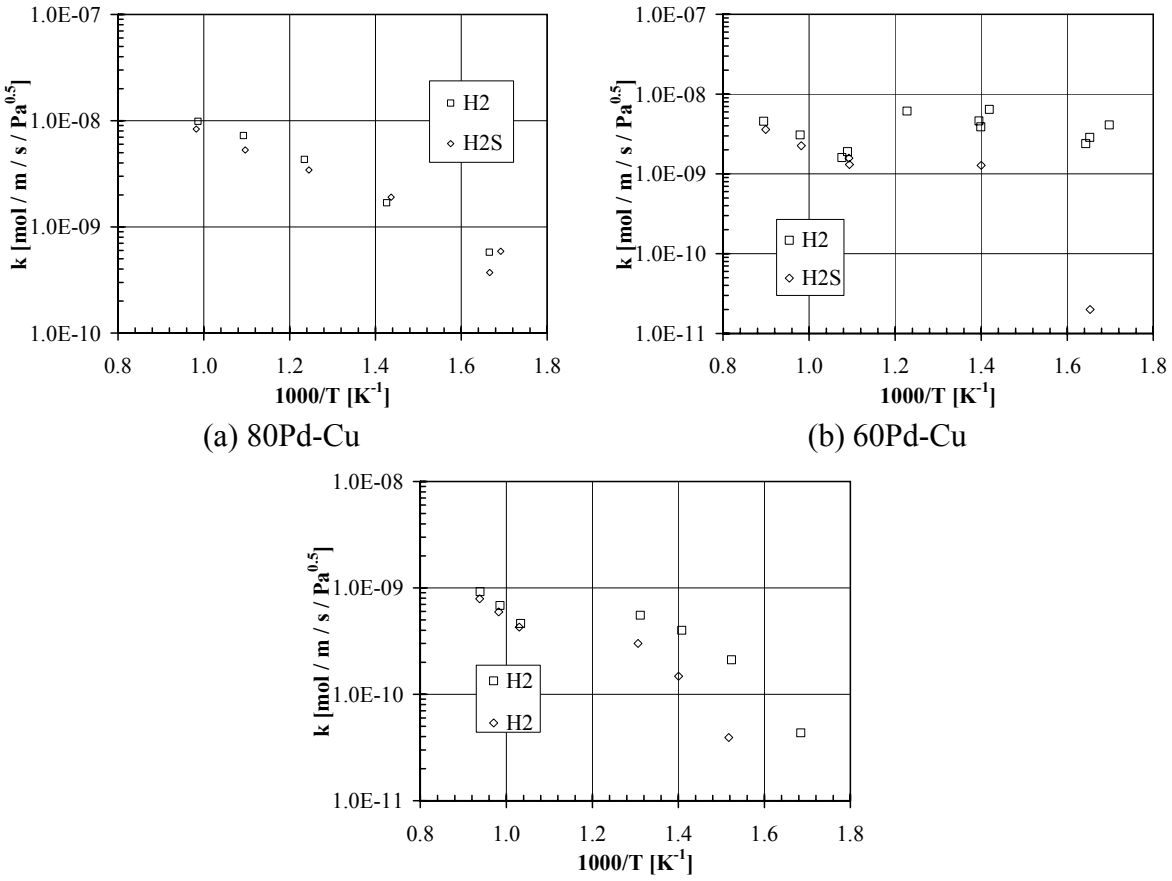

Figure 24. Permeability results for the (a) 80Pd-Cu, (b) 60Pd-Cu, and (c) 53Pd-Cu samples tested in the presence of H_2 and/or H_2/H_2S using the batch method.

While the aforementioned batch permeability testing of the Pd-Cu alloys in the presence of a H_2S gas mixture alludes to the relationship between crystalline phase and sulfur resistance, it was by no means a comprehensive study due to several limitations in the testing methodology. The first issue was the differences observed in the permeability values between the results in the batch (this section) and flowing systems (Section 4.1). The lower permeability values exhibited during batch testing is most likely attributed to the short durations of the tests not permitting a steady-state concentration profile within the membrane. Second was the finite amount of H_2S available for interaction with the membrane surface and the possible consumption of H_2S by other metal surfaces within the test unit. Lastly, the assumption that the interaction of H_2S with the membrane surface was rapid in comparison to the rate of hydrogen transport may have been erroneous. Although the abovementioned limitations warrants further analysis of the Pd-Cu-H_2S system, the qualitative observations resulting from batch testing gives insight of the trends to build upon in the evaluation in the presence of a flowing H_2S stream, which will be a of focus in following sections.

4.3 STEADY STATE PERFORMANCE IN THE PRESENCE OF H_2S

4.3.1 Initial investigation of 100 μm foils in the presence of H_2S

Initial studies of the influence of H_2S in a flowing system were conducted on membranes with thickness of ~100 μm. The foils were mounted using the brazing method illustrated in Figure 6. The permeability results of several 80Pd-Cu (6-176, 6-177 and 8-37) and 60Pd-Cu (6-

184 and 6-185) membranes are illustrated in Figure 25 as a function of temperature in the presence of 1000ppm H_2S/10% He/H_2 and compared to the results obtained from Section 4.1.3 and 4.1.4, respectively. All of the Pd-Cu alloys tested in this section were heated to 350^oC at a rate of ~120^oC/hr under inert gases. Upon completion of the heating ramp, a 10%He/H_2 mixture was introduced to the membrane to ensure the integrity of the membranes performance prior to the introduction of the H_2S containing gas mixture. Verification of the performance of the alloys in the presence of the 10%He/H_2 gas was attained in about 2 hours for the 80Pd-Cu and ~100 hours for the 60Pd-Cu samples. The hydrogen exposures for the 60Pd-Cu membrane were considerably longer to ensure phase transformation, which was accomplished by obtaining a steady-state flux. Upon verification of the membrane performance in the presence of H_2 gas mixture, a 1000ppm H_2S/ 10%He / H_2 gas mixture was introduced to the system at a pressure of ~620 kPa. The membranes were then operated at temperatures ranging from 450 to 635^oC in the presence of the aforementioned H_2S gas mixture. After the initial heating of the membranes in the presence of inert gases, all the membrane samples were ramped to the next temperature in the presence of the H_2S gas mixture. The temperature sequence used in testing went from low temperature to high temperature for all of the samples.

Three 80Pd-Cu membranes were studied in the presence of the H_2S gas mixture (6-176, 6-177, 8-37). All of the 80Pd-Cu membrane samples showed significant decreases (greater than an order of magnitude) at a membrane temperature of 350°C, illustrated in Figure 25 (a). As the temperature of the system was increased, the influence of H_2S on the permeability lessened. At temperatures above ~450°C minimal influence of H_2S on permeability was observed. The trends observed in the presence of a flowing H_2S stream were not in good agreement with the results obtained from the batch method, which may be a result of increased exposure times and the increased availability of H_2S in the flowing system studies.

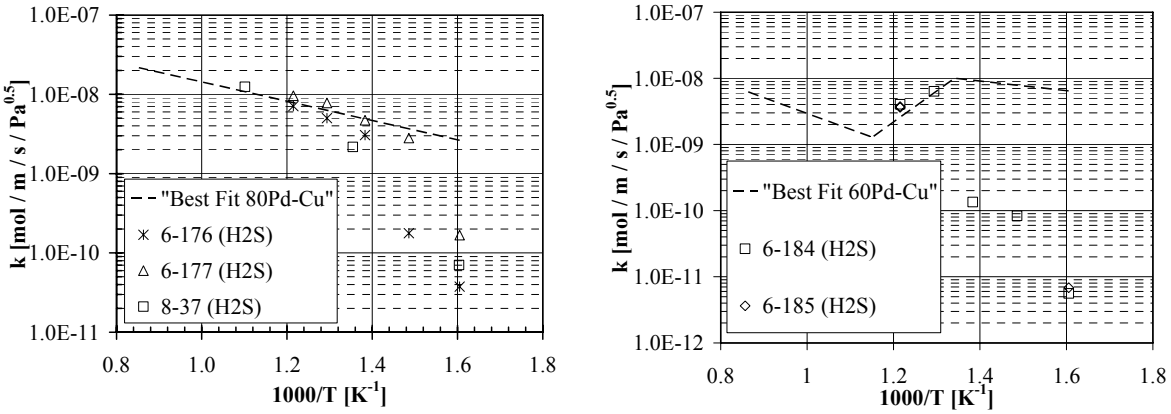

(a) 80Pd-Cu (b) 60Pd-Cu

Figure 25. Initial permeability results of the 100 μm thick, brazed membranes in the presence of 1000ppm H_2S/10% He/ H_2.

The 60Pd-Cu alloy set consisted of two membrane samples, 6-184 and 6-185. The 60Pd-Cu alloys exhibited decreases in permeability as large as 3 orders of magnitude at temperatures below 450°C, where the higher the temperature the less the severity of H_2S exposure on performance, Figure 25(b). At temperatures above ~500°C, no apparent decreases in

permeability were observed. The trends observed from the steady-state testing in the presence of H_2S for the 60Pd-Cu alloy agreed with the studies conducted using the batch method in the presence of H_2S.

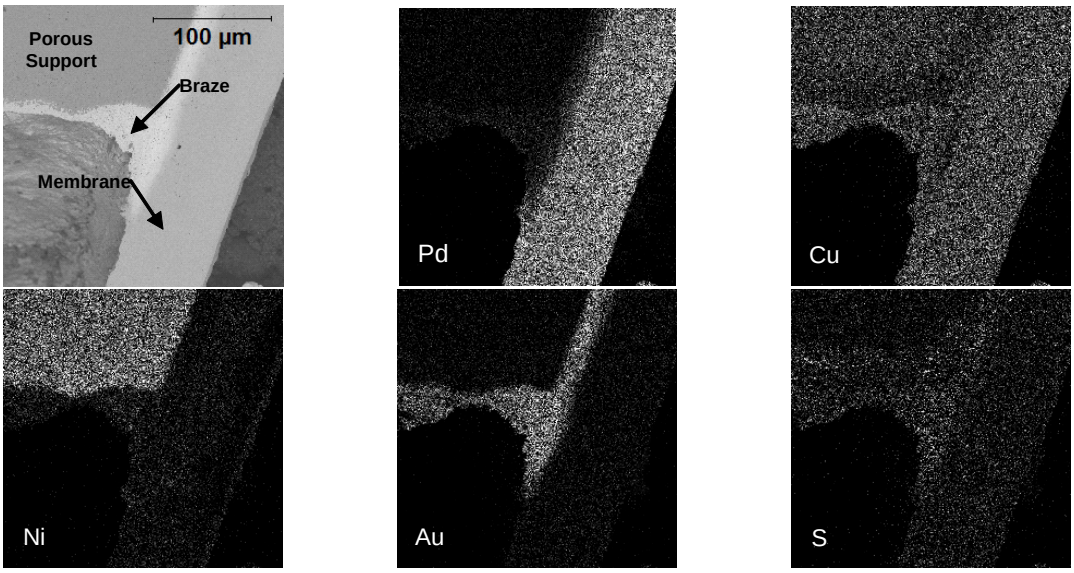

Figure 26. SEM/EDS cross section analysis of a Pd-Cu alloy membrane failure illustrating the formation of Ni-S.

Although several attempts were made in an effort to characterize the performance of the Pd-Cu alloys of interest in a flowing system, each attempt resulted in premature membrane failure. The membrane failure was evident by the detection of He in the sweep stream and occurred at temperatures between 550 and 635^{o}C for all of the membrane samples in this section. Following failure, samples were removed from the test assembly and examined using an optical microscope. Cracking of the alloys were evident at the membrane-braze interface suggesting a failure mechanism. Further examination of the membrane cross section by SEM/EDS revealed the presence of nickel-sulfide crystals within the braze and membrane region, Figure 26. Therefore, it is suspected that the formation of rather brittle Ni-S crystals within the sample and induced stress of the pressure differential and differences in the coefficient of thermal expansion led to the repeated membrane failures.

4.3.2 Investigation of 1000 μm foils in the presence of H_2S

Due to the technical barriers impeding the complete characterization of the 100 μm foils using the brazing mounting method, this study then focused on the influence of H_2S on the performance of 1000 μm thick Pd-Cu alloys. Although the thicknesses of these membranes are 2 to 3 orders of magnitude larger than thin-layered membranes being developed for commercial reactions, it was hypothesized based on the conclusions of previous researchers (adsorbed S blocks H_2 adsorption), that the surface reaction would limit the H_2 transport mechanism[77, 78, 84, 88, 107]. Thus, the thickness of the membrane sample would not dilute the impact observed on H_2 flux via competitive adsorption.

The 1000 μm thick membrane samples were all mounted using the method illustrated in Figure 5. The testing protocol used for the study of the influence of H_2S on the permeability of 1000 μm thick membranes was very similar to that of Section 4.3.1. The membrane samples were heated in the presence of inert gases at a rate of 120^{o}C/hr to the desired temperature, either 350 or 450^{o}C. Once the desired temperature was obtained, the test gas was switched to 10%He/ H_2 in an effort to verify the performance prior to testing in the presence of H_2S. Once again, due to the elevated temperatures associated with the mounting method employed, alloys which exhibit a phase transition (60Pd-Cu and 53Pd-Cu) were operated at a temperature corresponding to the B2 phase until no change in flux was observed prior to the introduction of a H_2S containing gas mixture.

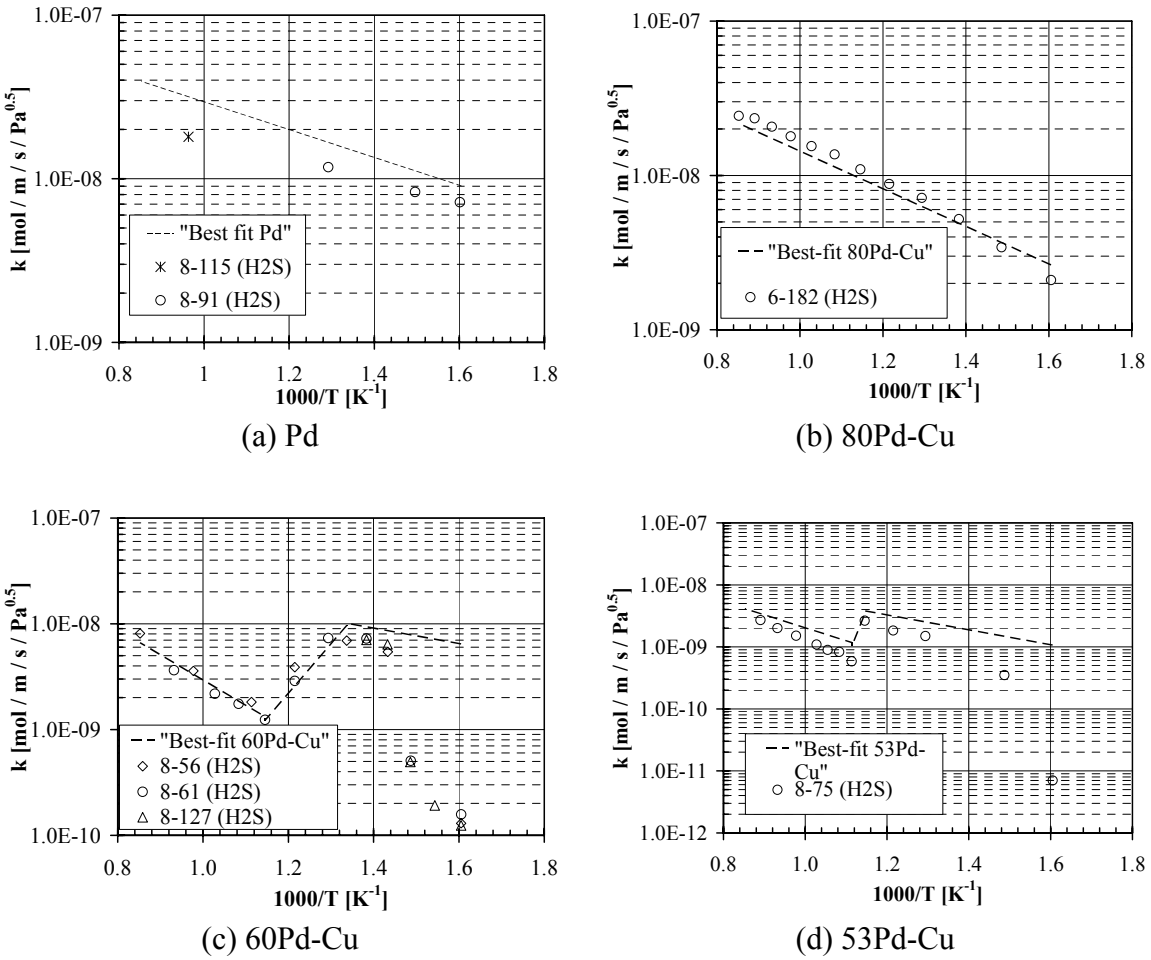

Figure 27. Permeability results of 1000 μm thick Pd and Pd-Cu membranes in the presence of 1000ppm H_2S/ 10%He/ H_2 as a function of temperature. The results are compared to the "best-fit" results from section 4.1.

After the performance of the membrane was verified in the presence of the H_2 gas mixture, a 1000ppm H_2S/ 10%He /H_2 was introduced to the system at a feed pressure of ~620 kPa. The membranes were operated in increasing temperature sequences for all of the samples with the temperature increases being conducted at a rate of 120^{o}C/hr in the presence of the H_2S containing gas mixture. Upon completion of testing in the presence of the H_2S containing gas mixture, the test gas was switched to UHP He and the membrane was cooled to room

temperature. The influence of the 1000ppm H_2S/10% He/ H_2 gas mixture on the permeability of 1000 μm Pd and Pd-Cu alloys is illustrated in Figure 27.

Two 1000 μm thick palladium membrane samples were operated in the presence of the 1000ppm H_2S/10%He/H_2 gas mixture. The first Pd sample (6-115) was operated at a temperature of 765^oC in the presence of H_2S for ~90hrs while the second sample (8-91) was operated at temperatures of 350, 465 and 635^oC and corresponding exposure durations of 63, 27 and 20 hrs, respectively. The results for the Pd samples exhibited a decrease in permeability ranging from 25 to 50% in the presence of the H_2S gas mixture, illustrated in Figure 27(a).

Only one 80Pd-Cu membrane was tested (6-182) with the results illustrated in Figure 27(b). The membrane was operated at temperatures ranging from 350 to 900 at 50^oC increments in the presence of the 1000ppm H_2S/10%He/H_2 gas mixture where the average exposure was approximately 20 hours at each temperature. The permeability values obtained for the 1000 μm sample in the presence of H_2S were comparable to the results in the presence of H_2 over the entire temperature range of study, 350 to 900^oC.

Evaluation of the 60Pd-Cu alloy consisted of testing three 1000 μm thick samples, again where the phase of the alloy was qualitatively verified by operation in the presence of H_2 until a "steady state" flux was obtained. The first sample (8-56) was operated at seven temperatures ranging from 350 to 900^oC in the presence of 1000ppm H_2S/10%He/H_2, with an average exposure duration of ~26 hours per temperature. The second sample (8-61) was evaluated over a temperature range from 350 to 800^oC in which eight temperatures were evaluated. The average

exposure time at each temperature was ~60 hours. Testing of the last sample (8-127) focused on temperatures ranging from 350 to 450^{o}C at 25^{o}C intervals with an average dwell time of 46hrs per temperature. A summary of the results of the 60Pd-Cu alloy in the presence of H_2S is illustrated in Figure 27(c) and compared to the previously described results in the presence of H_2. The permeability values obtained in the presence of H_2S gas mixtures compare very well to tests conducted in H_2 gas mixtures at temperatures above ~475^{o}C, but deviations as large as 2 orders of magnitude were observed at temperatures below ~475^{o}C.

Lastly, the performance of the 53Pd-Cu alloy was evaluated by flux testing of one membrane (8-75), where the permeability values are illustrated in Figure 27(d). The membrane was operated at thirteen temperatures ranging from 350 to 850^{o}C in the presence of 1000 ppm H_2S/ 10%He /H_2. The average exposure for each temperature was approximately 15hrs. The permeability values in the presence and absence of H_2S of the 53Pd-Cu alloy had very similar trends as compared to the 60Pd-Cu alloy. At elevated temperatures ($T \geq 500^{o}$C) the permeability values in the presence and absence of H_2S were comparable, while at temperatures below 500^{o}C decreases as large as two orders of magnitude were observed in the presence of the H_2S containing gas mixture.

The trends observed for the steady state exposure of the Pd-Cu alloys in the presence of H_2S were very similar to the batch testing results. In both tests, the 60Pd-Cu alloy and the 53Pd-Cu alloy exhibited significant decreases in performance at temperatures below ~500^oC and negligible changes at temperatures above. Negligible differences in permeability were observed for the 80Pd-Cu alloy in the presence and absence of H_2S over the entire temperature range of study for both the batch testing of 100 μm samples and stead-state testing of the 1000 μm samples.

Although the permeability trends observed for the batch (100 μm samples) and flowing studies conducted with 1000 μm membranes in the presence of H_2S were similar for the 80Pd-Cu alloy, the initial results for the 100 μm brazed samples (Section 4.3.1) in a flowing system were rather dissimilar at low temperatures ($T \leq 500^oC$). At temperatures above ~500^oC no deviation in the presence of H_2S was observed, while at temperatures below ~500^oC decreases as large as two ordered of magnitude was perceived.

The difference observed in the initial studies with the 100 μm brazed samples and the 1000 μm 80Pd-Cu sample in a flowing gas stream gives evidence that the thickness of the membranes samples may have masked the effect of H_2S on thicker samples. Therefore the next section will focus on mitigating the issues encountered in the preliminary testing of the 100 μm samples in the presence of H_2S and give a comparison between the two membrane thicknesses.

4.3.3 Long-term performance of 100 μm membranes in the presence of H_2S

As was demonstrated in the previous sections of this work, H_2S can have a significant influence on membrane performance and as the membrane thickness decreases, the influence of H_2S on performance may increase. Therefore, this section will focus on exposing 100 μm Pd, 80Pd-Cu, 60Pd-Cu and 53Pd-Cu membranes to a flowing gas stream containing H_2S for a fixed duration at a desired temperature to attempt to resolve these issues. The decreases in hydrogen flux observed in the presence of the H_2S containing gas mixture will attempt to be correlated with changes in surface phenomenon. All of the membrane samples in this section utilized the mounting procedure illustrated in Figure 7, which employed a Swagelok® compression fitting. The compression fitting allowed for operation at elevated temperatures by reducing the influence of Ni-sulfide incorporation at the seal while allowing the flexibility of ensuring the crystalline structure of the foil prior to installation into the ss-HMT. Therefore all of the membranes in this section went through the following sequence:

1) Modification of the crystalline structure by annealing in H_2 at an appropriate temperature followed by verification via XRD.

2) Mounting of the membrane foil using a Swagelok® VCR® fitting as illustrated in Figure 7 and installation into the ss-HMT unit.

3) Heating of the membrane sample at a rate of 120^{o}C/hr to the desired test temperature (350, 450 or 635^{o}C) under inert gases.

4) Verification of the permeability of the membrane in the presence of a 10%He/H_2 gas mixture, which typically lasted ~2 hrs at 620 kPa.

5) Introduction of a 1000 ppmH_2S/ 10%He/ H_2 gas mixture which was the test gas for the next 120 hrs of operation at 620 kPa.

6) Purging with inert gas to the process side of the membrane in an effort to remove any reactive gases prior to cooling.

7) Cooled sample at a maximum rate in an effort to preserve any surface changes that may have occurred during H_2S exposure and removed from the test unit, usually about 1.5 hrs.

8) The surface of the membrane was then analyzed by optical microscope, SEM/EDS and XRD in an effort to observe surface changes, recrystallization, elemental information, structure formations and compounds formed. Further SEM/EDS analysis was conducted on the specimen cross-section in an effort to evaluate the segregation or formation of surface compounds.

Preliminary testing using this methodology resulted in widely scattered flux values. Upon close inspection of the test parameters, test data and optical examination of the post tested membranes it was apparent that the unusual observations were due two phenomenon taking place. First, the membrane-H_2S system was very sensitive to the concentration of H_2S measured in the effluent. Variations in H_2S effluent concentration as large as 40% were observed and appeared to influence the resulting flux. Figure 28(a) illustrates a variance in H_2S concentration from ~800 to 1000 ppm H_2S resulting in a hydrogen flux of ~0.01 to 0.1 $cm^3/cm^2/min$, respectively.

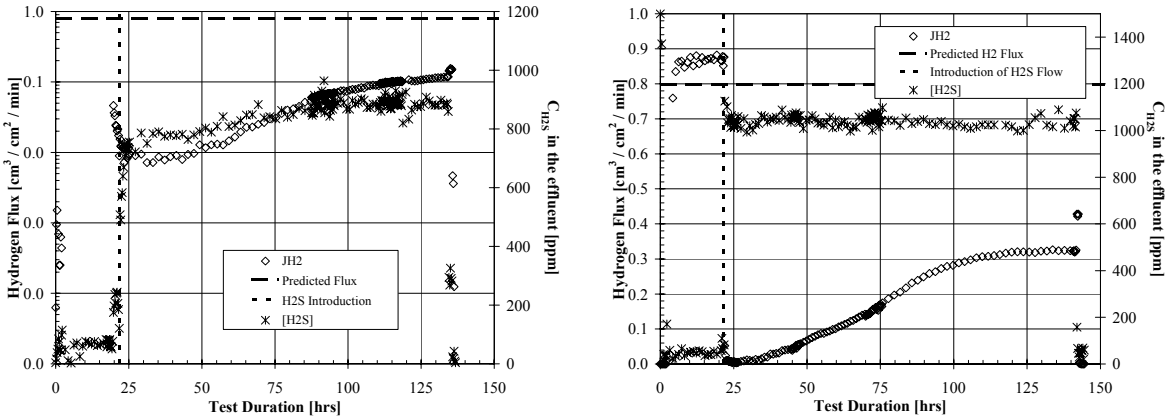

(a) 53Pd-Cu, 450°C (b) 53Pd-Cu, 450°C

Figure 28. Preliminary testing results in the presence of H_2S. (a) Apparent influence of changing [H_2S] on hydrogen flux. (b) Apparent influence of metal (Cr, Fe, and/or Ni) on the hydrogen flux observed during testing.

The change in H_2S concentration detected in the effluent was attributed to its consumption by the reactor materials (316 stainless steel and/or Inconel® 600) at elevated temperatures. The consumption of H_2S by the reactor materials was mitigated by the use of a quartz "sleeve" and annular feed tube which reduced or eliminated the contact of the reactive gases and the hot metal surfaces, Figure 29.

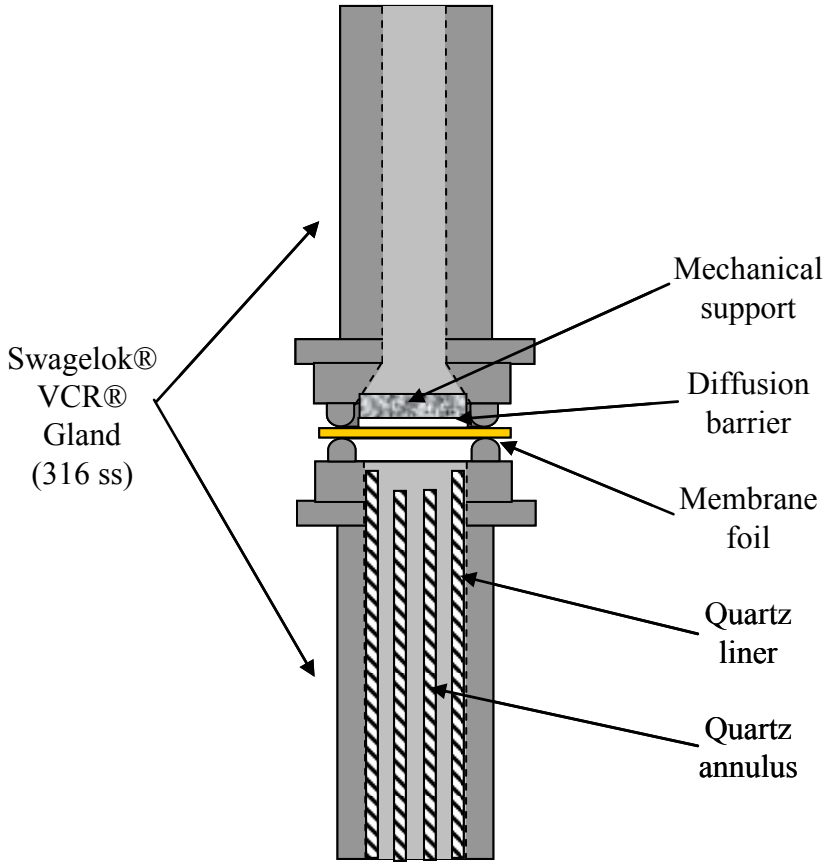

Figure 29. Schematic of the modified Swagelok® compression fitting and feed system.

The second phenomenon possibly attributing to the observed variation in hydrogen flux was the deposition of metal sulfides from the reactor walls onto the surface of the membrane, illustrated in Figure 30. Metals sulfides (Cr, Ni and/or Fe) were often detected by SEM/EDS on the surface of the membrane during preliminary testing and were attributed to the spalling of the corroded reactor material which was in close proximity to the membrane surface. The compression fittings used in this testing, illustrated in Figure 7, has an almost parallel, stainless steel surface which was less than 4 mm from the membrane surface. The apparent influence of the metal-sulfide deposition is illustrated in Figure 28(b). In an effort to reduce the contamination of the membrane surface by spalling scale of the reactor materials, the inside diameter of the compression fitting was reduced to minimize the stainless steel surface that was roughly parallel to the membrane surface, Figure 29.

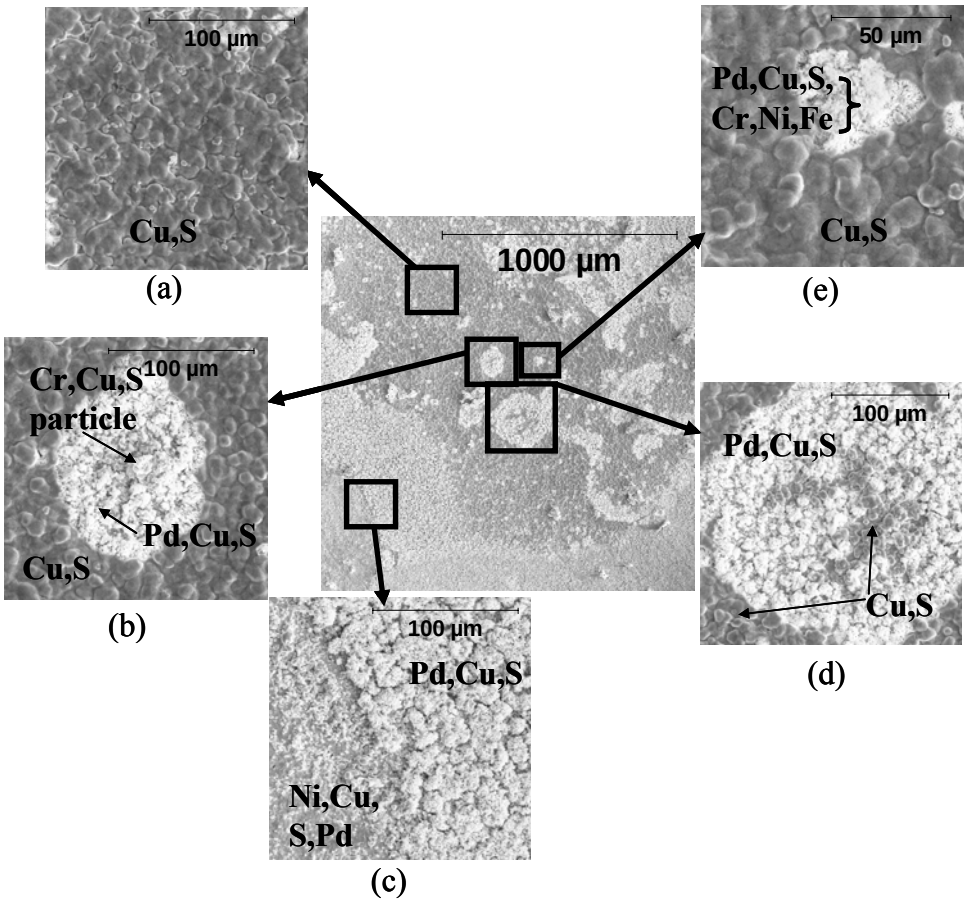

Figure 30. SEM/EDS analysis of the metal-sulfide contamination on the surface of a membrane.

Therefore, a quartz feed and exit system as well as a modified compression fitting was used for the following results in an effort to induce a constant H_2S exposure to the membrane surface exposure and reduce the influence of external scale contamination. Additionally, a Pt gasket was placed between the membrane surface and the sealing surface of the compression fitting. The Pt gasket was used in an effort to reduce possible intermetallic diffusion of the stainless-steel VCR® fitting into the membrane and thus reduce previously observed failures resulting from dissolved Ni-S particles in the brazed samples.

4.3.4.1 Palladium Three, 100 μm Pd foils were examined using this method. The first membrane sample was tested at 350°C, the second at 450°C and the third membrane was tested at a temperature of 635°C. Each sample was exposed to a 1000 ppmH_2S/ 10%He/ H_2 mixture for ~120hrs. Figure 31 illustrates the results of the H_2S exposures on Pd at 350, 450 and 635°C. At all of the temperatures studied, the Pd membranes exhibited a continuous decrease in the hydrogen flux in the presence the H_2S gas mixture. The resulting hydrogen flux after 120 hours of operation in the presence of the aforementioned H_2S gas mixture was approximately ~30% of the value expected in the presence of H_2 at 350°C and approximately 20% at 450 and 635°C.

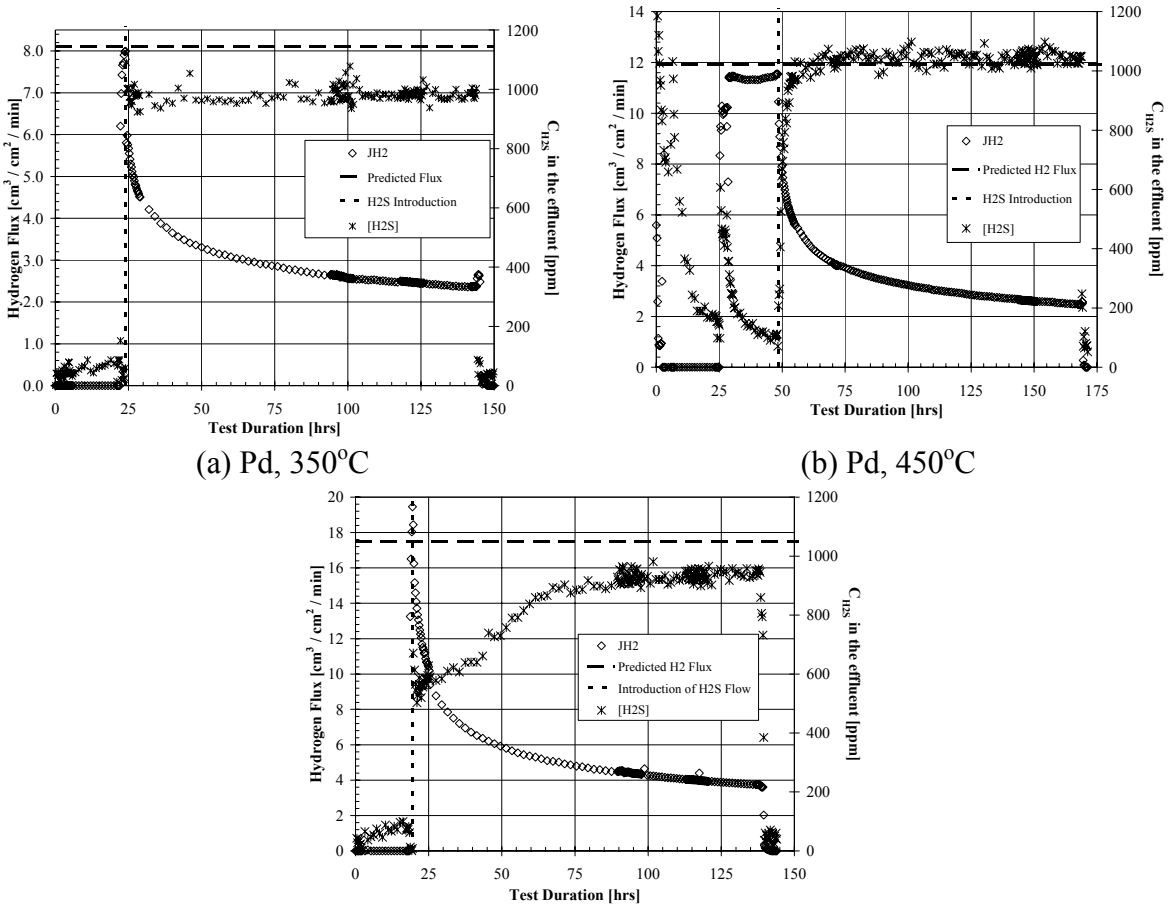

(a) Pd, 350°C

(b) Pd, 450°C

(c) Pd, 635°C

Figure 31. Flux results of the 100 μm Pd membrane samples in the presence of 1000ppm H_2S/ 10%He/ H_2 as a function of exposure. (a) Pd at 350°C. (b) Pd at 450°C. (c) Pd at 635°C.

Upon completion of the flux testing, the membrane samples were removed from the test apparatus and mounting hardware. The surfaces of the samples were analyzed by SEM/EDS, Figures 32, 33 and 34.

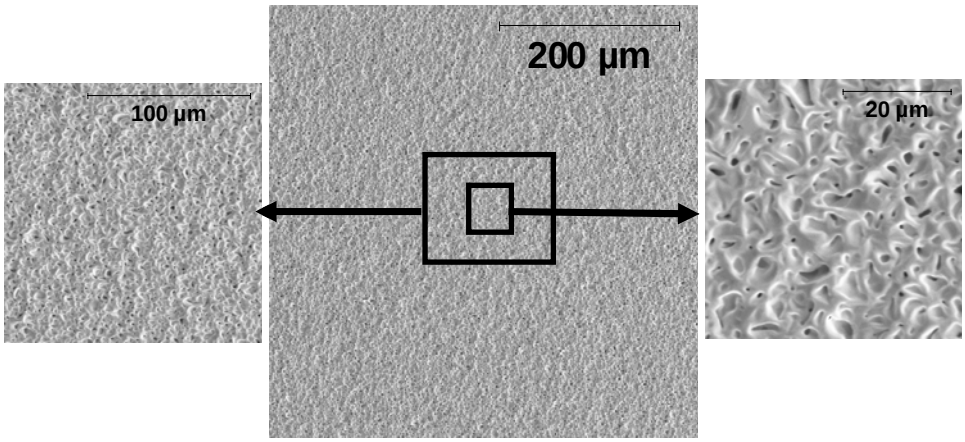

(a) Pd, 350°C – Surface SEM

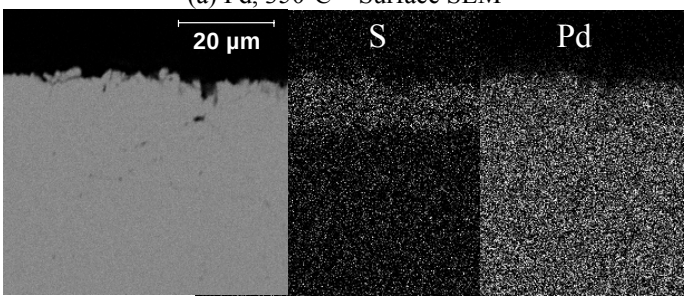

(b) Pd, 350°C-Cross Section Elemental Mapping

Figure 32. SEM/EDS analysis of the membrane surface and cross section of the 100 µm Pd membrane samples after exposure to 1000ppm H_2S / 10% He / H_2 for 120 hrs at 350°C and 600 kPa.

SEM images of the surfaces showed significant surface modification of the membranes while EDS analysis indicated the presence of Pd and S on all membrane surfaces. The surfaces of the Pd membranes were further analyzed by x-ray diffraction which indicated that both Pd and Pd_4S were present, which could allude to an impure Pd_4S layer or that the XRD analyzed deeper than the scale thickness. The membranes were then cross sectioned and analyzed by EDS elemental mapping to determine the penetration depth of the S within the metal. The elemental mapping indicated the presence of S containing layers of ~15, ~20 and ~30 µm at 350, 450 and 635°C, respectively.

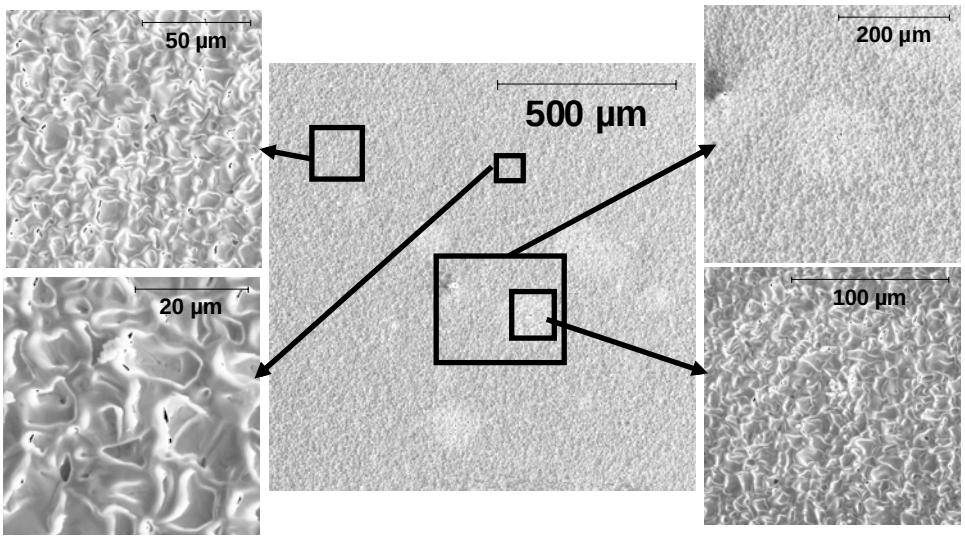

(a) Pd, 450°C – Surface SEM

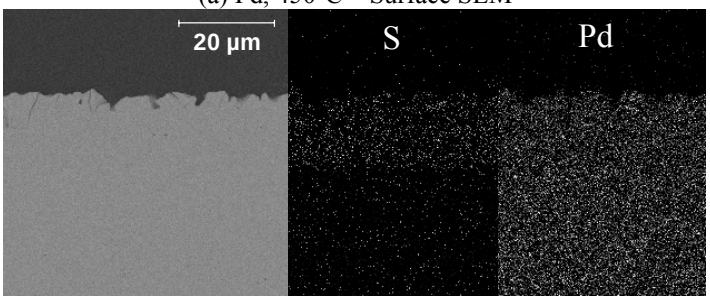

(b) Pd, 450°C-Cross Section Elemental Mapping

Figure 33. SEM/EDS analysis of the membrane surface and cross section of the 100 µm Pd membrane samples after exposure to 1000ppm H_2S / 10% He / H_2 for 120 hrs at 450°C and 600 kPa.

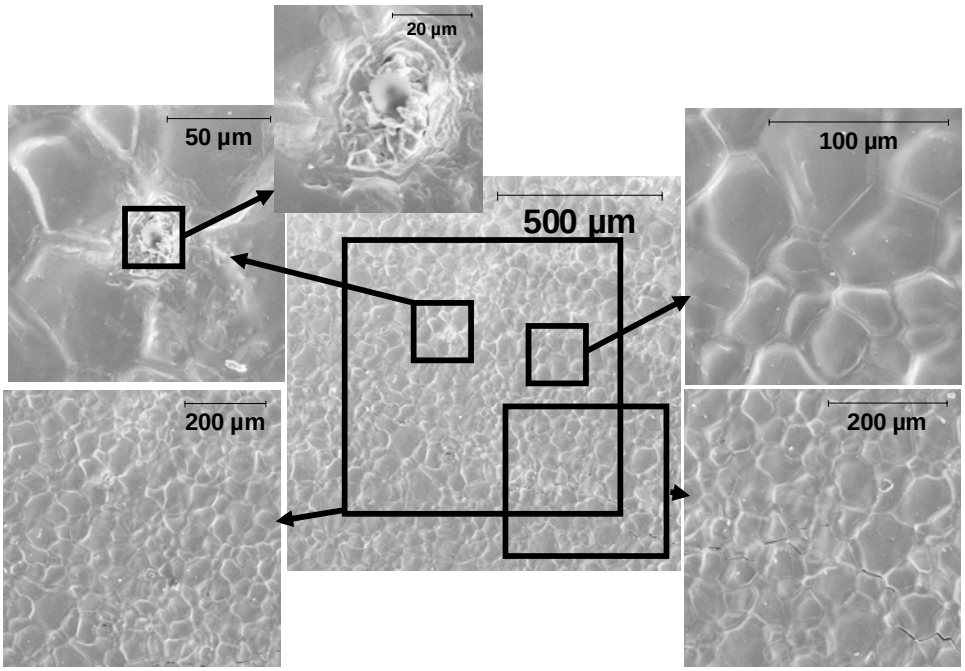

(a) Pd, 635°C – Surface SEM

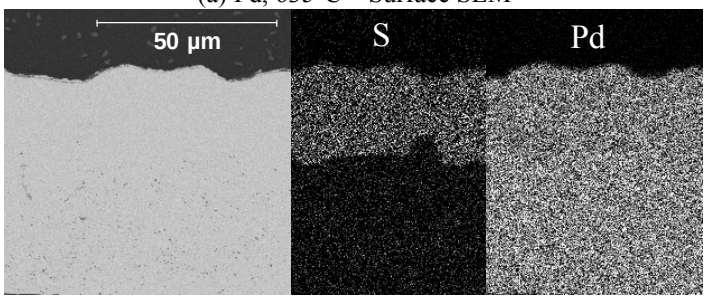

(b) Pd, 635°C-Cross Section Elemental Mapping

Figure 34. SEM/EDS analysis of the membrane surface and cross section of the 100 µm Pd membrane samples after exposure to 1000ppm H_2S / 10% He / H_2 for 120 hrs at 635°C and 600 kPa.

4.3.4.2 80Pd-Cu Three, 100 µm 80Pd-Cu membranes were evaluated in a similar fashion as the Pd samples in the presence of H_2S. Each membrane was tested at one temperature, 350°C, 450°C and 635°C, in the presence of 1000ppm H_2S / 10%He/ H_2 for 120 hrs at 600 kPa. Figure 35 shows the results for the 80Pd-Cu membranes as a function of exposure time in the presence of the H_2S gas mixture.

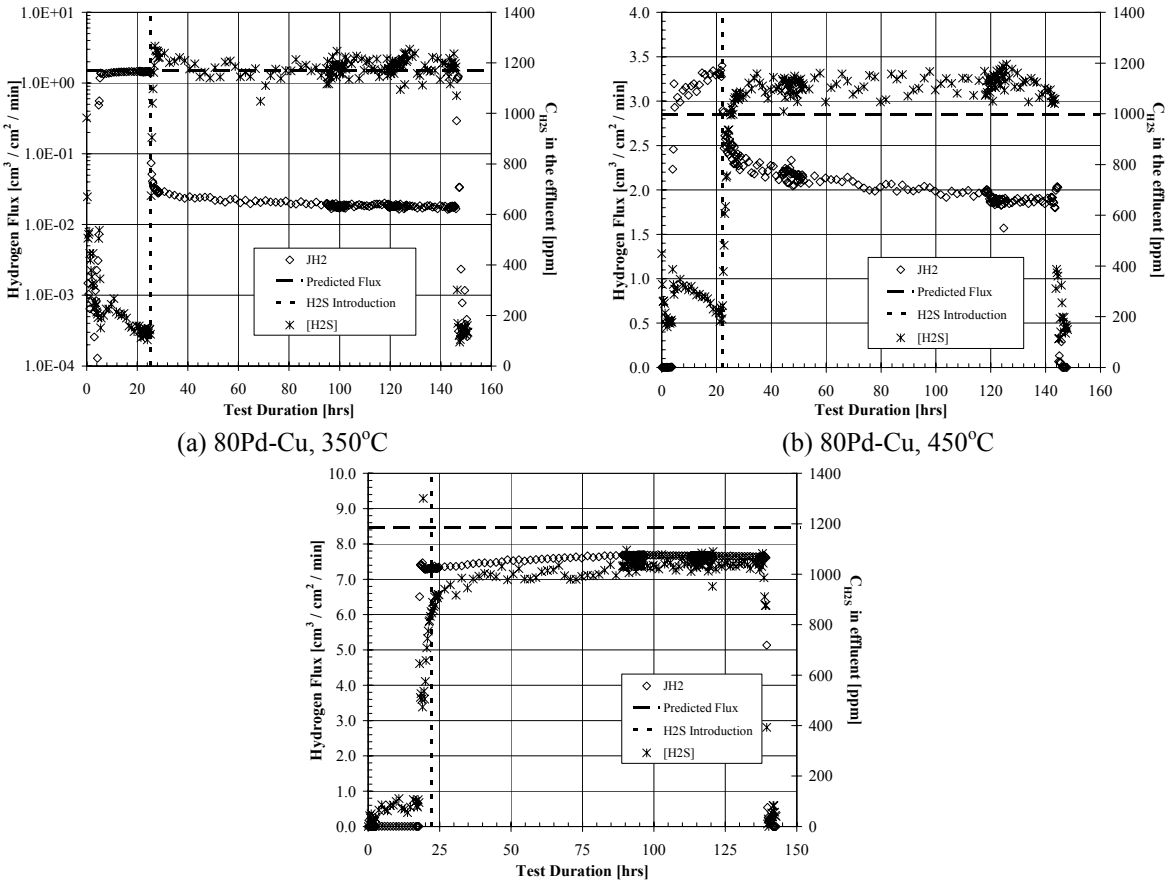

(a) 80Pd-Cu, 350°C

(b) 80Pd-Cu, 450°C

(c) 80Pd-Cu, 635°C

Figure 35. Flux results of the 100 μm 80Pd-Cu membrane samples in the presence of 1000ppm H_2S/ 10%He/ H_2 as a function of exposure time. (a) 80Pd-Cu at 350°C. (b) 80Pd-Cu at 450°C. (c) 80Pd-Cu at 635°C.

The influence of H_2S on hydrogen flux through the 80Pd-Cu membranes was more significant at lower temperatures. At 350°C, the hydrogen flux dramatically decreased in the first 30 minutes of exposure followed by a continuous decrease to 1% of the expected value in hydrogen. A similar, but less severe trend was observed at 450°C for the 80Pd-Cu sample resulting in a total decrease of ~35% after 120 hrs of operation. At 635°C, the flux in the absence of the H_2S feed gas was approximately 14% lower than predicted and remained relatively constant over the duration of H_2S exposure.

Upon completion of the flux testing, the membrane samples were removed from the test apparatus and mounting hardware. The surfaces of the samples were analyzed by SEM/EDS, Figures 36, 37 and 38. SEM images of the surfaces shows surface modification of all the 80Pd-Cu membranes tested. The surface roughening of the 80Pd-Cu membranes was less significant than that observed for the pure Pd samples at similar conditions.

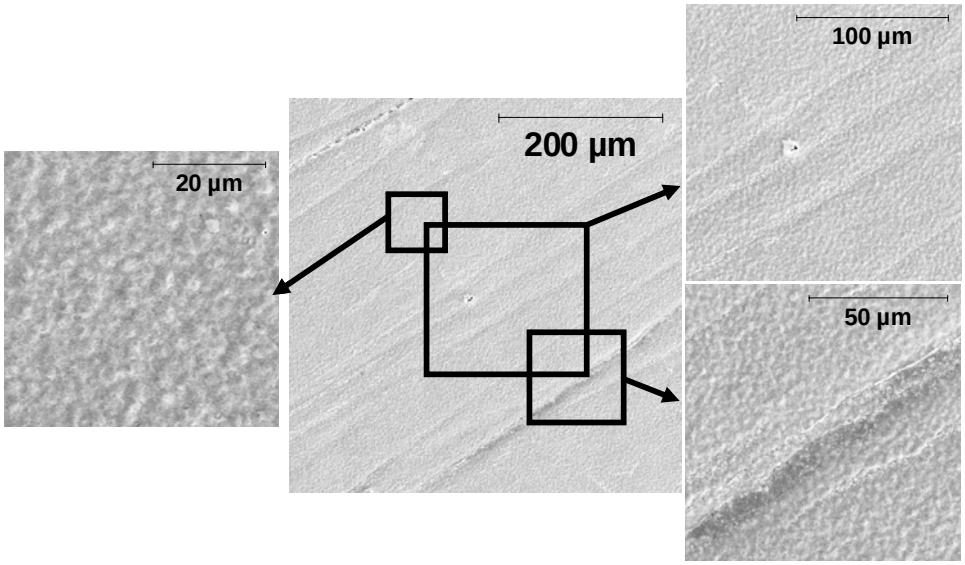

(a) 80Pd-Cu Surface, 350°C

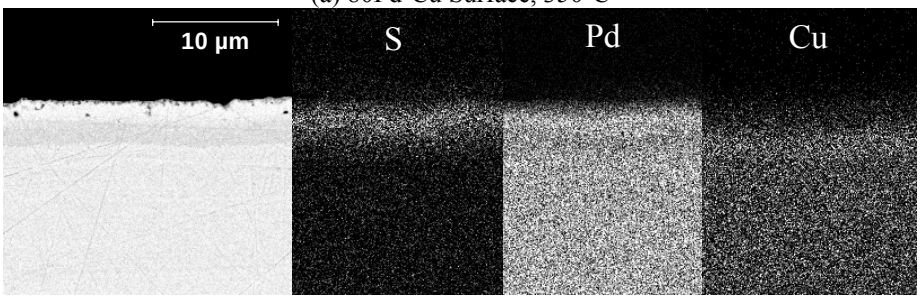

(b) 80Pd-Cu Cross Section Elemental Mapping, 350°C

Figure 36. SEM/EDS analysis of the membrane surface and cross section of the 100 µm80Pd-Cu membrane samples after exposure to 1000ppm H_2S / 10% He / H_2 for 120 hrs at 350°C and 620 kPa.

EDS analysis of the surfaces indicated the presence of Pd, Cu and S at temperatures of 350 and 450°C, however, no S was detected after exposure at 635°C. The surfaces of the 80Pd-Cu membranes were further analyzed by XRD. After H_2S exposure at 350°C, XRD revealed the presence of Pd_4S, $Pd_{13}Cu_3S_7$ and B2 Pd-Cu alloy. The membrane sample exposed to H_2S at 450°C showed the presence of Pd_4S and $Pd_{13}Cu_3S_7$, but no detectable metal while the sample exposed at 635°C had trace amounts of $Pd_{13}Cu_3S_7$ and B2 alloy along with a significant amount of fcc alloy.

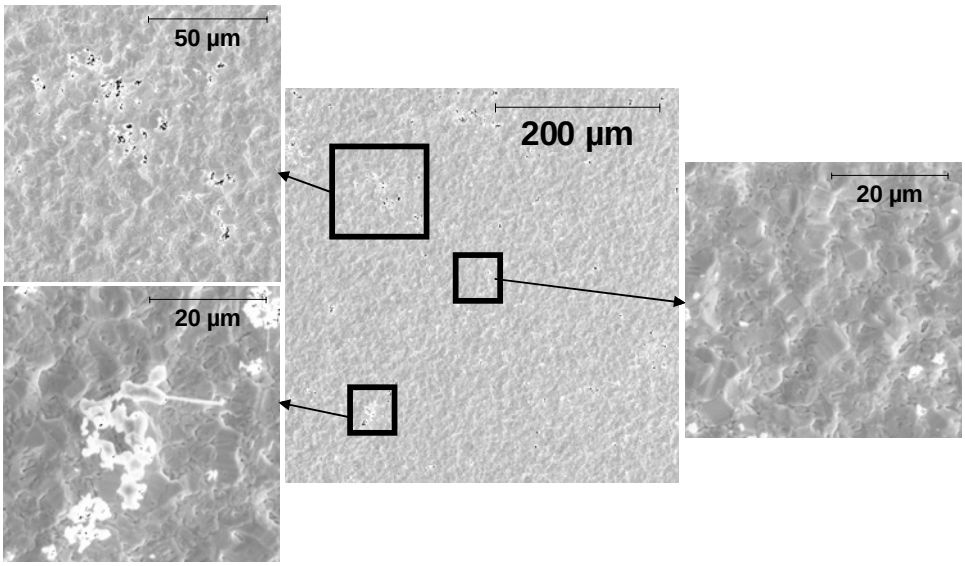

(a) 80Pd-Cu Surface, 450°C

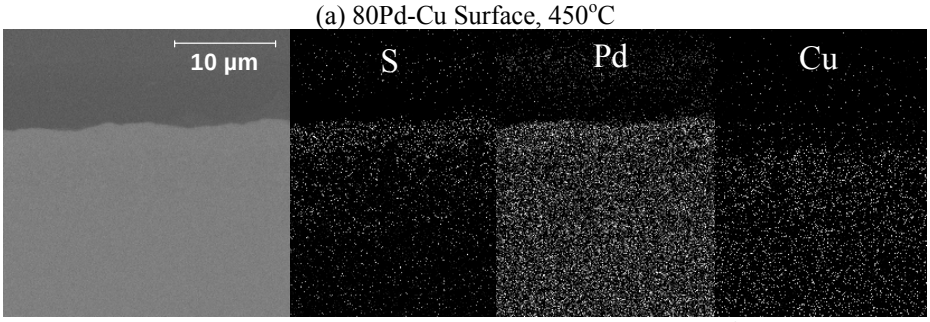

(b) 80Pd-Cu Cross Section Elemental Mapping, 450°C

Figure 37. SEM/EDS analysis of the membrane surface and cross section of the 100 µm80Pd-Cu membrane samples after exposure to 1000ppm H_2S / 10% He / H_2 for 120 hrs at 450°C and 620 kPa.

The membranes were then cross sectioned and analyzed by EDS elemental mapping to determine the sulfide thickness. The cross section of the sample exposed to H_2S at 350°C along with the XRD results revealed a layered sulfide with a total thickness of ~4-5 µm, with Pd_4S on the outermost surface followed by $Pd_{13}Cu_3S_7$ and lastly by a Pd-Cu metal. The cross section of the samples exposed at 450 and 635°C revealed a relatively thin sulfide layer and no detectable sulfide scale, respectively.

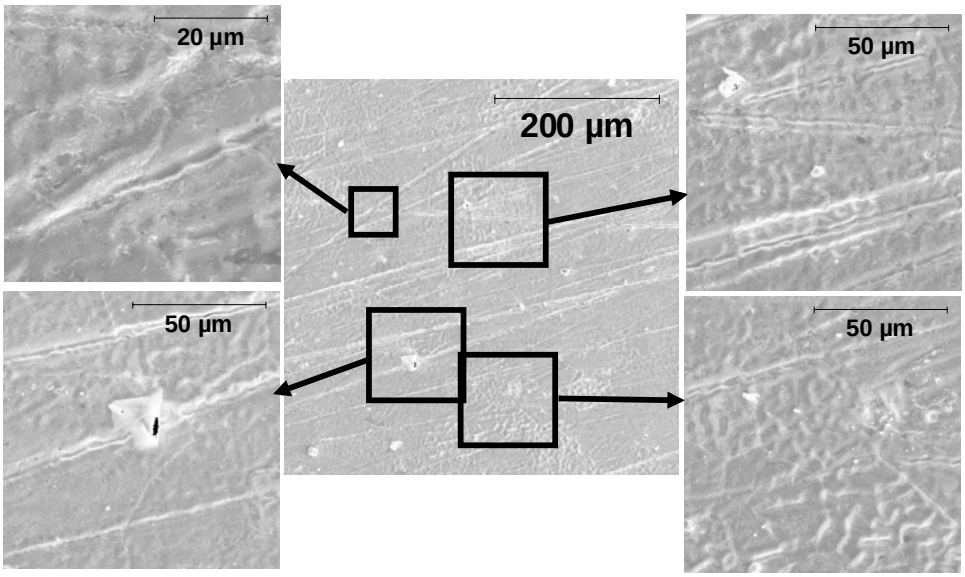

(e) 80Pd-Cu Surface, 635°C

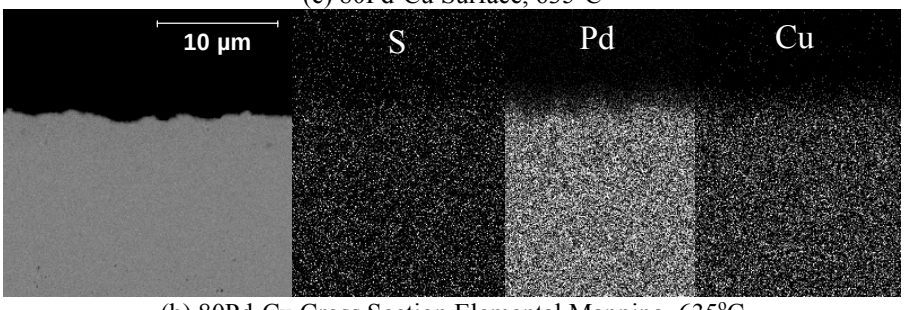

(b) 80Pd-Cu Cross Section Elemental Mapping, 635°C

Figure 38. SEM/EDS analysis of the membrane surface and cross section of the 100 µm80Pd-Cu membrane samples after exposure to 1000ppm H_2S / 10% He / H_2 for 120 hrs at 635°C and 620 kPa.

4.3.4.3 60Pd-Cu Three, 100 μm 60Pd-Cu membranes were examined in a similar fashion as the Pd and 80Pd-Cu samples. Each membrane was tested at one temperature, 350°C, 450°C or 635°C, in the presence of 1000ppm H_2S / 10%He/ H_2 for 120 hrs at 600 kPa. Figure 39 illustrates the hydrogen flux results of the 60Pd-Cu membrane as a function of exposure time in the presence of the H_2S gas mixture.

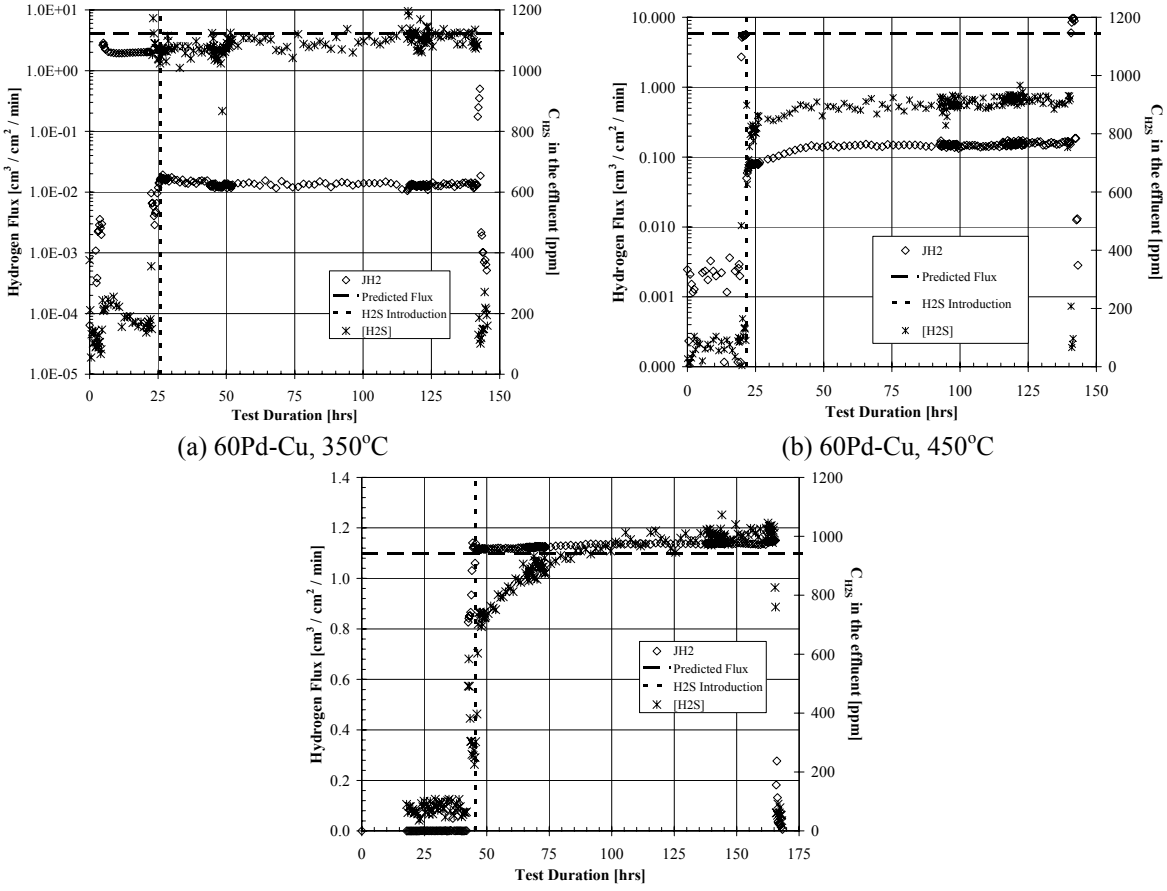

(a) 60Pd-Cu, 350°C

(b) 60Pd-Cu, 450°C

(c) 60Pd-Cu, 635°C

Figure 39. Flux results of the 100 μm 60Pd-Cu membrane samples in the presence of 1000ppm H_2S/ 10%He/ H_2 as a function of exposure time. (a) 60Pd-Cu at 350°C. (b) 60Pd-Cu at 450°C. (c) 60Pd-Cu at 635°C.

The influence of H_2S on the hydrogen flux through the 60Pd-Cu membranes was more significant at lower temperatures. At 350°C and 450°C, the hydrogen flux dramatically decreased in the first 30 min of operation to only ~1% of the expected value. At 635°C, the flux showed no significant change as a function of test exposure time, and was approximately 3.5% higher than the predicted values based on the results from previous sections.

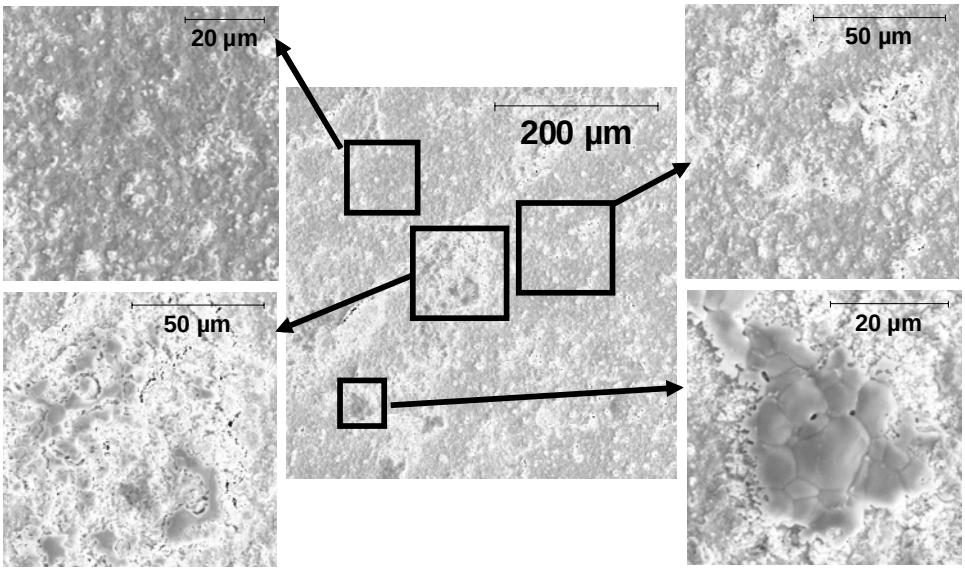

(a) 60Pd-Cu surface, 350°C

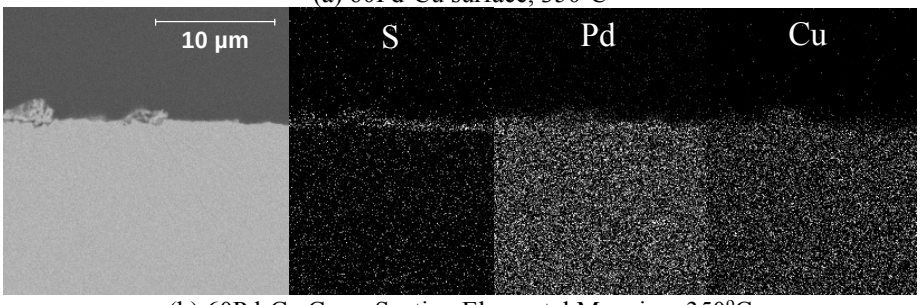

(b) 60Pd-Cu Cross Section Elemental Mapping, 350°C

Figure 40. SEM/EDS analysis of the membrane surface and cross section of the 100 µm 60Pd-Cu membrane samples after exposure to 1000ppm H_2S / 10% He / H_2 for 120 hrs at 350°C and 620 kPa.

Upon completion of the flux testing, the 60Pd-Cu membrane samples were removed from the test apparatus and mounting hardware. The surfaces of the samples were analyzed by SEM/EDS, Figures 40, 41 and 42.

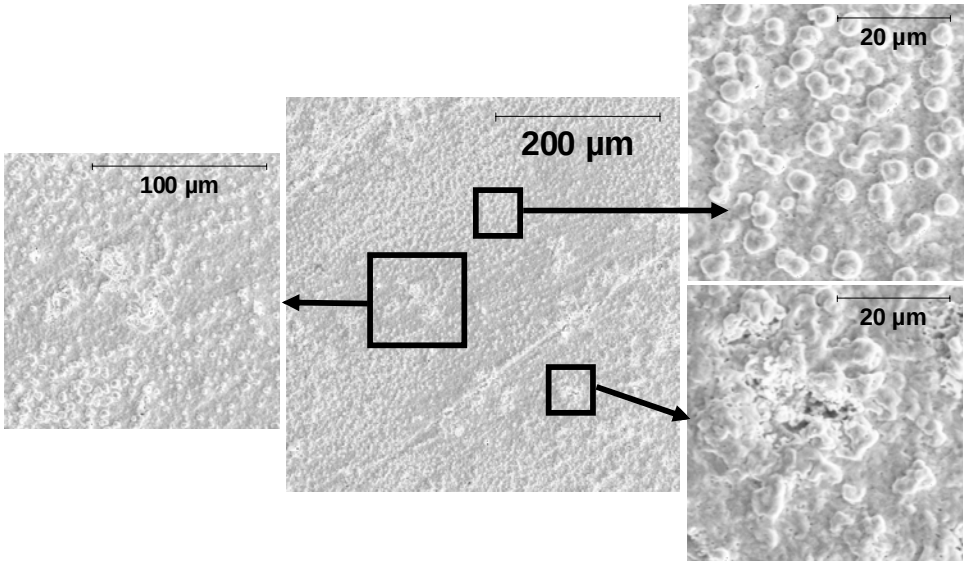

(a) 60Pd-Cu surface, 450°C

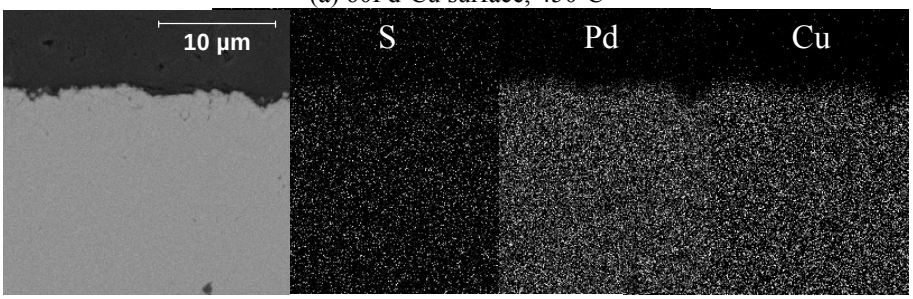

(b) 60Pd-Cu Cross Section Elemental Mapping, 450°C

Figure 41. SEM/EDS analysis of the membrane surface and cross section of the 100 µm60Pd-Cu membrane samples after exposure to 1000ppm H_2S / 10% He / H_2 for 120 hrs at 450°C and 620 kPa.

The membrane sample operated at 350°C exhibited a roughened surface, mostly attributed to the presence of small particles and islands, Figure 40(a). The small particles, which were generally less than 1 µm in diameter, did not appear to have a significant compositional

difference as compared to the bulk surface by EDS analysis, where Cu, Pd, and S were detected. However, the larger islands (~500 μm^2) exhibited grain definition within the islands and appeared to contain only Cu and S by EDS. XRD analysis of the surface revealed a predominant B2 Pd-Cu alloy with trace amounts of Cu_2S, Pd_4S, $Pd_{16}Cu_3S_7$ and fcc Pd-Cu alloy. Therefore, based on EDS and XRD data, the islands were most likely Cu_2S while the membrane surface was a mixture of Pd-Cu alloy, Pd_4S and $Pd_{13}Cu_3S_7$. EDS mapping of the membrane cross section exhibited a very thin sulfide layer on the surface, which indicates that the corrosion phenomenon for the 60Pd-Cu alloy was much less than that observed for the Pd and 80Pd-Cu alloy at 350°C.

The membrane sample operated at 450°C also exhibited surface roughening and particle formation, Figure 41. EDS analysis of the surface of this membrane sample showed the presence of Pd, Cu and S, similar to that observed for the sample operated at 350°C. However, the particles observed on the surface were much larger (~5 μm diameter) and more regular in shape than that observed at lower temperatures. EDS analysis indicated that the particles contained only Pd and Cu. XRD analysis revealed a significant amount of B2 alloy, fcc alloy and trace amounts of $Pd_{13}Cu_3S_7$. Therefore, based on the EDS and XRD results, the "top" most surface of the membrane is $Pd_{13}Cu_3S_7$, with the particles and membrane subsurface containing a combination of B2 and fcc Pd-Cu alloy. EDS mapping of the membrane cross section revealed no detectable sulfide scale on the surface of the sample.

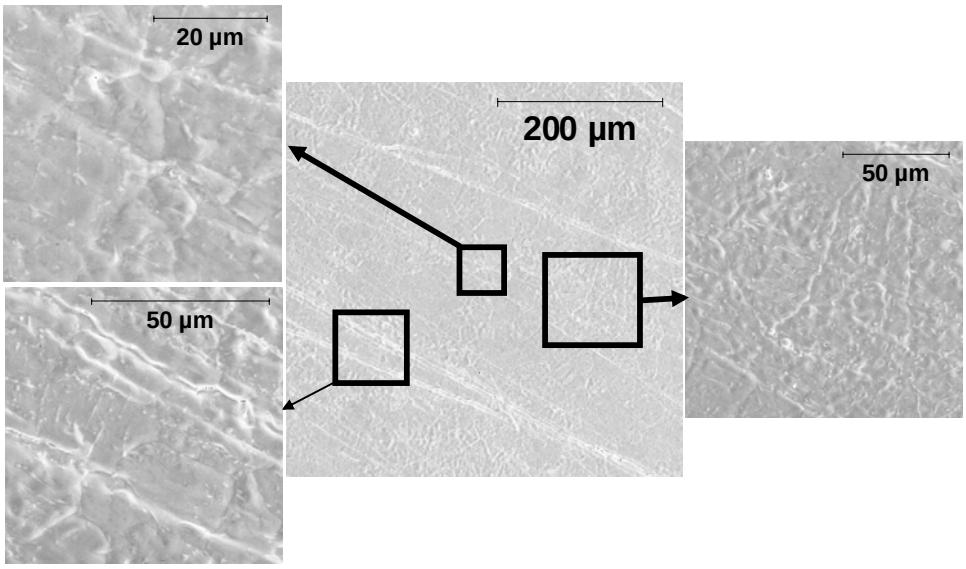

(a) 60Pd-Cu surface, 635°C

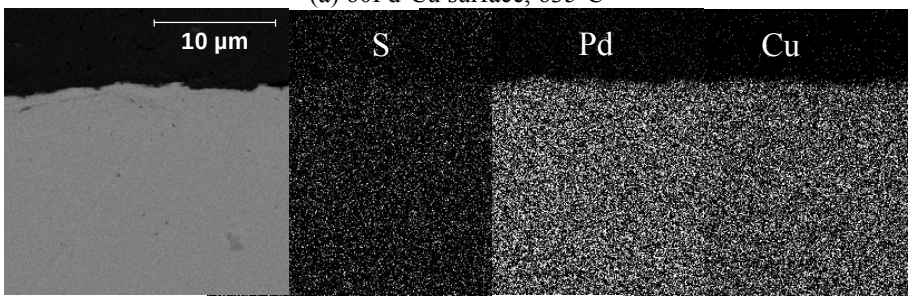

(b) 60Pd-Cu Cross Section Elemental Mapping, 635°C

Figure 42. SEM/EDS analysis of the membrane surface and cross section of the 100 µm 60Pd-Cu membrane samples after exposure to 1000ppm H_2S / 10% He / H_2 for 120 hrs at 635°C and 620 kPa.

The sample operated in the presence of the H_2S-gas mixture at 635°C appeared to have a much smoother surface as compared to the two previously described 60Pd-Cu samples, Figure 42. SEM analysis of the sample revealed what appeared to be several parallel lines and the formation of faint grain boundaries on the surface. The parallel lines on the surface were determined to be residual markings from pre-test polishing. EDS and XRD analysis of the sample surface as well as EDS elemental mapping of the membrane cross section revealed no detectable sulfur as well as no discernable elemental differences over the entire surface.

4.3.4.4 53Pd-Cu Three, 100 μm 53Pd-Cu membranes were examined in a similar fashion as the other membrane samples studied in this section. Each membrane was tested at one temperature, 350°C, 450°C or 635°C, in the presence of 1000ppm H_2S/ 10%He/ H_2 for 120 hrs. Figure 43 shows the hydrogen flux results of the 53Pd-Cu membranes as a function of exposure time in the presence of the H_2S gas mixture.

The trends in hydrogen flux in the presence of H_2S observed for the 53Pd-Cu membrane samples were very similar to those observed for the 60Pd-Cu samples. At 350°C and 450°C, the hydrogen flux exhibited a significant decrease, greater than 97% at each temperature. However, at 635°C no significant changes in hydrogen flux was observed upon the introduction of the H_2S gas mixture although the flux was approximately 22% lower than the predicted values based on Figure 21.

The 53Pd-Cu membrane sample operated at 350°C exhibited significant particle formation on the surface, Figure 44. The particles examined were of varying size (sub-micron to 10 microns in diameter) and contained S with varying combinations of Pd and Cu. Although XRD analysis revealed only trace amounts of Cu_2S and $Pd_{13}Cu_3S_7$, EDS analysis indicated that only a very small portion of the membrane surface did not contain sulfur. Additionally, XRD analysis revealed mostly B2 Pd-Cu alloy present, while EDS elemental mapping indicated that the sulfur surface scale was very thin.

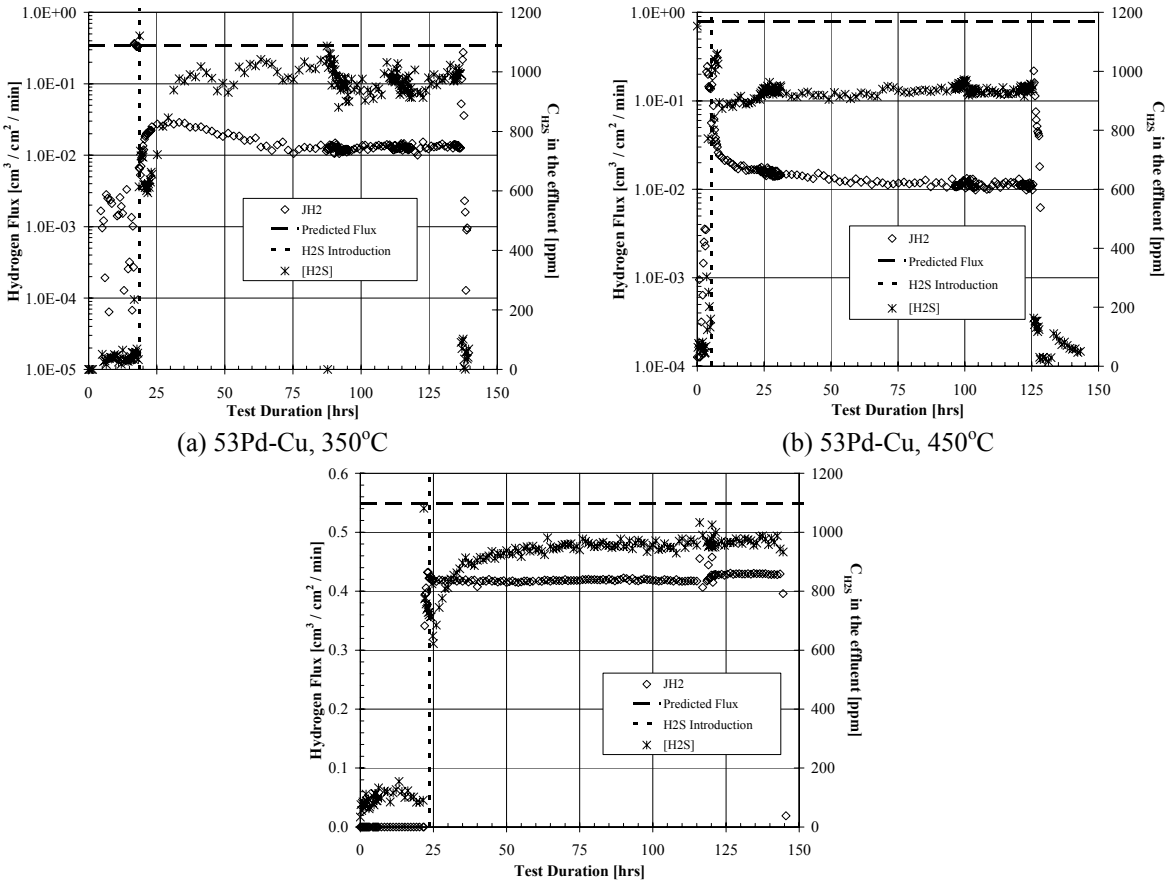

(a) 53Pd-Cu, 350°C

(b) 53Pd-Cu, 450°C

(c) 53Pd-Cu, 635°C

Figure 43. Flux results of the 100 μm 53Pd-Cu membrane samples in the presence of 1000ppm H_2S/ 10%He/ H_2 as a function of exposure time. (a) 53Pd-Cu at 350°C. (b) 53Pd-Cu at 450°C. (c) 53Pd-Cu at 635°C.

Figure 45 shows the SEM images of the 53Pd-Cu alloy after exposure at 450°C and the elemental mapping of the membrane cross-section. The SEM/EDS analysis revealed surface islands containing Cu and S on top of a surface of Pd, Cu and S while XRD analysis showed the presence of B2 Pd-Cu alloy and Cu_2S. Similar to the 53Pd-Cu sample operated at 350°C, the 450°C sample showed no significant sulfur scale by EDS elemental mapping.

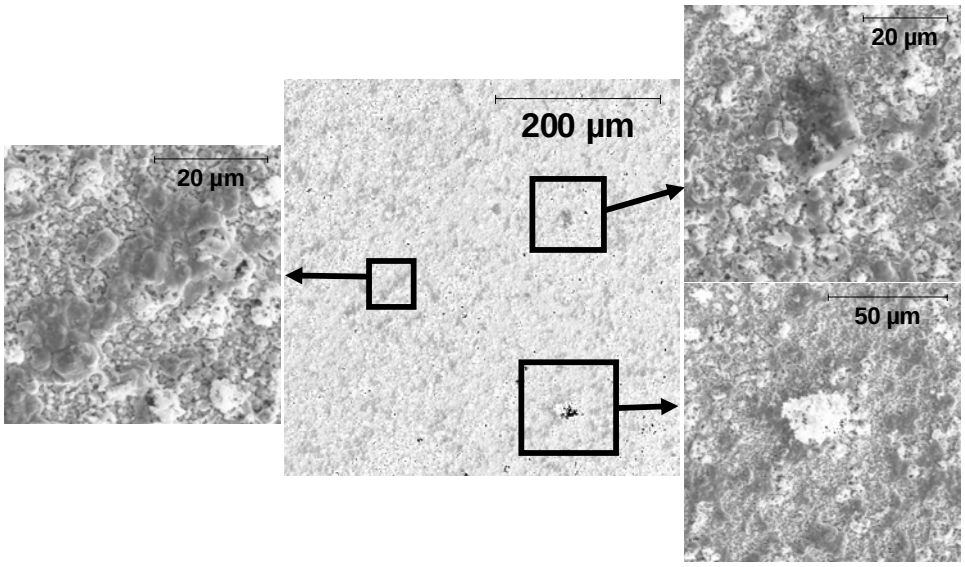

(a) 53Pd-Cu surface, 350°C

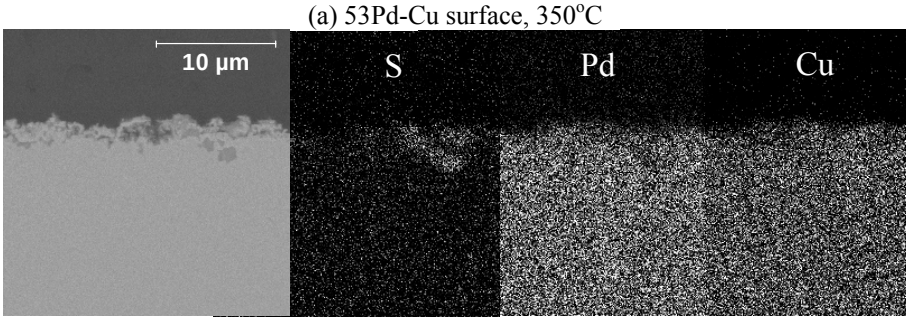

(b) 53Pd-Cu Cross Section Elemental Mapping, 350°C

Figure 44. SEM/EDS analysis of the membrane surface and cross section of the 100 µm53Pd-Cu membrane samples after exposure to 1000ppm H_2S / 10% He / H_2 for 120 hrs at 350°C and 620 kPa.

SEM images of the membrane sample operated at 635^{o}C in the presence of the H_2S-containing gas mixture are shown in Figure 46. Similar to the 60Pd-Cu sample operated at 635^{o}C, the 53Pd-Cu sample exhibited relatively small changes in surface morphology. The 53Pd-Cu sample showed significant evidence of residual polishing lines as well as the formation of faint grain definition. However, XRD analysis coupled with EDS surface analysis and EDS elemental mapping of the membrane cross-section revealed no sulfide surface scale and the presence of only B2 Pd-Cu alloy. The presence of B2 alloy at an operating temperature of fcc stability was attributed to a rapid phase transition of the alloy during the post-test cooling process.

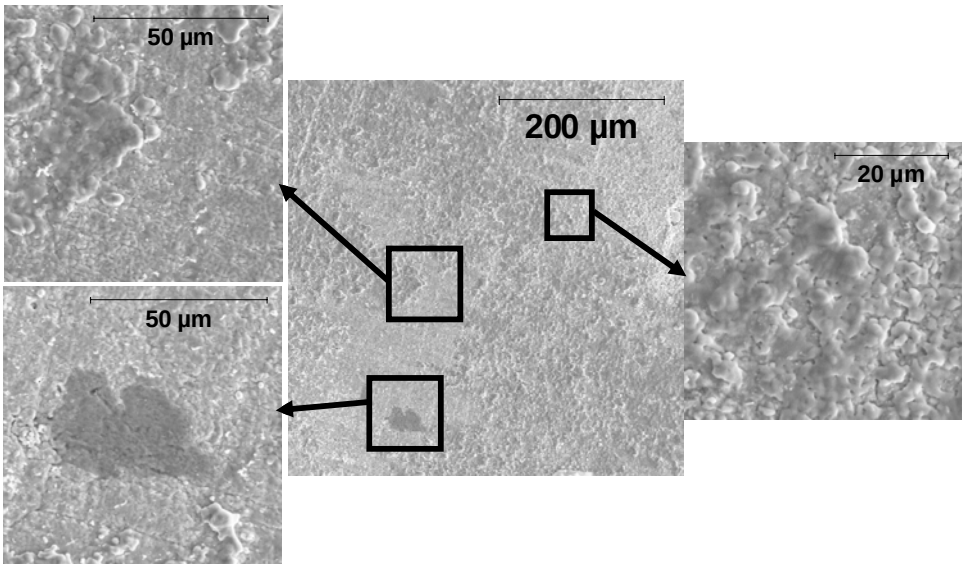

(a) 53Pd-Cu surface, 450°C

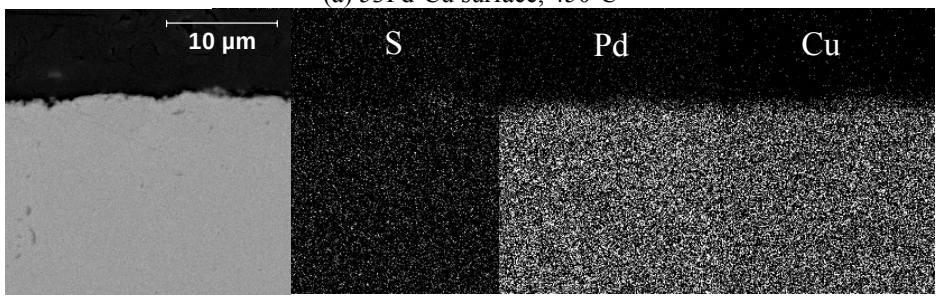

(b) 53Pd-Cu Cross Section Elemental Mapping, 450°C

Figure 45. SEM/EDS analysis of the membrane surface and cross section of the 100 µm53Pd-Cu membrane samples after exposure to 1000ppm H_2S / 10% He / H_2 for 120 hrs at 450°C and 620 kPa.

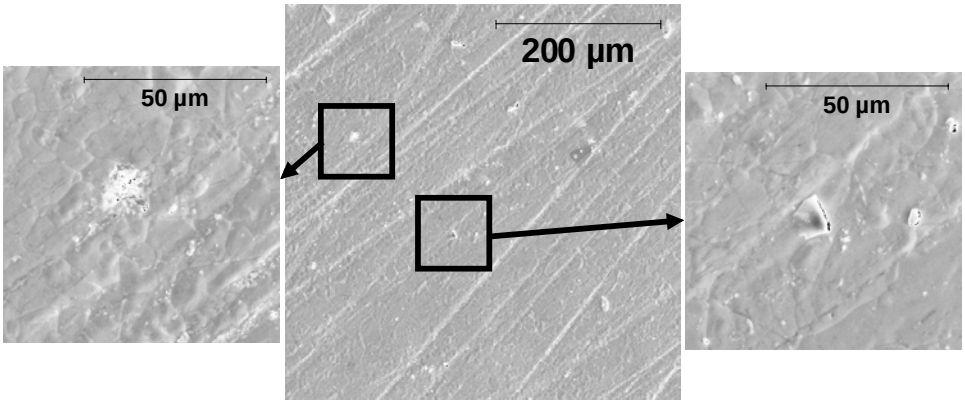

(a) 53Pd-Cu surface, 635°C

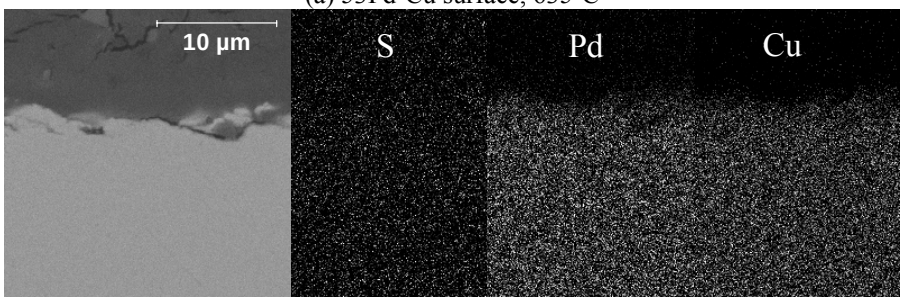

(b) 53Pd-Cu Cross Section Elemental Mapping, 635°C

Figure 46. SEM/EDS analysis of the membrane surface and cross section of the 100 µm53Pd-Cu membrane samples after exposure to 1000ppm H_2S / 10% He / H_2 for 120 hrs at 635°C and 620 kPa.

4.3.4.5 Long Term H2S Exposure Summary The flux results and sulfur uptake of the Pd and Pd-Cu alloys exposed to the 1000 ppm H_2S/ 10% He / H_2 mixture after ~120 hours is summarized in Figure 47. The Pd samples all exhibited a gradual decline in hydrogen flux with increasing exposure time and a significant Pd_4S scale. Decreases in flux for the Pd membranes of 71%, 79% and 80% were observed at 350, 450 and 635°C, and corresponded to a Pd_4S scale thickness of ~9, ~15 and ~25 microns, respectively.

The 80Pd-Cu sample, which also has an fcc crystal structure throughout the entire temperature range of study, exhibited scale growth only at 350 and 450°C, with a complex, ~5

μm multi-layered scale (Pd_4S-$Pd_{13}Cu_3S_7$-Pd-Cu metal) and a ~3 μm Pd_4S scale, respectively. Additionally, at exposures where the multilayered scale was observed (350°C) the flux decreased 98% within the first hour of exposure and continued to decrease continuously, resulting in a total reduction of 99%. At an exposure of temperature of 450°C, where a ~3 μm Pd_4S scale was observed, the flux of the 80Pd-Cu alloy gradually decreased over the 120 hour exposure time to a value of ~65% of the expected value in H_2. At 635°C, no sulfide growth was detected on the 80Pd-Cu alloy and no changes in H_2 flux was observed with increasing exposure time to the H_2S gas mixture. These results give strong implications that the 80Pd-Cu is resistant to poisoning and corrosion at a temperature of 635°C, but suffers significantly from sulfidation at temperatures of 350 and 450°C.

The 53Pd-Cu and 60Pd-Cu alloys, which exhibit B2 crystalline structure at temperatures below 600 and 475°C, respectively, showed no significant scale growth at any of the temperatures studied. At exposure temperatures of 350 and 450°C, the B2 alloys showed trace amounts of Cu_2S, Pd_4S, and/or $Pd_{13}Cu_3S_7$ and exhibited decreases in flux of greater than 75%. However, during exposure at 635°C, where the alloys have an fcc crystalline structure, a negligible change in hydrogen flux was observed for the 60Pd-Cu alloy while a 20% reduction in flux was observed for 53Pd-Cu alloy.

In summary, in alloys exhibiting an fcc crystalline structure and form rather thick sulfides scales, it appears that the observed hydrogen flux may be directly linked to the corresponding growth rate of the sulfide scale. As the sulfide scale grows, the hydrogen flux through the scale will also decrease (assuming the scale has a lower permeability than the membrane), due to the hydrogen flux being inversely proportionally to the membrane (or scale) thickness.

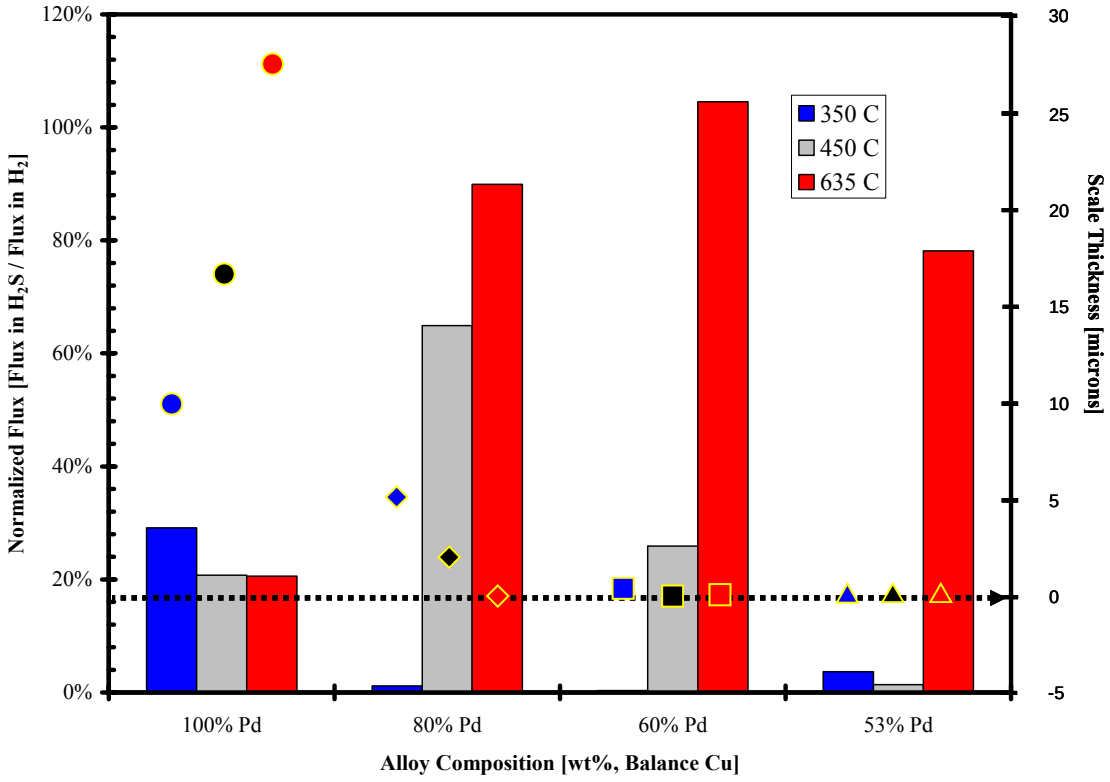

Figure 47. Summary of the influence of the H_2S gas mixture on alloy flux after 120hrs of exposure. The data in the form of solid boxes correspond to the sulfide scale thickness determined by elemental mapping of the membrane cross-sections and XRD of the membrane surface.

Membrane samples which do not exhibit significant sulfide scale growth but still demonstrate a significant decrease in hydrogen flux, the membrane surface is probably not providing the atomic hydrogen needed for the hydrogen transport process and thus inhibiting membrane flux, via a competitive adsorption mechanism.

However, several membrane and temperature combinations were observed where neither scale growth occurred nor a decrease in hydrogen flux was observed (i.e. 60Pd-Cu at 635^{o}C). The conditions where H_2S appears to have insignificant impact on performance are possibly attributed to insufficient blocking of adsorption sites by adsorbed sulfur and thermodynamic instability of low permeability, metal sulfides.

4.4 PD, CU AND PD-CU CORROSION

In an effort to determine influence of H_2S on the mechanical and chemical stability along with the influence of corrosion rate on the performance of the aforementioned potential membrane alloys, several experiments were conducted in attempt to study the sulfide growth rate. Metal coupons with compositions of Pd, 80Pd-Cu, 60Pd-Cu, 53Pd-Cu and Cu were studied at temperatures of 350, 450 and 635^{o}C at a pressure slightly above atmospheric. Figure 48 illustrates the results of the corrosion studies at temperatures of 350, 450, and 635^{o}C.

The change in mass per unit area of the sample coupons was fit to Equation 4-7 for the corrosion of metals[148]. The constants developed from the kinetic experiments allowed for the

quantification of sulfide thickness ($X_{M\text{-}S}$) for simple scale formations (single sulfide scale) or sulfur uptake for more complex scales (multiple sulfide scale) as a function of exposure time, which are detailed in **Table 5**.

$$\frac{\Delta m}{SA} = kt^{y} \text{ or } X_{M-S} = k't^{y} \qquad (4\text{-}7)$$

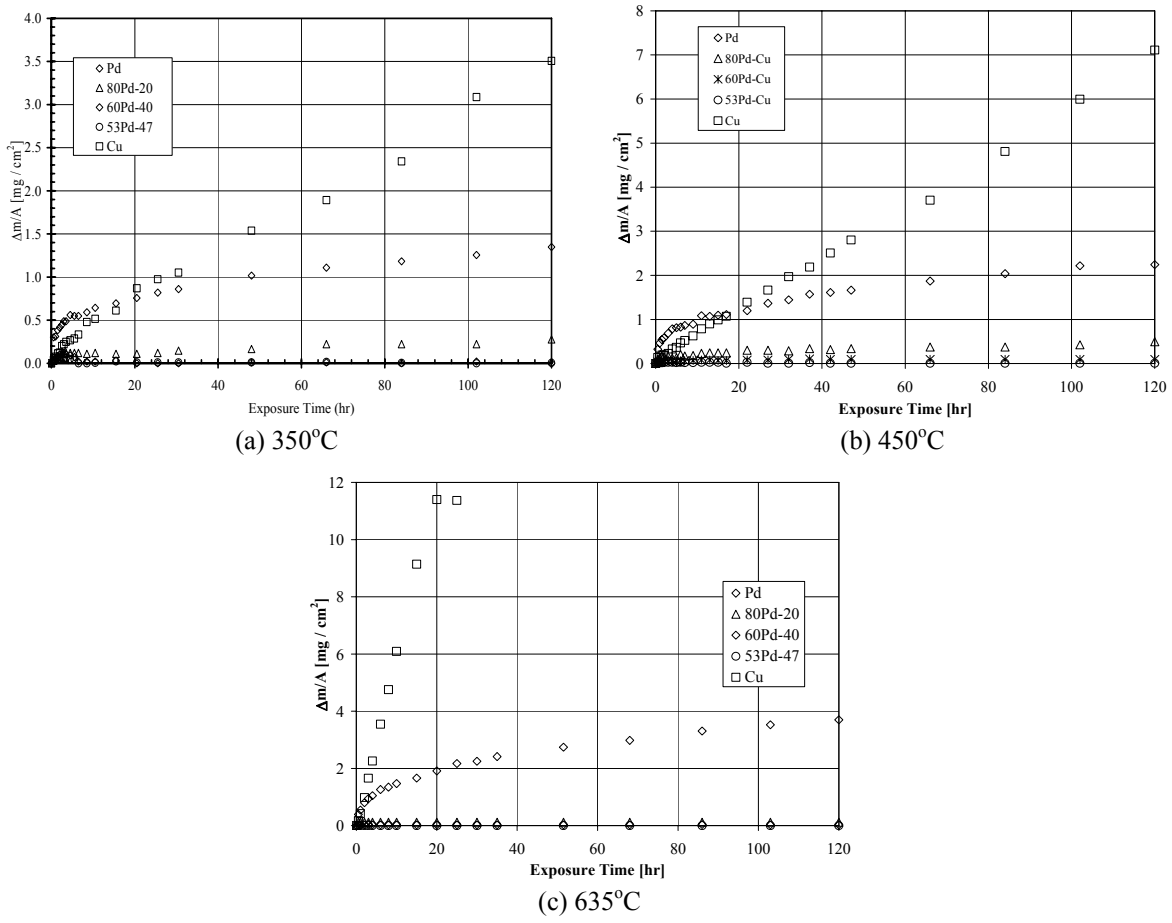

(a) 350°C (b) 450°C

(c) 635°C

Figure 48. Kinetic evaluation of Pd, 80Pd-Cu, 60Pd-Cu, 53Pd-Cu and Cu samples as a function of exposure time at (a) 350°C, (b) 450°C and (c) 635°C.

Table 5. Kinetic parameters of sulfur uptake for various Pd-Cu alloys in the presence of 1000ppm H_2S / 10%He / H_2 at atmospheric pressure for equation (4-7).

Alloy	350°C			450°C			635°C		
	k	y	R^2	k	y	R^2	k	y	R^2
Pd	0.341	0.278	0.991	0.453	0.338	0.993	0.578	0.397	0.995
80Pd-Cu	0.065	0.272	0.768	0.115	0.278	0.909	NA	NA	NA
60Pd-Cu	NA	NA	NA	0.043	0.196	0.867	NA	NA	NA
53Pd-Cu	NA	NA	NA	NA	NA	NA	NA	NA	NA
Cu	0.081	0.775	0.993	0.059	1	0.998	0.587	1	0.977

Note: k has units of [mg cm^{-2} hr^{-y}]. * The Cu foil was totally sulfided after 30 hrs of exposure at 635°C.

At all of the temperatures evaluated, the sulfur uptake of the Pd samples was highest as low exposure times, less than approximately 20 hrs. The rapid uptake by the Pd samples at short exposures illustrates the high reactivity of the metal with respect to S (the most reactive material in this study at short durations). However, at exposure times greater than approximately 20 hrs, the Cu samples exhibited the largest sulfur uptake. The change in uptake trends for the Pd and Cu samples at exposures greater than ~20 hrs is attributed to the sulfide growth becoming "more" diffusion limited in the Pd samples, as evident by the time exponents given in Table 5. The diffusion path for new sulfide growth may be the transport of M-cations to the scale gas interface or the S-anions to the metal-scale interface. Figure 49 gives evidence of the primary growth mechanism exhibited for the Pd sample at 635°C. A strand of reactor insulation, which was inadvertently placed on the surface of the coupon sample, was consumed by the scale growth. This observation gives evidence of the scale growth is attributed to the diffusion of Pd-cations to the scale-gas interface, followed for the formation of new scale. Thus, at times greater than ~20 hrs, it appears that the diffusion of Pd-cations to the scale-gas interface limits the growth rate of the Pd-S system as compared to the Cu-S system.

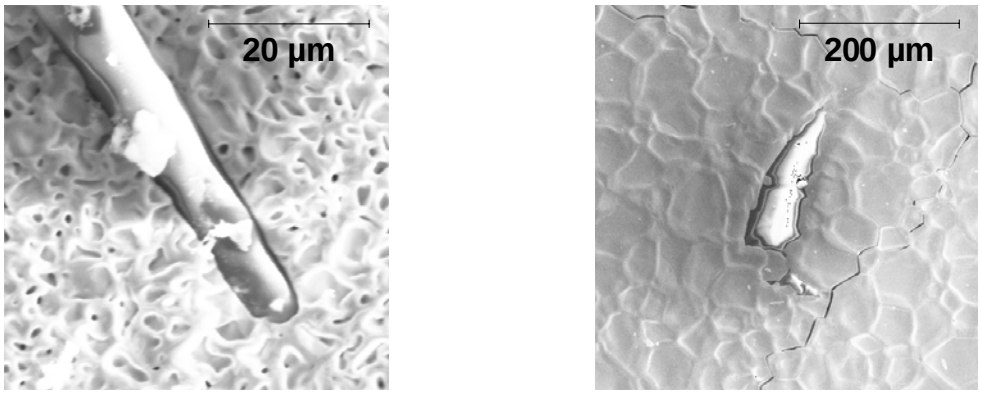

(a) 350°C (b) 635°C

Figure 49. Illustration of Pd based scale growth over a "non-reactive" surface deposit at (a) 350°C and (b) 635°C as observed during membrane testing.

The sulfur uptake of the 80Pd-Cu alloy was much less than that observed for the Pd samples at all of the temperatures studied, 79% less at 350°C, 78% less at 450°C while no sulfur uptake was observed for the 80Pd-Cu alloy at 635°C. The weight change for the 60Pd-Cu and 53Pd-Cu samples were negligible as a function of exposure time and temperature for all of the conditions studied. Additionally, the weight changes observed for the abovementioned alloys qualitatively agrees with the scales observed by SEM/EDS elemental mapping of the coupon cross sections, Figures 50, 51 and 52.

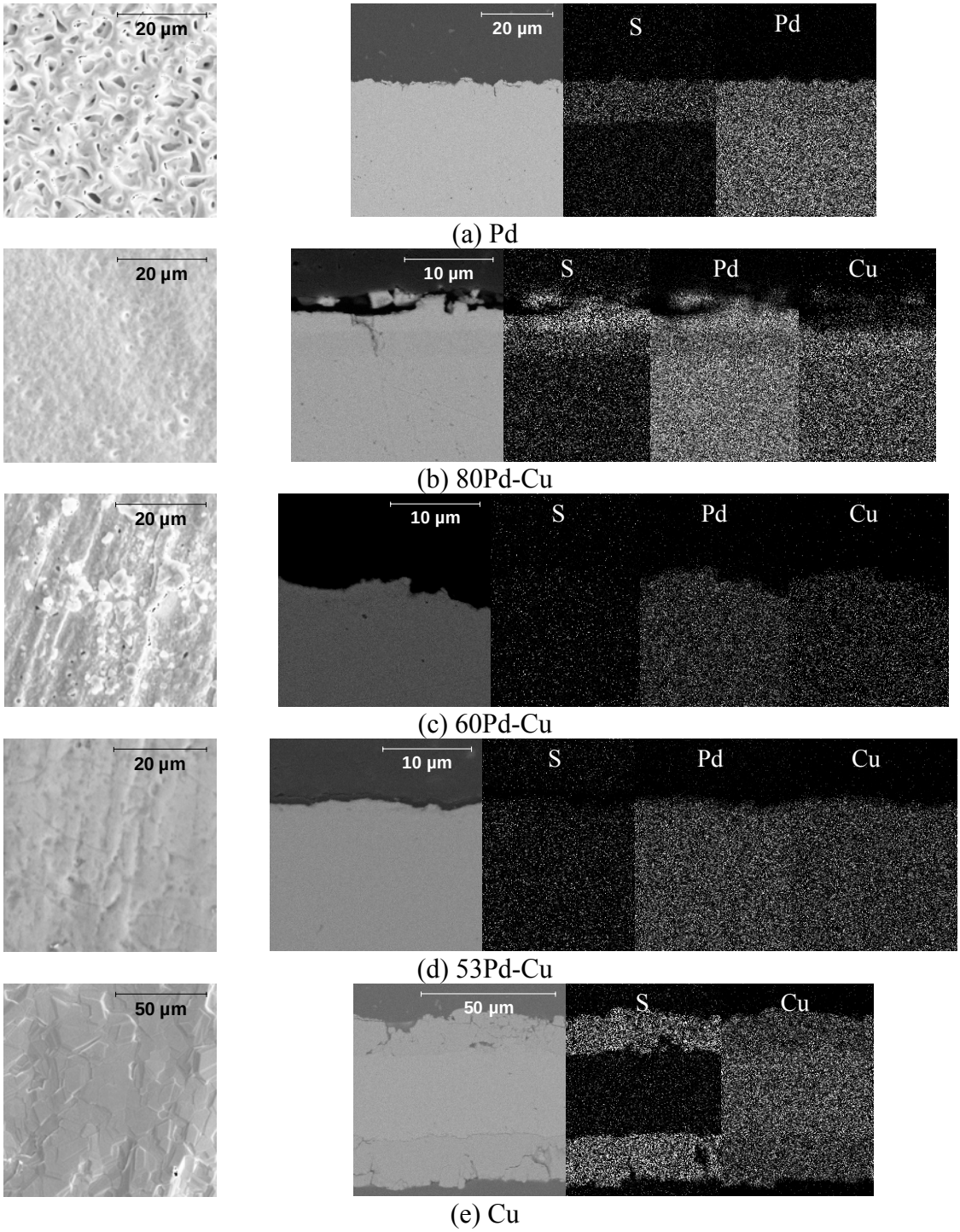

Figure 50. SEM surface images and EDS mapping of the cross sections of the coupon samples after exposure to 1000ppm H_2S / 10%He / H_2 at 350^oC for 120 hrs. (a) Pd, (b) 80Pd-Cu, (c) 60Pd-Cu, (d) 53Pd-Cu, (e) Cu.

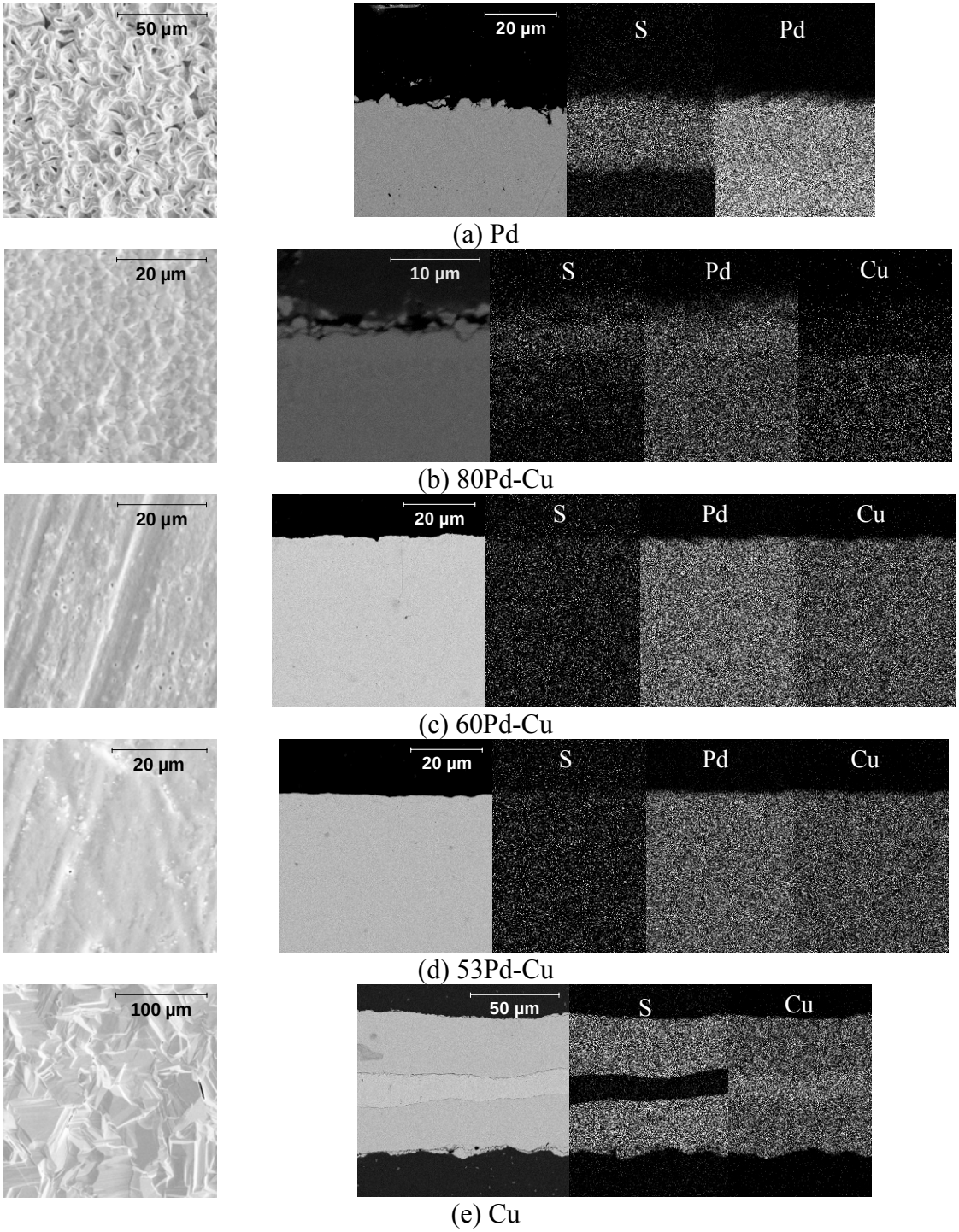

Figure 51. SEM surface images and EDS mapping of the cross sections of the coupon samples after exposure to 1000ppm H_2S / 10%He / H_2 at 450^oC for 120 hrs. (a) Pd, (b) 80Pd-Cu, (c) 60Pd-Cu, (d) 53Pd-Cu, (e) Cu.

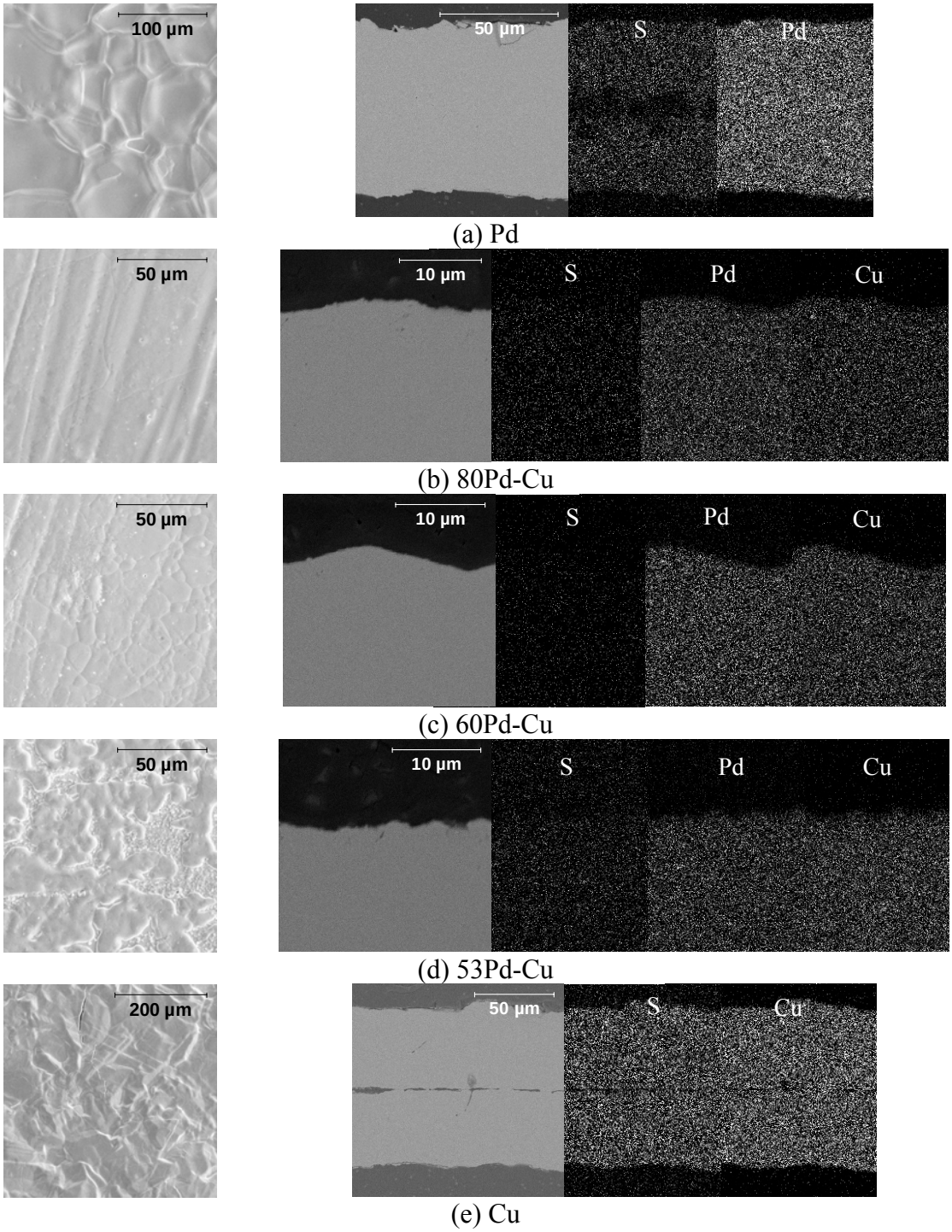

Figure 52.SEM surface images and EDS mapping of the cross sections of the coupon samples after exposure to 1000ppm H_2S / 10%He / H_2 at 635^oC for 120 hrs. (a) Pd, (b) 80Pd-Cu, (c) 60Pd-Cu, (d) 53Pd-Cu, (e) Cu.

The scales observed on the coupon samples during the corrosion study varied from an apparently pure sulfide scale, to a multi-layered sulfide scale, to no sulfide growth. The scales observed on the pure Pd and Cu scales were rather simple, where only Pd_4S and CuS_2 were detected by XRD, respectively. The rather simple scale formation of the pure Pd and Cu samples allowed for the direct correlation of the weight gain of the coupon sample to the thickness of the sulfide. Figure 53 illustrates the scale growth of the Pd and Cu samples as a function of exposure time.

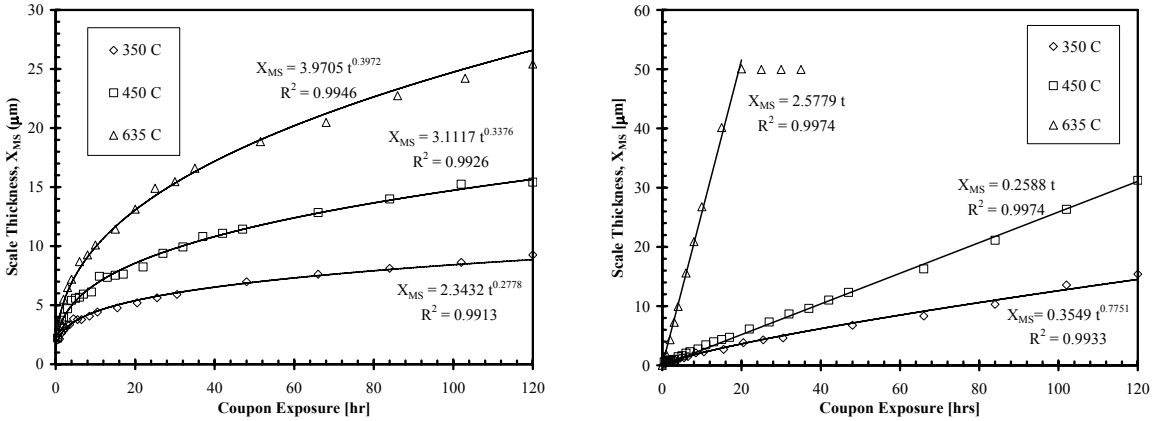

(a) Pd (b) Cu

Figure 53. Evaluation of the scale thickness of the (a) Pd and (b) Cu coupons as a function of time in the presence of 1000 ppm H_2S / 10%He / H_2.

A comparison of the estimated sulfide thickness by SEM cross section and the thickness calculated by the weight gain of the pure Pd and Cu samples was within 10% over all of the temperatures studied in the work. Moreover, the weight gain by the pure Cu at 635^oC corresponded to a total sulfidation of the specimen (Figure 53), and was verified by SEM (Figure 52(e). Therefore, the agreement observed between the thickness of the scales on the pure Pd and Cu samples validated the methodology of the sulfide thickness determination by specimen weight change.

The 80Pd-Cu alloy was somewhat more complex than any of the pure metals studied. At a temperature of 350°C, the 80Pd-Cu coupon exhibited a multi-layered scale. EDS elemental mapping of the specimen cross section coupled with XRD results gave evidence that the layers observed on the coupon were Pd_4S at the gas/scale interface, $Pd_4S/Pd_{13}Cu_3S_7$ at the scale/scale interface and $Pd_{13}Cu_3S_7$/B2 Pd-Cu alloy at the scale/metal interface, Figure 50. These results give evidence that enough of the Pd and/or copper were removed from the metal to induce the formation of a B2 alloy. The corrosion phenomenon for the 80Pd-Cu alloy at 450 and 635°C were much simpler than that observed at 350°C. The scale observed by EDS cross section analysis and XRD at 450°C appeared to consist only of a Pd_4S surface scale with a thickness of ~1-2 μm (Figure 51 (b)) while at 635°C no surface scale was observed (Figure 52(b)).

The corrosion study of the 60Pd-Cu and 53Pd-Cu alloys were the simplest of all the alloys studied in that at all of the temperatures studied, no sulfides scales were observed on any of the test specimens.

The trends observed during the coupon testing (this section) and those observed during the long-term membrane exposure testing (Section 4.3) were very similar. For example, the palladium coupons exhibited a sulfide thickness of ~ 10, 20 and 30 microns at 350, 450 and 635°C, respectively, while Pd membranes exposed to similar conditions during flux testing exhibited thicknesses of ~9, 15 and 25 μm at similar temperatures.

Additionally, the 80Pd-Cu alloys exhibited a similar corrosion behavior in the corrosion study and the membrane testing in the presence of the H_2S gas mixture. At 350°C, the 80Pd-Cu

alloy exhibited a multi-layered corrosion product with a thickness of ~4-5 μm for both the corrosion and membrane testing while at 450°C only a thin (~1-2 μm) Pd_4S layer was observed in both test methods.

At all temperatures studied, the coupon exposures resulted in no detectable surface sulfides for the 60Pd-Cu and 53Pd-Cu alloys. However, similar trends were not observed for the membranes exposed at similar conditions and durations. Although no significant sulfide growth was observed during membrane testing via elemental mapping of the membrane cross sections, significant surface modification and "surface" sulfides was observed by SEM/EDS and XRD analysis of the membrane surface. The 60Pd-Cu and 53Pd-Cu alloys often exhibited surface segregation and the presence of varying combinations of Pd, Cu and S. The differences observed between the membrane testing and the coupon exposures may be attributed to the mobility of H_2 in the membrane samples inducing alloy segregation and thus producing thermodynamically stable metal-sulfide systems.

4.5 INFLUENCE OF SCALE GROWTH ON HYDROGEN FLUX

The decreases observed in hydrogen flux for several of the membranes during the long term exposure testing in the presence of the H_2S gas mixture was attempted to be correlated with the trends observed for sulfide growth rate. The methodology used to determine the influence of scale growth on the hydrogen flux is analogous heat conduction through a composite wall or a multi-layered membranes and is illustrated in Figure 54. The first assumption in the development of the governing equation used in this methodology is that the hydrogen flux through the sulfide scale must be equal to the hydrogen flux through the metal membrane, Equation 4-8.

$$J_{H2}=J_S\,(\text{flux through the sulfide})=J_M\,(\text{flux through the metal}) \qquad (4\text{-}8)$$

Thus, assuming steady-state, the hydrogen flux through each layer of the membrane may be expressed by the generalized Richardson's Equation (4-9), where $P_{H2,1}$, $P_{H2,2}$ and $P_{H2,3}$ is an equivalent hydrogen pressure at the gas-scale interface, scale-metal interface and the metal-gas interface, respectively.

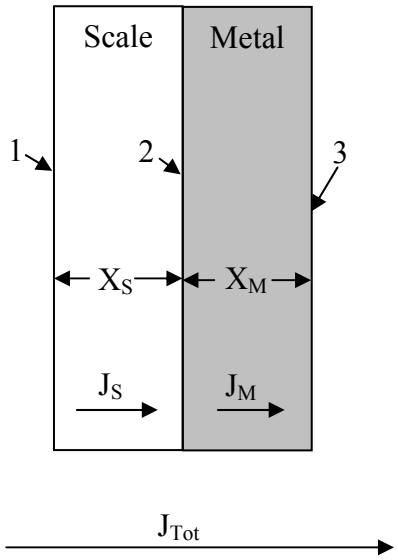

Figure 54. Illustration of the multi-layered membrane.

$$J_S = \frac{k_S}{X_S}\left(P^n_{H2,1} - P^n_{H2,2}\right) = \frac{1}{R_S}\left(P^n_{H2,1} - P^n_{H2,2}\right) \quad (4\text{-}9)$$

$$J_M = \frac{k_M}{X_M}\left(P^{0.5}_{H2,2} - P^{0.5}_{H2,3}\right) = \frac{1}{R_M}\left(P^{0.5}_{H2,2} - P^{0.5}_{H2,3}\right) \quad (4\text{-}10)$$

Since it is unclear if the hydrogen transport through the metal sulfide follows an diffusion limited atomic transport mechanism or a transport mechanism limited by surface reaction, Equation 4-9 is written in general terms, where n =0.5 or 1.0. Substitution of equations 4-10 into 4-9 and implementing the sulfide growth rate obtained in previous section, and assuming that the entire membrane thickness is roughly constant, the permeability of the sulfide layer and pressure driving force can be estimated by optimizing Equation 4-11.

$$J_T = \frac{k_M}{X_M}\left[\left(P_{H2,1}^{n} - \frac{J_T X_S}{k_S}\right)^{0.5/n} - P_{H2,3}^{0.5}\right] \qquad (4\text{-}11)$$

Figure **55**, Figure 56 and Figure 57 illustrates the optimized models for Equation 4-11 fit to the data presented in Section 4.1 (Figure 31) at 350, 450 and 635^{o}C in the presence of a H_2S gas mixture, respectively as well as the predicted scale thickness.

At all of the temperatures studied the decreases in hydrogen flux observed due to the growth of a sulfide scale on Pd is well characterized by equation 4-11 assuming that the Pd is diffusion limited and that the sulfide scale is either diffusion limited (n=0.5) or surface reaction limited (n=1.0). The hydrogen flux through the membrane and scale system is best described by the model when assuming that the rate limiting step in the process is the surface reaction at the sulfide scale (n=1.0). However, in both transport assumptions, the model appears to slightly underestimate the hydrogen flux at low exposure times and overestimate the flux at high exposure times, which was more significant for n=0.5.

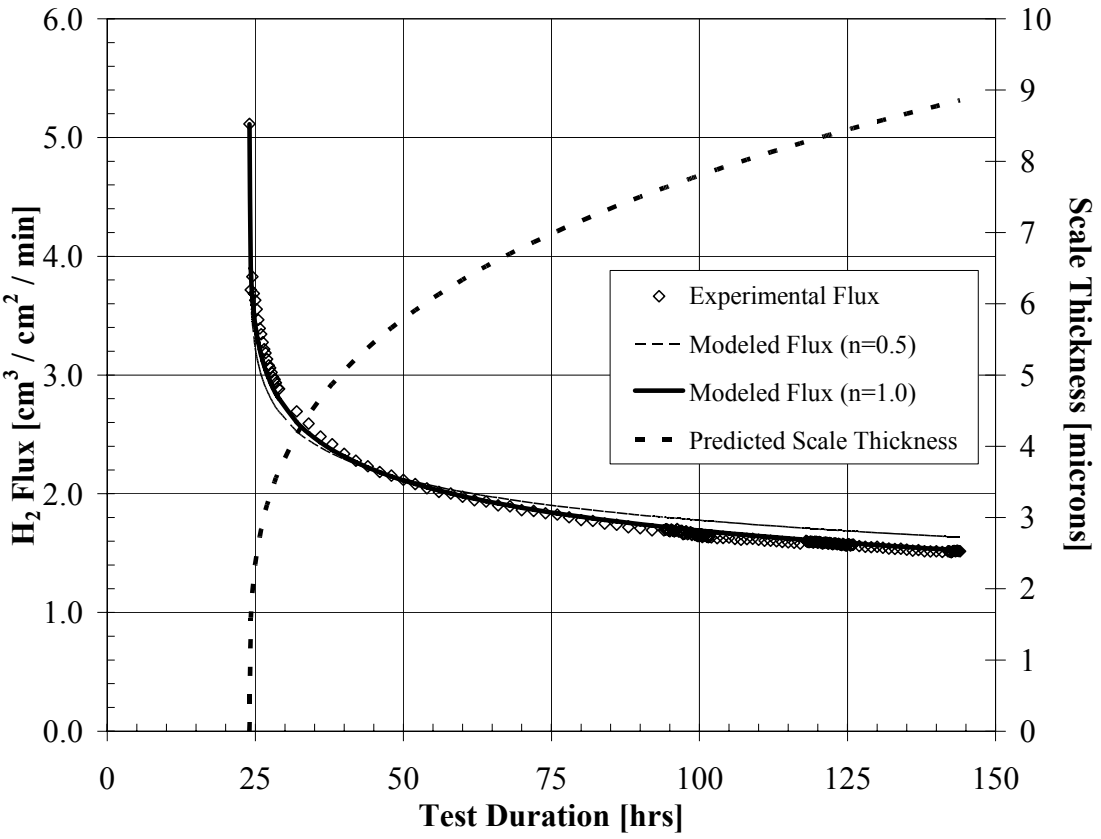

Figure 55. Model of the predicted flux through the continuously sulfiding Pd membrane as a function of exposure time at 350°C.

The permeability values for the Pd_4S sulfide scale obtained from Figures 55, 56 and 57 are illustrated in Figure 58 as a function of temperature and are compared to the permeability values obtained for Pd and several Pd-Cu alloys. Although the permeability of Pd_4S is better described by n=1.0, for comparative purposes the permeability is illustrated with both pressure exponents. The permeability values obtained for the Pd_4S (assuming a pressure exponent of 0.5) are approximately 20, 14 and 10 times lower than the pure palladium at 350, 450 and 635°C.

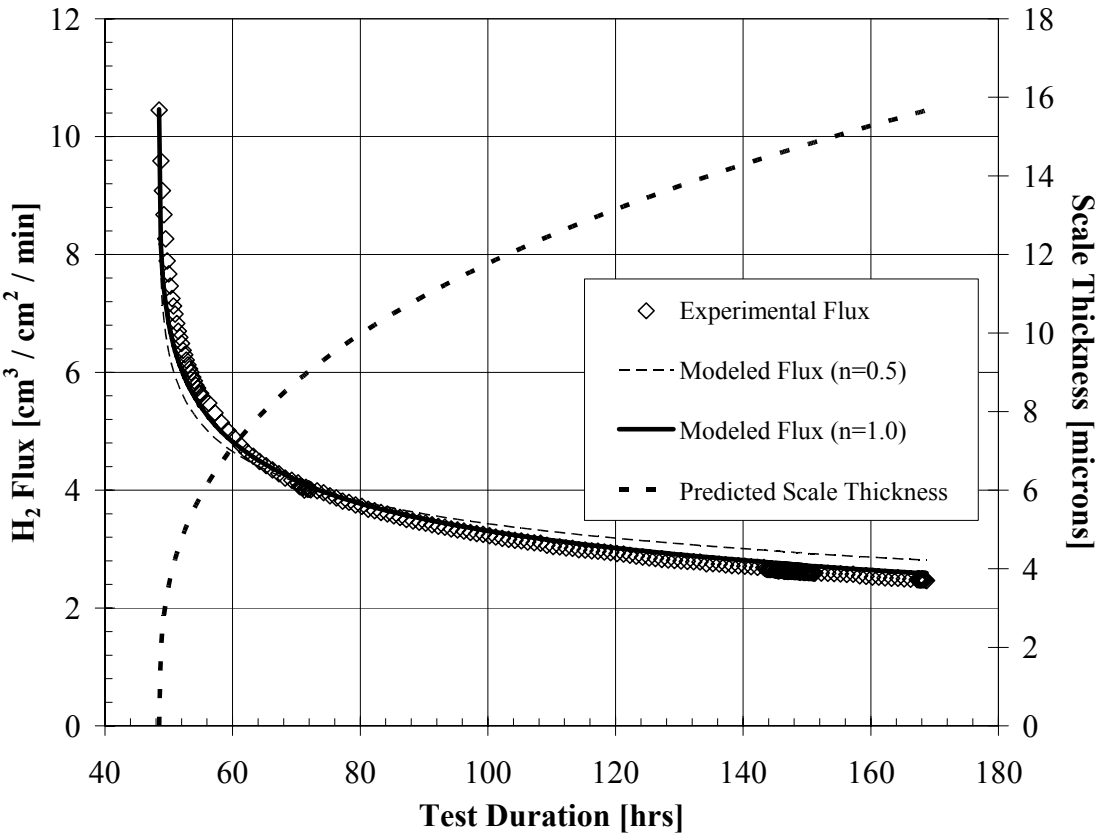

Figure 56. Model of the predicted flux through the continuously sulfiding Pd membrane as a function of exposure time at 450°C.

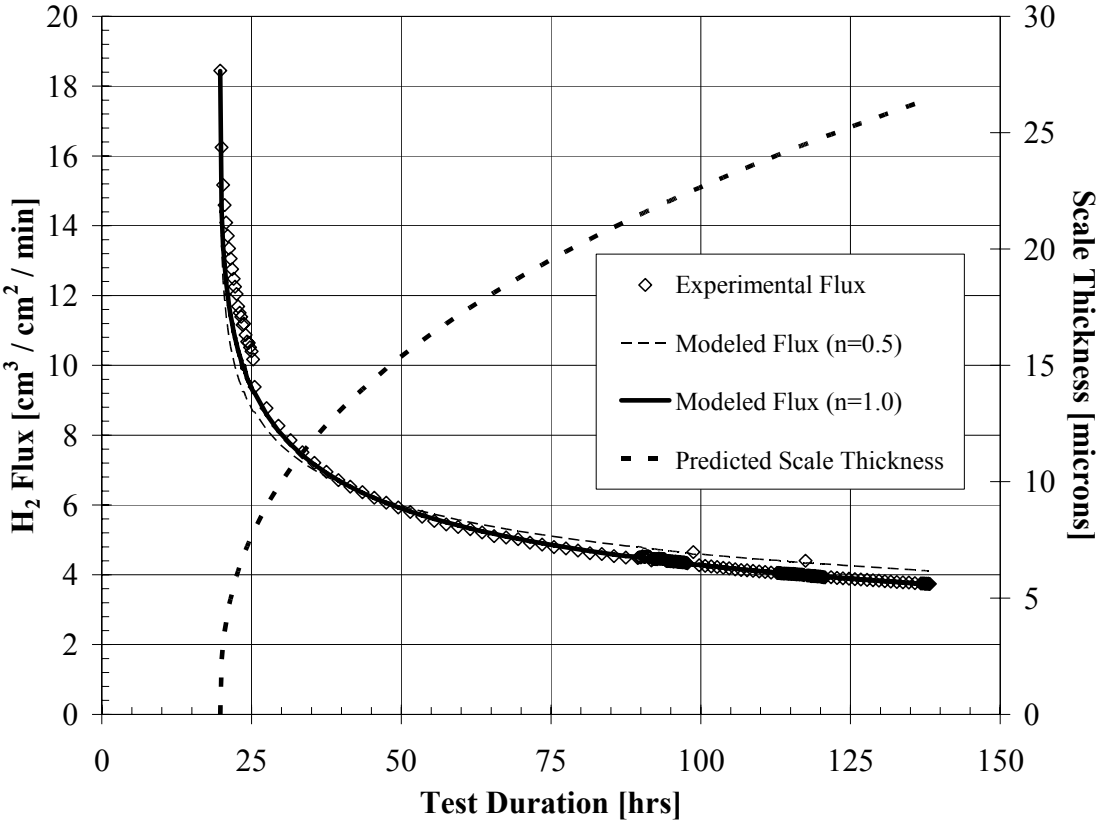

Figure 57. Model of the predicted flux through the continuously sulfiding Pd membrane as a function of exposure time at 635°C.

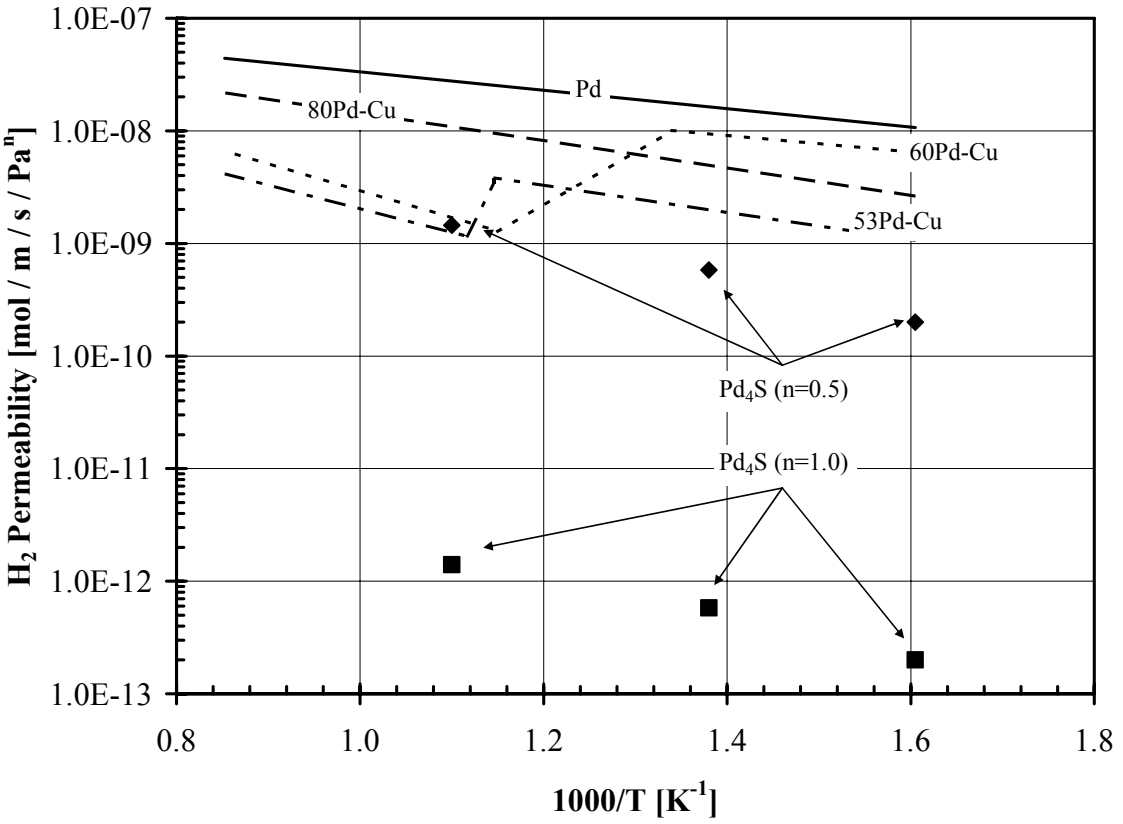

Figure 58. Permeability results of Pd_4S as a function of temperature and compared to the results from Section 4.0

5.0 SUMMARY

The intent of this work was to provide a through study of the permeability of the Pd-Cu system both in the presence and absence of hydrogen sulfide. The permeability of several metal foils (Pd, 80wt%Pd-Cu, 60wt%Pd-Cu, 53wt%Pd-Cu, Cu) were evaluated at temperatures which could be encountered in the gasification process, 350 to 900^{o}C. The metals selected for evaluation included pure Pd and Cu (end members of the Pd-Cu system), the 60wt%Pd-Cu alloy (the most widely investigate alloy of the system), the 80wt% alloy (due its crystalline homogeneity throughout the temperature range of study and its intermediate composition between pure palladium and the 60wt%Pd-Cu alloy) and lastly the 53wt%Pd-Cu alloy (which undergoes a direct crystalline phase transition from B2 to fcc).

Of the metals tested, palladium (both 100 and 1000 micron) exhibited the highest permeability in the presence of a 10%He-H_2 gas mixture at all of the temperatures studied. The performance of the alloy systems, assuming crystalline homogeneity (either all B2 or fcc), appeared to be proportionally to the atomic concentration of Pd (performance increases as Pd content increases).

The 60wt%Pd-Cu alloy exhibited the highest permeability of the Pd-Cu alloys tested at temperatures between 350 and ~475^{o}C, corresponding to a B2 crystalline structure. When the alloy was tested at temperatures ranging from ~475 to 600^{o}C, the permeability decreased with

increasing temperature, corresponding to a mixed B2-fcc crystalline region. At temperatures above 600^{o}C, corresponding to an fcc crystalline structure, the permeability of the alloy increased with increasing temperature, but was significantly lower than the B2 permeability.

The 80wt%Pd-Cu alloy, which exhibited an fcc crystalline structure through the entire temperature range of study, showed a trend of increasing permeability with increasing temperature. Additionally, the 80wt%Pd-Cu alloy had the highest permeability values of the Pd-Cu system at temperatures above ~475^{o}C. As compared to pure palladium, the 80wt%Pd-Cu alloy was roughly 75% and 50% lower at 350 and 900^{o}C, respectively.

The 53wt%Pd-Cu alloy exhibited similar trends with crystalline phase and performance as compared to the 60wt%Pd-Cu alloy. At temperatures corresponding to crystalline homogeneity (all B2 or fcc phase), the permeability increased with increasing temperature. Furthermore, the permeability of the 53wt%Pd-Cu alloy exhibited decreasing permeability trends associated with the transformation from B2 to fcc crystalline phase.

The performance of the palladium and palladium-copper alloys was more complex to evaluate in the presence of a 1000 ppm H_2S - 10% He - H_2 gas mixture. The complexity of characterizing the permeability of the alloys arose due to the use of several different test methods, the changing composition of the alloys with time due to metal extraction by the corrosion products, varying exposure durations, availability of H_2S, varying membrane thicknesses, incompatibility of membrane mounting methods with the H_2S atmosphere, the consumption of H_2S by the reactor materials, the deposition of sulfide scale from the reactor onto the membrane surface and the apparent differences in degradation mechanism.

The pure palladium membranes studied, with thickness of 100 and 1000 microns, showed significant decreases in performance in the presence of the H_2S gas mixture. The decrease in hydrogen flux observed with these membrane materials was dependent on the thickness of the membrane samples and the duration of exposure. A general trend of continually decreasing permeability with increasing exposure time was exhibited for all of the palladium membranes tested in the presence of the H_2S gas mixture. The 1000 microns thick sample exhibited decreases in hydrogen flux ranging from 25 to 50% (for exposure on the order of 25 hours at each temperature) while the 100 micron thick samples exhibited decreases ranging from 70 to 80% (for durations of 120 hours at each temperature) over 350 to 765^{o}C. XRD analysis, SEM images of the membrane surface, and elemental mapping of the membrane cross section of the post-exposed 100 micron palladium membrane samples revealed significant surface modification and the presence of a Pd_4S surface scale with thicknesses up to 30 microns.

In an effort to better understand the growth rate of the sulfide on palladium and in an attempt to correlate the decreases in hydrogen flux observed during membrane testing in the presence of the H_2S gas mixture, gravimetric studies were conducted using palladium coupons. The sulfide growth rate on palladium followed a parabolic rate law with the growth rate increasing with increasing temperature. Modeling of the flux decline observed during membrane testing along with the kinetics developed from the gravimetric studies resulted in the first reported value of the permeability of Pd_4S. Over the 350 to 635^oC temperature range, the permeability of Pd_4S is roughly 50 to 20 times less than pure palladium, respectively, assuming a partial pressure exponent of 0.5.

The permeability of the 80Pd-Cu alloy in the presence of the H_2S gas mixture was also evaluated using several experimental techniques, including the batch testing of 100 micron samples and steady-state testing of both 100 and 1000 micron membranes. The permeability results obtained using the batch testing method, which utilized a finite amount of H_2S and relatively short test exposures (typically less than 4 hours), suggested that the 80Pd-Cu alloy did not suffer any significant influence by the gas mixture at temperatures ranging from 350 to 900^oC. Similar results were observed during steady-state testing of 1000 micron 80Pd-Cu membranes, where no significant decreases in permeability under H_2S exposures typically in the range of 20 hours per temperature from 350 to 900^oC.

Due to the dependence of membrane thickness and test duration observed for the pure palladium membranes, additional testing of the 100 micron 80Pd-Cu alloys was conducted in a flowing gas system with a typical exposure time of 120 hours. The results obtained for the 100

micron samples in the flowing system were significantly different from the batch test of the100 micron samples and steady-state testing of the 1000 micron membranes. Following 120 hours of exposure to the H_2S gas mixture, a flux decrease of ~99% was observed at 350^oC. Characterization of the post-tested membrane revealed a modified surface topography and the presence of a layered sulfide (~2 micron thick Pd_4S on the outer most surface and ~2 micron thick sub-layer of $Pd_{13}Cu_3S_7$). At 450^oC, the 100 micron 80Pd-Cu membrane exhibited a decrease in hydrogen flux of ~35% after 120 hours of H_2S exposure. Post-test characterization of the membrane revealed a roughened membrane surface and the formation of a Pd_4S surface scale which had a thickness of ~2 microns. The membrane tested at a temperature at 635^oC did not appear to be influenced by H_2S. No decreases in flux or surface sulfide scales were observed.

The 80Pd-Cu alloy exhibited a negligible effect of H_2S on the permeability for short test exposures of 100 micron membranes and also for steady state testing of 1000 micron membranes, but significant permeability decreases were observed for long steady-state exposures of the 100 micron membranes at temperatures of 350 and 450^oC. These results suggest that the mechanism of permeability loss for the 80Pd-Cu over this temperature range was the formation of a surface sulfide scale with low hydrogen transport properties. Unfortunately, the decreases in hydrogen flux observed at 350 and 450^oC could not be correlated to the kinetic expression of the sulfide growth obtained from the gravimetric studies of the alloy. The correlation of sulfide growth and flux decrease could not be modeled due to the complexity of the corrosion product on the surface of the alloy and/or the uncertainty of the composition of the Pd-Cu alloy as a function of time. Where assuming the formation of a significant Pd_4S scale on the surface of an 80Pd-Cu membrane, the composition of the bulk may no longer be 80%Pd due to the extraction

of Pd, but will probably have a copper rich composition as compared to the starting alloy. At a temperature of 635^{o}C, long H_2S exposures of the 80Pd-Cu membranes to the H_2S gas mixture resulted in no detectable corrosion or poisoning phenomena, suggesting a condition of true sulfur resistance.

The 53Pd-Cu and the 60Pd-Cu alloys were tested in a similar fashion as the 80Pd-Cu alloy. The permeability of the alloys in the presence of the H_2S gas mixture was evaluated using experimental methods including the batch testing of 100 micron samples and steady-state testing of both 100 and 1000 micron foils. The batch testing of the 100 micron foils (finite amount of H_2S and exposure durations on the order of 2-hours) and the 1000 micron steady-state tests (infinite amounts of H_2S and exposure duration on the order of 24-hours) resulted in similar trends with respect to hydrogen flux and temperature. In both test methods, at temperatures greater than ~500^{o}C, the permeability of the alloys did not appear to be influenced by the H_2S containing gas mixture. However, at temperatures below ~500^{o}C significant decreases in hydrogen permeability were observed in both the 100 micron batch testing and the steady-state testing of 1000 micron foils. The decrease in permeability observed for the alloys was more significant at lower temperatures, where reductions as large as two orders of magnitude were observed at 350^{o}C.

Due to the differences observed in the previous alloys studied using the various test methods, the 53Pd-Cu and 60Pd-Cu alloys were evaluated in the presence of a flowing H_2S gas stream for exposures of ~120 hours. At test temperatures of 350 and 450^{o}C, the 53Pd-Cu and 60Pd-Cu alloys exhibited an immediate reduction in hydrogen flux upon the introduction of H_2S.

The reduction observed at 350 and 450°C for these alloys was greater than 97% and remained relatively invariant with respect to exposure time. Post-test characterization of the 53Pd-Cu and 60Pd-Cu membranes revealed surface particles and surface segregation which contained varying amounts of Cu, S and Pd. However, elemental mapping of the post-tested membrane cross sections revealed no significant sulfide scale for the 53Pd-Cu and 60Pd-Cu alloys. The 100 micron 53Pd-Cu and 60Pd-Cu alloys tested at a temperature of 635°C showed no change in hydrogen flux upon the introduction of the H_2S containing gas as well as no significant surface morphological changes or surface scale.

Therefore, it is apparent from the results of the 53Pd-Cu and 60Pd-Cu alloys which demonstrated significant decreases in hydrogen permeability for both thick and thin membrane samples in the presence of finite and infinite amounts of H_2S and varying exposure durations at temperatures below ~450°C that the mechanism inhibiting hydrogen flux is classical poisoning of a catalytic surface by the blocking of adsorption sites by adsorbed S. The competitive adsorption mechanism for decreasing the performance of palladium-based membranes has been hypothesized by many researchers[9, 77, 78, 84, 88]. However, at temperatures greater than ~635°C, it is apparent that the influence of H_2S on the poisoning and corrosion phenomena of the 53Pd-Cu and 60Pd-Cu is negligible for the thicknesses of the membranes studied.

In conclusion, it is apparent from the results presented in this study that Pd-Cu alloys with high Pd-content and having an fcc crystalline structure (80Pd-Cu and Pd) that the poisoning mechanism at temperatures of 350 and 450°C is attributed to the formation of a thick sulfide scale with low transport properties for hydrogen. The alloys studied that exhibit a B2 crystalline

phase, 53Pd-Cu and 60Pd-Cu, it is apparent that the competitive adsorption or the blocking of adsorption sites by S inhibits hydrogen flux at temperatures of 350 and 450^{o}C. Lastly, at a temperature 635^{o}C, all of the Pd-Cu alloys studied showed no significant permeability reductions or scale formation was observed in the presence of the H_2S gas mixture.

6.0 OUTLOOK

Although the pure palladium membrane had the highest performance value in the presence of hydrogen, the 60Pd-Cu alloy showed promise with respect to cost reduction potential. At current prices of Pd (~$10/gram), the 60Pd-Cu alloy has the potential of as large as a 20% savings in capital costs assuming similar surface area and thickness.

Membranes with high palladium content (pure palladium and 80Pd-Cu) suffer deleterious effects in the presence of H_2S. While the permeability of these metals is influenced by H_2S, mechanical impacts from sulfidation make them impractical where relatively thin foils are required (a 25 micron palladium membrane will completely sulfide in less than 1-yr at 350^oC).

Maybe the most significant observation of this study is the relative stable surface of the 60Pd-Cu and 53Pd-Cu alloys with respect to corrosion. Although the hydrogen flux through these membranes was considerably altered in the presence of a H_2S containing gases, the metal alloys remained relatively corrosion free. These observations may lead to the use of these alloys as membrane during intermittent H_2S exposure or as a method of protecting other highly corrosive metals.

Additionally of significant importance, was the observation that all of the Pd-Cu alloys tested appeared sulfur resistant at test temperatures of 635^{o}C. Upon the introduction of the H_2S containing gas mixture, no decreases in hydrogen flux were observed while characterization of the post-tested 80Pd-Cu, 60Pd-Cu and 53Pd-Cu alloys showed no formation of surface sulfides.

APPENDIX A

NOMENCLATURE

Symbol	Definition
X	Membrane thickness
K	Permeability
k´	Permeance
N	Hydrogen flux
P	Pressure
T	Temperature
C	Concentration
R	Universal gas constant
k_O	Pre-exponential constant
E_P	Activation energy of permeation
A	Area
T	Time
V	Volume
M	Mass
SA	Surface area
J	Flux

Subscript	Definition
M	Membrane / Metal
Ret	Retentate
M-S	Scale
S	Scale

APPENDIX B

DERIVATION OF THE "TRANSIENT" FLUX EQUATION

The diffusion of hydrogen through the Pd-Cu alloy membrane can be modeled from Fick's Law, Equation 1,

$$N_H = -D_H \frac{dC_H}{dx} \qquad (7\text{-}1)$$

For thick membranes (>0.1 mm), the rate-limiting step is the diffusion of the hydrogen atoms in the metal, i.e. the adsorption and dissociation, and reassociation and desorption steps are at equilibrium. This permits the relation to the concentrations of the hydrogen atoms in the surface to that of hydrogen molecules in the gas phase by the application of Sieverts Law, Equation 7-2,

$$C_H = K_S P_{H2}^{0.5} \qquad (7\text{-}2)$$

From Equation 7-1 and 7-2, and considering that the flux of H_2 is half the flux of H, and given the relative small thickness of the membrane, Equation 7-3 follows

$$N_{H2} = -\frac{D_H K_S}{2X_M}(P_{H2,retentate}^{0.5} - P_{H2,permeate}^{0.5}) \quad (7\text{-}3)$$

Under our experimental conditions hydrogen was considered as an ideal gas and the partial pressure of hydrogen on the permeate side of the membrane was negligible. Further it was assumed and subsequently verified) that the time required to poison the membrane was very short relative to the duration of the transient test, therefore the permeability of the membrane was invariant with respect to time. Under these conditions the variation of the retentate pressure is related to the permeance of the membrane (k'), Equation 7-4,

$$\frac{dP_{H2,retentante}}{dt} = \frac{k'}{X_M} P_{H2,retentate}^{0.5} \quad (7\text{-}4)$$

An integrated form of Equation 4 was used to correlate the transient hydrogen retentate pressure with the membrane in terms of hydrogen permeance, k', Equation 7-5,

$$P_{H2,Ret}(t) = \left[P_{H2,Ret,Initial}^{0.5} - \frac{1}{2} A_M k' \left(\frac{RT}{V} \right) t \right]^2 \quad (7\text{-}5)$$

APPENDIX C

DERIVATION OF THE STEADY-STATE FLUX EQUATION

Fick's law, equation (7-6), defines the transient mass transfer of species A in the direction of decreasing concentration of A.

$$\frac{dN}{dt} = -D\frac{dC}{dx} \tag{7-6}$$

In the relation to the hydrogen membrane processes, the direction of mass transfer would be defined from the retentate (hydrogen rich feed stream) to the permeate (hydrogen poor stream). Assuming a steady state permeation process and integrating Equation (7-6) yields the governing, steady state form of Fick's law for membrane processes (Perry's Chemical Engineer's Handbook, 1984).

$$N_H = 2N_{H_2} = -D_M\frac{\Delta C_H}{t_M} \tag{7-7}$$

Where N_H is the atomic flux of hydrogen, N_{H2} is the molecular flux of hydrogen, D_M is the diffusivity of the membrane material, ΔC_H is the atomic concentration gradient across the membrane thickness, t_M.

The rate-limiting step in the membrane mechanism is sought to be the diffusion of the hydrogen through the membrane, because of the rapid dissociation of the hydrogen molecules on the membrane surface. As a result of the slow diffusion process, it can be assumed that the atomic concentrations at the membrane surfaces are at equilibrium with the retentate and permeate hydrogen gases. Application of Sieverts thermodynamic relation (Sievert et al.,), equation (7-8), gives the atomic concentration of hydrogen in terms of the partial pressure of the hydrogen gas at the membrane surface.

$$C_H = K_S P_{H_2}^{0.5} \tag{7-8}$$

Combining equations (7-7) and (7-8) gives the governing membrane permeation equation in terms of the hydrogen partial pressures of the retentate and permeate, the Richardson Equation, (7-9), as proposed by Buxbaum and Marker, 1993.

$$N_{H_2} = -\frac{D_M K_S}{2} \frac{\left(P_{H_2,Ret}^{0.5} - P_{H_2,Per}^{0.5}\right)}{t_M} \tag{7-9}$$

Defining the isothermal permeability constant of a membrane material by half of the product of the membrane diffusivity and the Sieverts constant and substituting into the Richardson Equation, (7-9), yields Equation (7-10), which is the governing equation for diffusion limited, atomic transport membrane processes.

$$N_{H_2} = -k_M \frac{\left(P_{H_2,Ret}^{0.5} - P_{H_2,Per}^{0.5}\right)}{t_M} \tag{7-10}$$

The rate of the molecular dissociation on the membrane surface and atomic-diffusion through the membrane has a large influence on the exponent of the partial pressure drop across the membrane. If dissociation of the membrane mechanism is the rate-limiting step, then the exponent of the partial pressure is 1.0, while membranes whose mechanism is governed by a rate-limiting step of diffusion have an exponent of 0.5 on the partial pressure expression. However, it has been established that for some atomic- or ionic-diffusion processes it is not uncommon to experience exponents ranging form 0.5 to 1.0 due to the competing rates of dissociation and diffusion (Hurlbert et al. 1961). Thus, equation (7-12) represents a more generic form of the membrane governing equation, which compensates for the competing "rate-determining steps" associated with the applicable mechanism.

$$N_{H_2} = -k_M \frac{\left(P^n_{H_2,Ret} - P^n_{H_2,Per}\right)}{t_M} \text{ or } R_{H_2} = -\frac{k_M A_M}{t_M}\left(P^n_{H_2,Ret} - P^n_{H_2,Per}\right) \qquad (7\text{-}12)$$

REFERENCES

1. Fain, D. E.; Roettger, G. E., Coal Gas Cleaning and Purification with Inorganic Membranes. *Transcript of the ASME Journal of Engineering for Gas Turbines and power* **1993,** 115, 628-633.

2. Gasification Technologies Training Course, Part 1: Fundamentals and operational experience". **2003**.

3. Bustamante, F., The high-temperature, high-pressure homogeneous water-gas shift reaction in a membrane reactor. *Ph.D. Thesis, University of Pittsburgh* **2004**.

4. Group, P. I. a. T., Hydrogen production facilities - plant performance and cost comparisons. *DE-AM26-99FT40465* **2002**.

5. Grashoff, G. J.; Pilkington, C. E.; Corti, C. W., The Purification of Hydrogen: A Review of the Technology Emphasizing the Current Status of Palladium Membrane Diffusion. **1983**, 157.

6. US.DOE.EERE, Report of the DOE Workshop on Hydrogen Separations and purification. **2004**.

7. Philpott, J.; Coupland, D. R., Metal Membranes for Hydrogen Diffusion and Catalysis. *Hydrogen Effects in Catalysis* **1988**, 679.

8. Hsieh, H. P., Inorganic membranes for separation and reaction. **1996**.

9. Darling, A. S., Hydrogen separtaion by diffusion through palladium alloy membranes. *Symposium on the less common means of separation, Institution of chemical engineers* **1963**.

10. Deville, H.; Troost, L., *Comptes rendus* **1863,** 57, 965.

11. Deville, H., *Comptes rendus* **1864,** 59, 102.

12. Graham, T., *Phil. Trans. Roy. Soc* **1866,** 156, 399.

13. Balovnev, Y. A., Diffusion of Hydrogen in Palladium at Low Pressures. *Russian Journal of Physical Chemistry* **1969,** 43, (10), 1382.

14. Davis, W. D. *Diffusion of Hydrogen Through Palladium*; General Electric Company: Schenectady, 1954.

15. Holleck, G. L., Diffusion and Solubility of Hydrogen in Palladium and Palladium-Silver Alloys. *The Journal of Physical Chemistry* **1970,** 74, (3), 503.
16. Katsuta, H.; Farraro, R. J.; McLellan, R. B., The Diffusivity of Hydrogen in Palladium. *Acta Metallurgica* **1979,** 27, 1111.

17. Koffler, S. A.; Hudson, J. B.; Ansell, G. S., Hydrogen Permeation Through Alpha-Palladium. *Transactions of the Metallurgical Society of AIME* **1969,** 245, 1735.

18. Toda, G., Rate of Permeation and Diffusion Coefficient of Hydrogen Through Palladium. *Journal of the Research Institute for Catalysis* **1958**, 13.

19. Paglieri, S. W., D., Innovations in Palladium Membrane Research. *Separation and Purification Methods* **2002,** 31 (1), 1-169.

20. Steward, S. A., Review of Hydrogen Isotope Permeability Through Materials. In Livermore, 1983; pp 1-21.

21. Buxbaum, R. E. Composite Metal Membrane for Hydrogen Extraction. 1993.

22. Athayde, A. L.; Baker, R. W.; Nguyen, P., Metal composite membranes for hydrogen separation. *Journal of Membrane Science* **1994,** 94, (1), 299.

23. Collins, J. P.; Way, J. D., Preparation and Characterization of a Composite Palladium-Ceramic Membrane. *Industrial & Engineering Chemistry Research* **1993,** 32, 3006.

24. Edlund, D. J.; McCarthy, J., The relationship between intermetallic diffusion and flux decline in composite-metal membranes: implications for achieving long membrane lifetime. *Journal of Membrane Science* **1995,** 107, (1-2), 147.

25. Fernandes, N. E.; Fisher, S. M.; Poshusta, J. C.; Vlachos, D. G.; Tsapatsis, M.; Watkins, J. J., Reactive Deposition of Metal Think Films within Porous Supports from Supercritical Fluids. *Chemical Materials* **2001,** 13, 2023.

26. Hou, K.; Hughes, R., Preparation of thin and highly stable Pd/Ag composite membranes and simulative analysis of transfer resistance for hydrogen separation. *Journal of Membrane Science* **2003,** 214, (1), 43.

27. Hsu, C.; Buxbaum, R. E., Electroless and Immersion Plating of Palladium on Zirconium. *Journal of the Electrochemical Society* **1985,** 132, (10), 2419.

28. Huang, L.; Chen, C. S.; He, Z. D.; Peng, D. K.; Meng, G. Y., Palladium membranes supported on porous ceramics prepared by chemical vapor deposition. *Thin Solid Films* **1997,** 302, (1-2), 98.

29. Itoh, N.; Tomura, N.; Tsuji, T.; Hongo, M., Deposition of palladium inside straight mesopores of anodic alumina tube and its hydrogen permeability. *Microporous and Mesoporous Materials* **2000,** 39, (1-2), 103.
30. Jemaa, N.; Shu, J.; Kaliaguine, S.; Grandjean, B. P. A., Thin Palladium Film Formation on Shot Peening Modified Porous Stainless Steel Substrates. *Industrial & Engineering Chemistry Research* **1996,** 35, 973.

31. Juda, W.; Krueger, C. W.; Bombard, T. R. Diffusion-bonded palladium-copper alloy framed membrane for pure hydrogen generators and the like and method of preparing the same. 1999.

32. Juda, W.; Krueger, C. W.; Bombard, T. R. Method of producing thin palladium-copper and the like, palladium alloy membranes by solid-solid metallic interdiffusion, and improved membrane. 2001.

33. Jun, C.-S.; Lee, K.-H., Palladium and palladium alloy composite membranes prepared by metal-organic chemical vapor deposition method (cold-wall). *Journal of Membrane Science* **2000,** 176, (1), 121.

34. Keuler, J. N.; Lorenzen, L., Developing a heating procedure to optimise hydrogen permeance through Pd-Ag membranes of thickness less than 2.2 [mu]m. *Journal of Membrane Science* **2002,** 195, (2), 203.

35. Keuler, J. N.; Lorenzen, L.; Maichon, S., Preparing and Testing Pd Films of Thickness 1-2 Micrometer With High Selectivity and High Hydrogen Permeance. *Separation Science and Technology* **2002,** 37, (2), 379.

36. Keuler, J. N.; Lorenzen, L.; Sanderson, R. D.; Prozesky, V.; Przybylowicz, W. J., Characterization of electroless plated palladium-silver alloy membranes. *Thin Solid Films* **1999,** 347, (1-2), 91.

37. Kishimoto, S.; Inoue, M.; Yoshida, N., Solution of Hydrogen in Thin Palladium FIlms. *Journal of the Chemical Society. Faraday Transactions* **1986,** 82, 2175.

38. Krueger, C.; Juda, W.; Bombard, T. *Opportunities for High Temperature Metal Hydrogen Separation Membranes*; Hy9 Corporation: Woburn.

39. Krueger, C. W. Method of improving and optimizing the hydrogen permeability of a palladium-copper membrane and novel membranes manufactured thereby. 2002.

40. Kusakabe, K.; Yokoyama, S.; Morooka, S.; Hayashi, J. i.; Nagata, H., Development of supported thin palladium membrane and application to enhancement of propane aromatization on Ga-silicate catalyst. *Chemical Engineering Science* **1996,** 51, (11), 3027.

41. Kusakabe, K.; Takahashi, M.; Maeda, H.; Morooka, S., Preparation of Thin Palladium Membranes by a Novel Method Based on Photolithography and Electrolysis. *Journal of Chemical Engineering of Japan* **2001,** 34, (5), 703.

42. Li, A.; Liang, W.; Hughes, R., Characterisation and permeation of palladium/stainless steel composite membranes. *Journal of Membrane Science* **1998,** 149, (2), 259.

43. Li, A.; Liang, W.; Hughes, R., Fabrication of defect-free Pd/[alpha]-Al2O3 composite membranes for hydrogen separation. *Thin Solid Films* **1999,** 350, (1-2), 106.

44. Li, A.; Liang, W.; Hughes, R., Repair of a Pd/[alpha]-Al2O3 composite membrane containing defects. *Separation and Purification Technology* **1999,** 15, (2), 113.

45. Li, A.; Liang, W.; Hughes, R., Fabrication of dense palladium composite membranes for hydrogen separation. *Catalysis Today* **2000,** 56, (1-3), 45.

46. Mardilovich, P. P.; She, Y.; Ma, Y. H.; Rei, M.-H., Defect-Free Palladium Membranes on Porous Stainless-Steel Support. *AIChE Journal* **1998,** 44, (2), 310.

47. McCool, B.; Xomeritakis, G.; Lin, Y. S., Composition control and hydrogen permeation charateristics of sputter deposited palladium-silver membranes. *Journal of Membrane Science* **1999,** 161, 67-76.

48. Moss, T. S.; Peachey, N. M.; Snow, R. C.; Dye, R. C., Multilayer Metal Membranes for Hydrogen Separation. *International Journal of Hydrogen Energy* **1998,** 23, (2), 99.

49. Nam, S.-E.; Lee, S.-H.; Lee, K.-H., Preparation of a palladium alloy composite membrane supported in a porous stainless steel by vacuum electrodeposition. *Journal of Membrane Science* **1999,** 153, (2), 163.

50. Nam, S.-E.; Lee, K.-H., A study on the palladium/nickel composite membrane by vacuum electrodeposition. *Journal of Membrane Science* **2000,** 170, (1), 91.

51. O'Brien, J.; Hughes, R.; Hisek, J., Pd/Ag membranes on porous alumina substrates by unbalanced magnetron sputtering. *Surface and Coatings Technology* **2001,** 142-144, 253.

52. Pan, X. L.; Stroh, N.; Brunner, H.; Xiong, G. X.; Sheng, S. S., Pd/ceramic hollow fibers for H2 separation. *Separation and Purification Technology* **2003,** 32, (1-3), 265.

53. Peachey, N. M.; Snow, R. C.; Dye, R. C., Composite Pd/Ta metal membranes for hydrogen separation. *Journal of Membrane Science* **1996,** 111, (1), 123.

54. Pick, M. A.; Davenport, J. W.; Strongin, M.; Dienes, G. J., Enhancement of Hydrogen Uptake Rates for Nb and Ta by Thin Surface Overlays. *Physical Review Letters* **1979,** 43, (4), 286.

55. Pick, M. A.; Greene, M. G.; Strongin, M., Uptake Rates for Hydrogen by Niobium and Tantalum: Effect of Thin Metallic Overlayers. *Journal of the Less Common-Metals* **1980,** 73, 89.
56. Roa, F.; Way, J. D.; McCormick, R. L., Preparation of Micron Scale, Pd-Cu Composite Membranes for H_2 Separations. In *ACS*, Colorado School of Mines: Golden, 2001.

57. Shu, J.; Grandjean, B. P. A.; Kaliaguine, S., Methane steam reforming in asymmetric Pd- and Pd-Ag/porous SS membrane reactors. *Applied Catalysis A: General* **1994,** 119, (2), 305.

58. So, J.-H.; Yang, S.-M.; Bin Park, S., Preparation of silica-alumina composite membranes for hydrogen separation by multi-step pore modifications. *Journal of Membrane Science* **1998,** 147, (2), 147.

59. Souleimanova, R. S.; Mukasyan, A. S.; Varma, A., Study of structure formation during electroless plating of thin metal-composite membranes. *Chemical Engineering Science* **1999,** 54, (15-16), 3369.

60. Strokes, C. L.; Buxbaum, R. E., Analysis of Palladium Coatings to Remove Hydrogen Isotopes from Zirconium Fuel Rods in Canada Deuterium Uranium-Pressurized Heavy Water Reactors: Thermal and Neutron Diffusion Effects. *Nuclear Technology* **1992,** 98, 207.

61. Uemiya, S.; Kude, Y.; Sugino, K.; Sato, N.; Matsuda, T.; Kikuchi, E., A Palladium/Porous-Glass Composite Membrane for Hydrogen Separation. *The Chemical Society of Japan* **1988**, 1687.

62. Uemiya, S., State-Of-The-Art of Supported Metal Membranes for Gas Separation. *Separation and Purification Methods* **1999,** 28, (1), 51.

63. Uemiya, S.; Sato, N.; Ando, H.; Kude, Y.; Matsuda, T.; Kikuchi, E., Separation of hydrogen through palladium thin film supported on a porous glass tube. *Journal of Membrane Science* **1991,** 56, (3), 303.

64. Uemiya, S.; Kato, W.; Uyama, A.; Kajiwara, M.; Kojima, T.; Kikuchi, E., Separation of hydrogen from gas mixtures using supported platinum-group metal membranes. *Separation and Purification Technology* **2001,** 22-23, 309.

65. Wu, L.-Q.; Xu, N.; Shi, J., Preparation of a Palladium Composite Membrane by an Improved Electroless Plating Technique. *Industrial & Engineering Chemistry Research* **2000,** 39, 342.

66. Yan, S.; Maeda, H.; Kusakabe, K.; Morooka, S., Thin Palladium Membrane Formed in Support Pores by Metal-Organic Chemical Vapor Deposition Method and Application to Hydrogen Separation. *Industrial & Engineering Chemistry Research* **1994,** 33, 616.

67. Yeung, K. L.; Varma, A., Novel Preparation Techniques for Thin Metal-Ceramic Composite Membranes. *AIChE Journal* **1995,** 41, (9), 2131.

68. Yeung, K. L.; Sebastian, J. M.; Varma, A., Novel preparation of Pd/Vycor composite membranes. *Catalysis Today* **1995,** 25, (3-4), 231.
69. Yeung, K. L.; Christiansen, S. C.; Varma, A., Palladium composite membranes by electroless plating technique: Relationships between plating kinetics, film microstructure and membrane performance. *Journal of Membrane Science* **1999,** 159, (1-2), 107.

70. Zhao, H. B.; Pflanz, K.; Gu, J. H.; Li, A. W.; Stroh, N.; Brunner, H.; Xiong, G. X., Preparation of palladium composite membranes by modified electroless plating procedure. *Journal of Membrane Science* **1998,** 142, (2), 147.

71. Okamoto, H., Phase Diagrams for binary alloys. **2000**.

72. Callister, W. D., Materials Science and Engineering, An Introduction. **2003**.

73. Gao, H.; Lin, Y. S.; Li, Y.; Zhang, B., Chemical Stability and Its Improvement of Palladium-Based Metallic Membranes. *Industrial & Engineering Chemistry Research* **2004,** 43, 6920.

74. Roa, F.; Way, J. D., The effect of air exposure on palladium-copper composite membranes. *Applied Surface Science* **2005,** 240, 85-104.

75. Hurlbert, R. C.; Konecny, J. O., Diffusion of Hydrogen through Palladium. *The Journal of Chemical Physics* **1961,** 34, (2), 655.

76. Collins, J. P.; Way, J. D., Catalytic decomposition of ammonia in a membrane reactor. *Journal of Membrane Science* **1994,** 96, (3), 259.

77. Ali, J. K.; Newson, E. J.; Rippin, D. W. T., Deactivation and regeneration of Pd=Ag membranes for dehydrogenation reactions. *Journal of Membrane Science* **1994,** 89, (1-2), 171.

78. Lalauze, R.; Gillard, P.; Pijolat, C., Hydrogen permeatioin through a thin film of palladium: influence of surface impurities. *Sensors and Actuators* **1988,** 14, (3), 243.

79. Paglieri, S. N.; Foo, K. Y.; Way, J. D.; Collins, J. P.; Harper-Nixon, D. L. *A New Preparation Technique for Pd/Alumina Membranes with Enhanced High-Temperature Stability*; 1999.

80. Antoniazzi, A. B.; Haasz, A. A.; Auciello, O.; Stangeby, P. C., Atomic, ionic and molecular hydrogen permeation facility with in situ Auger surface analysis. *Journal of Nuclear Materials* **1984,** 128-129, 670.

81. Basile, A.; Criscuoli, A.; Santella, F.; Drioli, E., Membrane reactor for water gas shift reaction. 243.

82. Li, A.; Liang, W.; Hughes, R., The effect of carbon monoxide and steam on the hydrogen permeability of a Pd/stainless steel membrane. *Journal of Membrane Science* **2000,** 165, (1), 135.
83. Paturzo, L.; Basile, A., Kinetics, Catalysis, and Reaction Engineering. *Industrial & Engineering Chemistry Research* **2002,** 41, 1703.

84. McKinley, D. L.; Nitro, W. Metal Alloy for Hydrogen Separation and Purification. 1967.

85. Edlund, D.; Friesen, D.; Johnson, B.; Pledger, W., Hydrogen-permeable metal membranes for high-temperature gas separations. *Gas Separation & Purification* **1994,** 8, (3), 131.

86. Edlund, D. J.; Pledger, W. A., Thermolysis of hydrogen sulfide in a metal-membrane reactor. *Journal of Membrane Science* **1993,** 77, (2-3), 255.

87. Kajiwara, M.; Uemiya, S.; Kojima, T., Stability and hydrogen permeation behavior of supported platinum membranes in presence of hydrogen sulfide. *International Journal of Hydrogen Energy* **1999,** 24, 839.

88. Kulprathipanja, A.; Alptekin, G. O.; Falconer, J. L.; Way, J. D., Pd and Pd-Cu membranes: inhibition of H_2 permeation be H_2S. *Journal of Membrane Science* **2005,** 254, 49-62.

89. Mundschau, M.; Xie, X.; Everson, X., Nonporous Inorganic Membranes. **2006**.

90. Boes, N.; Zuchner, H., Diffusion of Hydrogen and Deuterium in Ta, Nb, and V. *Physica Status Solidi (a)* **1973,** 17, K111.

91. Veleckis, E.; Edwards, R. K., Thermodynamic Properties in the Systems Vanadium-Hydrogen, Niobium-Hydrogen, and Tantalum-Hydrogen. *The Journal of Physical Chemistry* **1969,** 73, (3), 683.

92. Simonovic, B. R.; Mentus, S.; Susic, M. V., Kinetics of tantalum hydriding: the effect of palladization. *International Journal of Hydrogen Energy* **2000,** 25, 1069.

93. Buxbaum, R. E.; Subramanian, R.; Park, J. H.; Smith, D. L., Hydrogen transport and embrittlement for palladium coated vanadium--chromium--titanium alloys. *Journal of Nuclear Materials* **1996,** 233-237, (Part 1), 510.

94. Paglieri, S. N.; Birdsell, S. A.; Snow, R. C.; Springer, R. W.; Smith, F. M., Development of Palladium Composite Membranes for Hydrogen Separation. In *AIChE - Advances in Gas Separation Membranes and Applications II*, Los Alamos National Laboratory: Los Alamos, 2003.

95. Buxbaum, R. E.; Hsu, P. C., Measurement of diffusive and surface transport resistances for deuterium in palladium-coated zirconium membranes. *Journal of Nuclear Materials* **1992,** 189, (2), 183.

96. Buxbaum, R. E.; Kinney, A. B., Hydrogen Transport through Tubular Membranes of Palladium-Coated Tantalum and Niobium. *Industrial & Engineering Chemistry Research* **1996,** 35, 530.

97. Buxbaum, R. E.; Marker, T. L., Hydrogen transport through non-porous membranes of palladium-coated niobium, tantalum and vanadium. *Journal of Membrane Science* **1993,** 85, (1), 29.

98. Makrides, A. C.; Newton, M. A.; Wright, H.; Jewett, D. N., US Patent # 3,350,846. **1964**.

99. Buxbaum, R. E., The Use of Zirconium-Palladium Windows for the Separation of Tritium from the Liquid Metal Breeder-Blanket of a Fusion Reactor. *Separation Science and Technology* **1983,** 18, (12&13), 1251.

100. Buxbaum, R. E.; Hsu, P. C. Method for plating palladium. 1992.

101. Simonovic, B. R.; Mentus, S.; Dimitrijevic, R.; Susic, M. V., Multiple hybriding/dehybriding of $Zr_{1.02}$ $Ni_{0.98}$ alloy. *International Journal of Hydrogen Energy* **1999,** 24, 449.

102. Perng, T. P.; Altstetter, C. J., On the Effective Hydrogen Permeability in Metastable Beta Titanium Alloy, Niobium and 2.25Cr-1 Mo Ferritic Steel. *Metallurgical Transactions* **1986,** 17A, 2086.

103. Rothenberger, K. S.; Howard, B. H.; Killmeyer, R. P.; Cugini, A. V.; Enick, R. M.; Bustamante, F.; Ciocco, M. V.; Morreale, B. D.; Buxbaum, R. E., Evaluation of tantalum-based materials for hydrogen separation at elevated temperatures and pressures. *Journal of Membrane Science* **2003,** 218, (1-2), 19.

104. Edlund, D. P., W., Catalytic Platinum-based membrane reactor for removal of H2S from natural gas streams. *Journal of Membrane Science* **1994,** 94, 111-119.

105. Shu, j.; Grandjean, B.; Kaliaguine, S., Catalytic palladium-based membrane reactors. *Applied Catalyst A: General 119* **1991**, 1036-1060.

106. Knapton, A. G., Palladium Alloys for Hydrogen Diffusion Membranes. *Platinum Metals Review* **1977,** 21, 44.

107. McKinley, D. L. Method for Hydrogen Separation and Purification. 1969.

108. Farr, J. P. G.; Harris, I. R., *British Patent # 1,346,422* **1974**.

109. Fort, D.; Farr, J. P. G.; Harris, I. R., *Less-Comon Met.* **1975,** 39, 293.

110. Edlund; Henry, A membrane process for hot gas clean-up and decomposition of H2S to elemental sulfur. *Phase II Final Report, DE-FG03-91ER81228* **1996**.
111. Hoang, H. T.; Tong, H. D.; Gielens, F. C.; Jansen, H. V.; Elwenspoek, M. C., Fabrication and characterization of dual sputtered Pd-Cu alloy films for hydrogen separation membranes. *Materials Letters* **2004,** 58, (3-4), 525.

112. Roa, F.; Block, M. J.; Way, J. D., The influence of alloy composition on the H2 flux of composite Pd---Cu membranes. *Desalination* **2002,** 147, (1-3), 411.

113. Way, J. D. *Palladium/Copper Alloy Composite Membranes for High Temperature Hydrogen Separation from Coal-Derived Gas Streams*; Colorado School of Mines: Golden, 2001.

114. Way, J. D.; McCormick, R. L.; Roa, F.; Paglieri, S. N. *Palladium Alloy Composite Membranes for High Temperature Hydrogen Separation from Coal-Derived Gas Streams*; Colorado School of Mines: Golden, 2002.

115. Bryden, K. J.; Ying, J. Y., Nanostructured palladium-iron membranes for hydrogen separation and membrane hydrogenation reactions. *Journal of Membrane Science* **2002,** 203, (1-2), 29.

116. Itoh, N.; Xu, W. C.; Sathe, A. M., Capability of Permeate Hydrogen through Palladium-Based Membranes for Acetylene Hydrogenation. *Industrial & Engineering Chemistry Research* **1993,** 32, 2614.

117. Tosti, S.; Bettinali, L.; Violante, V., Rolled thin Pd and Pd-Ag membranes for hydrogen separation and production. *International Journal of Hydrogen Energy* **2000,** 25, 319.

118. Tosti, S.; Adrover, A.; Basile, A.; Camilli, V.; Chiappetta, G.; Violante, V., Characterization of thin wall Pd-Ag rolled membranes. *International Journal of Hydrogen Energy* **2003,** 28, 105.

119. Fort, D.; Harris, I. R., *Less-Comon Met.* **1975,** 41, 313.

120. Hughes, D. T.; Harris, I. R., *Less-Comon Met.* **1978,** 61, 9.

121. Zetkin, A. S.; Kagan, G. E.; Varaksin, A. N.; Levin, E. S., DIffusion and penetrability of deuterium in the alloy Pd-53 at. % Cu. *Soviet Physics, Solid State* **1992,** 34, (1), 83.

122. Zetkin, A. S.; Kagan, G. Y.; Levin, Y. S., Influence of Structural Transformations on the Diffusion Parameters of Deuterium in Palladium-Copper Alloys. *Phys. Met. Metall.* **1987,** 64, (5), 130.

123. Piper, J., Diffusion of Hydrogen in Copper-Palladium Alloys. *Journal of Applied Physics* **1966,** 37, (2), 715.

124. Levin, E. S.; Zetkin, A. S.; Kagan, G. E., Solubility of deuterium in Pd-Cu alloys. *Russian Journal of Physical Chemistry* **1992,** 66, (2), 465.
125. Flanagan, T. B.; Chisdes, D. M., Solubility of hydrogen (1 atm, 298 K) in some copper/palladium alloys. *Solid State Communications* **1975,** 16, (5), 529.

126. Burch, R.; Buss, R. G., Pressure-composition isotherms in the palladium-copper-hydrogen system. *Solid State Communications* **1974,** 15, (2), 407.

127. Kuranov, A. A.; Berseneva, F. N.; Sasinova, R. A.; Laptevskiy, A. S., Ordering, and the Mechanical Properties of Palladium-Copper Alloys. *Phys. Met. Metall.* **1983,** 56, (3), 167.

128. Kulprathipanja, A.; Alpetkin, G. O.; Falconer, J. L.; Way, J. D., Effects of water gas shift gases on Pd-Cu alloy membrane surface morphology and separation properties. *Ind. Eng. Chem. Res.* **2004,** 43, 4188-4198.

129. Betteridge, W.; Hope, J., The Separation of Hydrogen from Gas Mixtures. *Platinum Metals Review* **1975,** 19, 50.

130. Campbell, C. T., H_2S/Cu(111): A Model Study of Sulfur Poisoning of Water-Gas Shift Catalysis. *Surface Science* **1987,** 183, 100.

131. Burke, M. L. M., R.J., Hydrogen on Pd(100)-S: the effect of sulfur on precursor mediated adsorption and desorption. *Surface Science* **1990,** 237, (1-3), 1-19.

132. Forbes, J. G.; Gellman, A. J.; Dunphy, J. C.; Salmeron, M., Imaging of sulfur overlayer structures on the Pd(111) surface. *Surface Science* **1992,** 279, 68-78.

133. Vazquez, A.; Pedraza, F.; Fuentes, S., Influence of sulfidation on the morphology and hydrodesulfurization activity of palladium particles on silica. *Journal of Molecular Catalysis* **1992,** 75, (1), 63.

134. Feuerriegel, U.; Klose, W.; Sloboshanin, S.; Goebel, H.; Schaefer, J. A., Deactivation of a Palladium-Supported Alumina Catalyst by Hydrogen Sulfide during the Oxidation of Methane. *Langmuir* **1994,** 10, (10), 3567.

135. Wilke, M.; Scheffler, M., Poisoning of Pd(100) for the dssociations of H_2: a theoretical study of co-adsorption of hydrogen and sulphur. *Surface Science Letters* **1995,** 329, L605-L610.

136. Gravil, P. A.; Toulhoat, H., Hydrogen, sulphur and chlorine coadsorption on Pd(111): a theoretical study of poisoning and promotion. *Surface Science* **1999,** 430, (1-3), 176.

137. Alfonso, D.; Cugini, A.; Sholl, D., Density functional theory studies of sulfur binding on Pd, Cu and Ag and their alloys. *Surface Science* **2003,** 546, 12.

138. Alfonso, D.; Cugini, A.; Sorescu, D., Adsorption and decomposition of H2S on Pd(111) surface: a first principle study. *Catalysis Today* **2005,** 99, 315.

139. Alfonso, D., First-principle study of sulfur overlayers on Pd(111) surface. *Surface Science* **2005,** 596, 229-241.

140. Barin, I.; Sauert, F.; Schultze-Rhonhof, E.; Sheng, W., Thermodynamic propertices of inorganic substances. **1993**.

141. Taylor, J. R., Phase relationships and thermodynamic properties of the Pd-S system. *Metallurgical Transactions B* **1985,** 16B, 143-148.

142. Niwa, K.; Yokokawa, T.; Isoya, T., Equilibria in the PdS-H2-Pd4S-H2S and Pd4S-H2-Pd-H2S Systems. *Bulletin of the 14th Annual Meeting of the Chemical Societ of Japan* **1962,** 35-9, 1543-1545.

143. Howard, B. H.; Killmeyer, R. P.; Rothenberger, K. S.; Cugini, A. V.; Morreale, B. D.; Enick, R. M.; Bustamante, F., Hydrogen permeance of palladium-copper alloy membranes over a wide range of temperatures and pressures. *Journal of Membrane Science* **2004,** 241, (2), 207.

144. Kamakoti, P.; Morreale, B. D.; Ciocco, M. V.; Howard, B. H.; Killmeyer, R. P.; Cugini, A. V.; Sholl, D. S., Prediction of Hydrogen Flux Through Sulfur-Tolerant Binary Alloy Membranes. *Science* **2005,** 307, (5709), 569-573.

145. Morreale, B. D.; Ciocco, M. V.; Howard, B. H.; Killmeyer, R. P.; Cugini, A. V.; Enick, R. M., Effect of hydrogen-sulfide on the hydrogen permeance of palladium-copper alloys at elevated temperatures. *Journal of Membrane Science* **2004,** 241, (2), 219.

146. Paglieri, S. N.; Birdsell, S. A. *Palladium Alloy Composite Membranes for Hydrogen Separation*; Los Alamos National Laboratory: Los Alamos.

147. Roa, F.; Way, J. D., Influence of Alloy Composition and Membrane Fabrication on the Pressure Dependence of the Hydrogen Flux of Palladium-Copper Membranes. *Industrial & Engineering Chemistry Research* **2003,** 42, 5827.

148. Meier, G. H.; Birks, N., Introduction of High Temperature Oxidation of Metals. **1983**.